5-2021

Development of Biomaterials for Drug Delivery

Raquel De Castro
University of Arkansas, Fayetteville

Development of Biomaterials for Drug Delivery

A dissertation submitted in partial fulfillment
of the requirements for the degree of
Doctor of Philosophy in Cell and Molecular Biology

by

Raquel de Castro
University of Arkansas
Bachelor of Science in Biology, 2012
University of Arkansas
Master of Arts in Teaching, 2013

May 2021
University of Arkansas

This dissertation is approved for recommendation to the Graduate Council.

_____
Audie K. Thompson, Ph.D.
Dissertation Director

_____
Robert Beitle, Ph.D.
Committee Member

_____
David McNabb, Ph.D.
Committee Member

_____
Francis Millett, Ph.D.
Committee Member

Abstract

Drug delivery systems (DDS) have highly evolved in the last decades with the development of hydrogels and nanoparticles. However, high systemic uptake, side effects, low bioavailability, and encapsulation efficiency continue to be a major hurdle faced by such DDSs.

Nanoparticles and hydrogels can be specifically designed for targeted DDSs to mitigate some of the problems. This dissertation aimed to design two DDSs for ocular drug delivery and one for cancer treatment. The first project sought to develop chitosan nanoparticles (Cs-NP) using PEGDA as a copolymer to encapsulate gentamicin (GtS) for ocular drug delivery. Cs-NPs contain positive charges that can interact with negatively charged ocular proteins to increase the NP residence time. Simultaneously, ocular enzymes degrade the chitosan β-(1→4)-glycosidic bonds to release GtS at the eye's surface, therefore, preventing premature release of GtS. PEGDA was used to increase drug encapsulation by shielding the repelling forces of like charges between Cs and GtS. The data shows PEGDA does not hinder enzymatic degradation while increasing drug encapsulation efficiency and producing more stable and homogeneous particles.

The second project utilized Michael's reaction to crosslink Cs, Cs-NPs, and PEGDA to produce a film designed for ocular drug delivery. The film serves as an anchor for the NPs to prevent drug removal by tears and blinking. The data shows that crosslinking of Cs and PEGDA does not affect lysozyme activity, and NPs could successfully release GtS without affecting GtS activity.

Finally, the third project sought to compare the cytotoxicity of the polysaccharide fucoidan (FU) encapsulated into chitosan nanoparticles (CFU) and without encapsulation (free-FU) and their effects on two cancer cell lines. The results indicate that free-FU has very little toxicity to MDA-MB-231 cancer cells compared to MCF-7. However, cytotoxicity to MDA-MB-

231 cells was increased by delivering encapsulated FU. Free-FU can enter MCF-7 cells using surface receptors that are not present in MDA-MB-231 cells. Therefore, by encapsulating FU into Cs-NPs, cytotoxicity can be increased as Cs-NPs containing FU are endocytosed into the MDA-MB-231 cells.

Dedication

Many friends and colleagues have helped me along this journey, and I am forever thankful for all the help, big or small, and words of encouragement.

Mom, you taught me to dream big and dare to follow my dreams, and dad, you taught me perseverance and to never give up. It was the best of you that gave me the tools I needed to get here and finish strong. Dinda and Gloria, thank you for the immeasurable help, prayers, and encouragement. Luis, thank you for being understanding and supportive during the difficult times, the late-night lab trips, and for cheering me on to the finish line. Lastly, I dedicate this dissertation to my son, my grandmother Regina and God. Grandma, you taught me to have the faith that sustained me through the many trials I have faced, the value of sacrifice, and you loved me so well even when I did not deserve it. Son, you have taught me how to love, have hope, and trust that God will never leave me or forsake me. Being your mom has been the greatest gift. Thank you for walking this journey by my side. God, thank you for making it all possible.

"So do not fear, for I am with you; do not be dismayed, for I am your God. I will strengthen you and help you; I will uphold you with my righteous right hand." Isaiah 41:10

Table of Contents

List of Abbreviations

BC	breast cancer
BSA	bovine serum albumin
CFU	chitosan fucoidan nanoparticle
CGNP	chitosan-gentamicin nanoparticle
Cs	chitosan
Cs Np	chitosan nanoparticle
Cs-GtS	chitosan-gentamicin
Cs-NP	chitosan nanoparticles
Cs-PEGDA-CG(NP) film	chitosan-PEGDA-(chitosan-gentamicin nanoparticle) film
Cs-PEGDA-GtS NP	chitosan-PEGDA-gentamicin nanoparticle
DD	drug delivery
DDS	drug delivery systems
ESC	equilibrium swelling content
FU	fucoidan
GtS	gentamicin
NP	nanoparticle
PEGDA	poly(ethylene glycol) diacrylate
PspA	pneumococcal surface protein A
PVA	polyvinyl alcohol
TPP	tripolyphosphate

List of Published Papers

Chapter 4

Aljewari, H., Castro, R. D., Solomon, O., Iii, Q. C. M., Nave, F., & Thompson, A. (2020). Study of Pneumococcal Surface Protein, PspA, Incorporated in Poly(Vinyl Alcohol) Hydrogel Membranes. *Journal of Biomaterials and Nanobiotechnology, 11*(01), 67-81. doi:10.4236/jbnb.2020.111005, published.

Introduction

The field of drug delivery (DD) has evolved from medicinal plants' liquid concoctions to developing the first pills in ancient Egypt. Although drug delivery systems (DDS) have vastly changed, many of the goals remain the same: improving patient compliance, drug stability, bioavailability, and efficacy while reducing side effects, doses, and overall costs (Figure 1) (Saikia & Gogoi, 2015). Today, we boast from various delivery systems, but some delivery routes such as topical ocular remain very inefficient due to high systemic uptake and physical barriers (Gaudana, Ananthula, Parenky, & Mitra, 2010). Another major obstacle to current DDSs is drug side effects. A recent study reported that 93% of women treated for early-stage invasive breast cancer experienced one or more toxicity from treatment (Friese et al., 2017). Thus, engineering DDSs for specific environments to provide targeted delivery and improve drug specificity to lower systemic uptake while simultaneously increasing drug bioavailability remains of utmost importance.

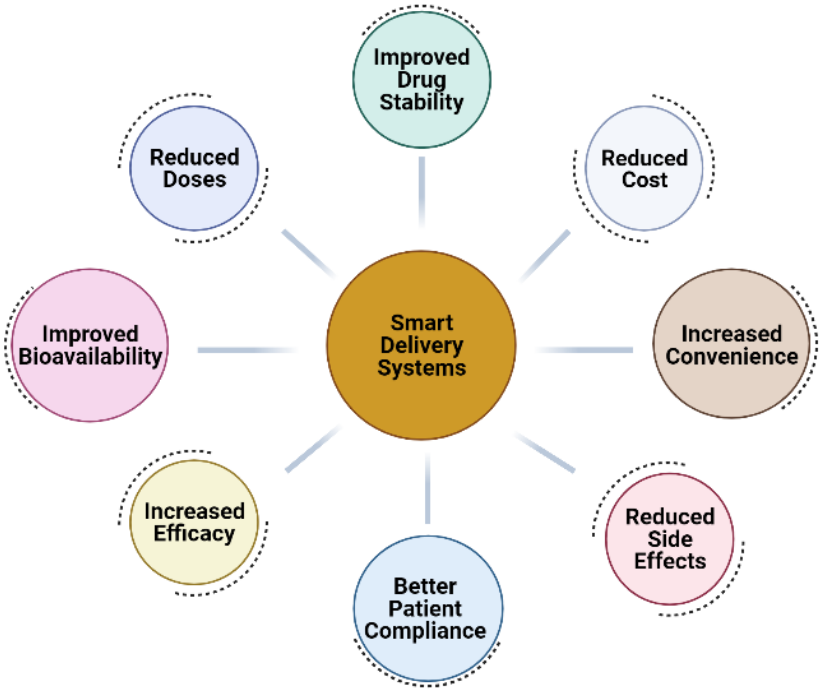

Figure 1 *Advantages of smart drug delivery systems.*

Drug bioavailability, the amount of drug that reaches its intended biological destination, and drug delivery rate depends on the route of administration (Price & Patel, 2020). For instance, 80-90% of solutions instilled into the anterior surface of the eye get drained into the nasal-lacrimal duct, and as little as 5% of eye drops reach the ocular target (Agrahari et al., 2016). The intravenous route is the most effective delivery method into the systemic circulation, and it yields the greatest bioavailability, but its invasiveness can lead to problems such as contamination and pain (Yalkowsky, Krzyzaniak, & Ward, 1998). This dissertation focuses on developing improved targeted drug delivery systems for (1) ocular and (2) topical delivery and (3) the use of a biological molecule with cancer cell specificity for cancer treatment.

The first system focused on designing a delivery system specific for the ocular surface to deliver aminoglycosides to the eye's anterior segment using chitosan nanoparticles (Cs-NP) while simultaneously increasing drug encapsulation. Chitosan (Cs) is a biocompatible polysaccharide derived from chitin that can form positively charged nanoparticles and become degraded by ocular enzymes. The benefits of encapsulating gentamicin (GtS) in Cs-NPs are many. It maintains drug stability during storage, prevents drug dilution, increases drug residency time due to the charge interactions between Cs and mucins in the eye, and degradation by ocular enzymes provides a controlled release system specific to the eye’s anterior segment. However, aminoglycosides such as gentamicin have low encapsulation efficiency into Cs-NPs due to charge repellence (Lu, Franzblau, Onyuksel, & Popescu, 2009). Therefore, to increase encapsulation efficiency, the biocompatible synthetic polymer poly(ethylene glycol) diacrylate (PEGDA) was used as a non-ionic dispersing agent (Figure 2).

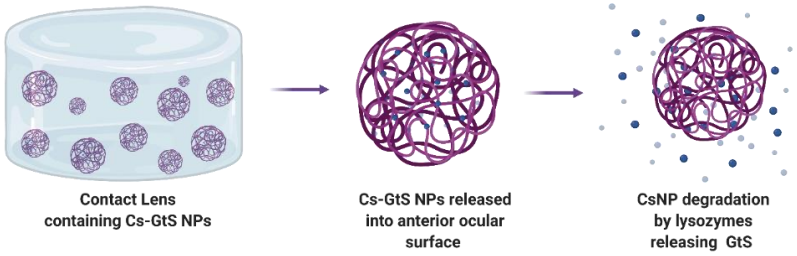

Figure 2 *Chitosan nanoparticles containing gentamicin can be added to therapeutic contact lenses to treat conjunctivitis.*

The second system sought to fabricate a chitosan-PEGDA film that can be functionalized with nanoparticles to deliver ocular medication. The film anchors the nanoparticles until contact with eye lysozymes release the drugs into the ocular surface. The film prevents the medication from being released prematurely and stops it from being removed from the eye surface due to blinking. Cs and PEGDA are both biocompatible materials used in hydrogel synthesis. Poly(ethylene glycol), the parent molecule of PEGDA, is a highly lubricating agent used in contact lens synthesis and dry eyes treatment, a symptom associated with bacterial eye infections. The diacrylate form of PEG can be crosslinked with Cs by Michaels addition reaction to form a hydrogel that can be functionalized with drug-loaded nanoparticles. As previously stated, Cs become degraded by ocular enzymes to release the nanoparticles at the eye's anterior surface (Figure 3).

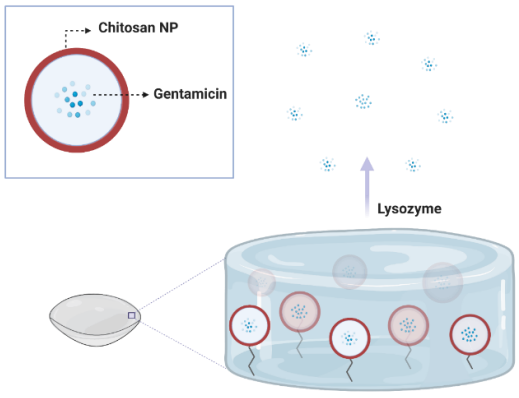

Figure 3 *Chitosan nanoparticles containing gentamicin chemically attached to chitosan-PEGDA film.*

The third system sought to use a polyvinyl alcohol (PVA) hydrogel to deliver a large protein, pneumococcal surface protein A (PspA), as a proof of concept for future microneedle vaccine delivery applications (Figure 4). The use of hydrogels in protein delivery is limited by protein size (Nikolaos A. Peppas & Mongia, 1997; N. A. Peppas & Simmons, 2004). PspA is a large protein of approximately 38kD shown to elicit protective immunity against pneumococcal infection. Successful incorporation and release of PspA from the hydrogel while maintaining protein stability and activity is the first step in developing a microneedle vaccine delivery (Leone, Mönkäre, Bouwstra, & Kersten, 2017).

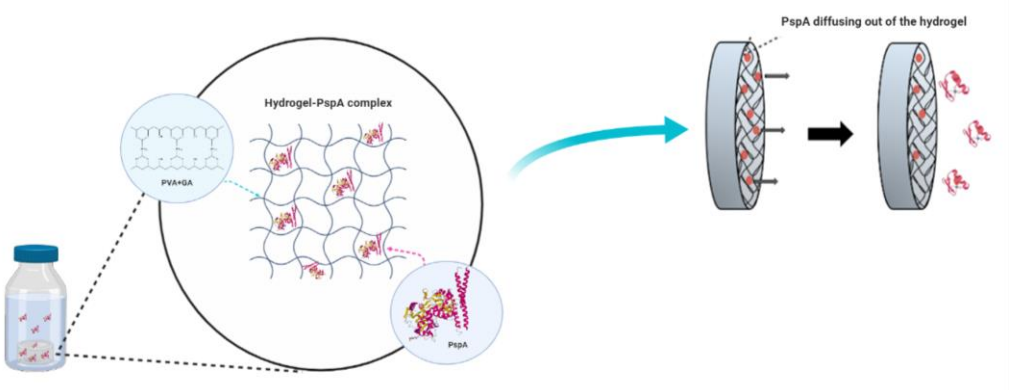

Figure 4 *Incorporation of PspA into the PVA hydrogel and diffusion of PspA graphic abstract.*

Finally, there is a need to design target-specific delivery systems to enhance bioavailability and reduced off-target effects, especially in cancer treatment, where the lack of target-specificity and high cancer heterogeneity often leads to debilitating side effects. As drug resistance increases, expanding the anticancer drug arsenal is also equally important, and bioactive molecules with cancer specificity are great candidates (Workman & Collins, 2008). A potential anticancer treatment for breast cancer is the naturally occurring polysaccharide fucoidan (FU). FU has been extensively investigated as an oral supplement and a component for drug delivery vehicles, but its use as an anticancer drug delivered by nanoparticles to enhance cytotoxicity to breast cancer cells has not been investigated (Wang et al., 2019). Chitosan is a polysaccharide with anticancerous properties that can synthesize biocompatible

and non-toxic NPs with target specificity. Targeted delivery is possible due to the enhanced permeability effect (EPR), in which small molecules such as NPs accumulate at the tumor site while normal tissue is left unharmed.

By delivering FU to the tumor site, side effects can be reduced, and efficacy increased by reducing systemic uptake. This study aimed to encapsulate FU into chitosan NPs to investigate their effects on MCF-7 and MDA-MB-231 cell lines compared to non-encapsulated FU. Furthermore, this study examines the cytotoxic effects of FU on cancerous and normal cell lines as a way of establishing the safety of using FU in breast cancer treatment (Figure 5).

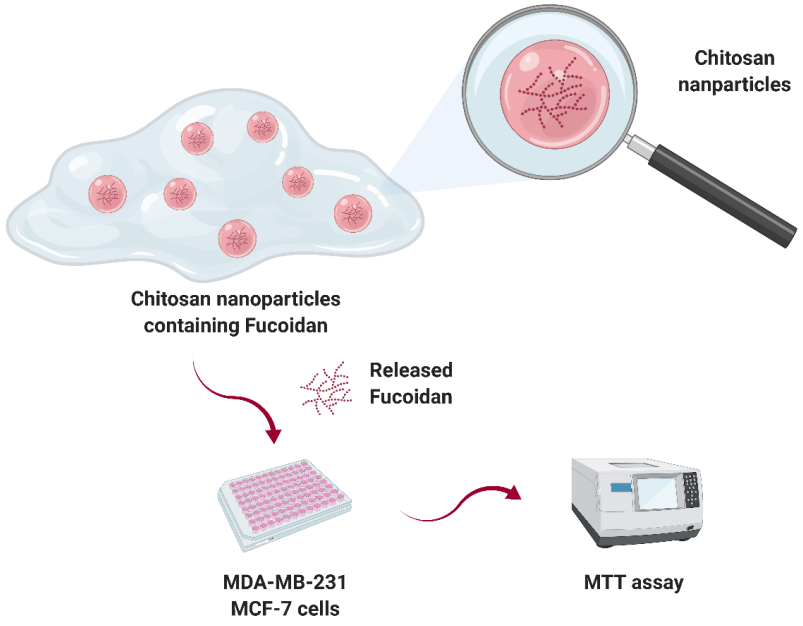

Figure 5 *Testing cytotoxicity of chitosan nanoparticles containing fucoidan using MTT assay.*

Agrahari, V., Mandal, A., Agrahari, V., Trinh, H. M., Joseph, M., Ray, A., . . . Mitra, A. K. (2016). A comprehensive insight on ocular pharmacokinetics. *Drug Delivery and Translational Research, 6*(6), 735-754. doi:10.1007/s13346-016-0339-2

Friese, C. R., Harrison, J. M., Janz, N. K., Jagsi, R., Morrow, M., Li, Y., . . . Hofer, T. P. (2017). Treatment-associated toxicities reported by patients with early-stage invasive breast cancer. *Cancer, 123*(11), 1925-1934. doi:10.1002/cncr.30547

Gaudana, R., Ananthula, H. K., Parenky, A., & Mitra, A. K. (2010). Ocular drug delivery. *AAPS J, 12*(3), 348-360. doi:10.1208/s12248-010-9183-3

Leone, M., Mönkäre, J., Bouwstra, J. A., & Kersten, G. (2017). Dissolving Microneedle Patches for Dermal Vaccination. *Pharmaceutical Research, 34*(11), 2223-2240. doi:10.1007/s11095-017-2223-2

Lu, E. X., Franzblau, S., Onyuksel, H., & Popescu, C. (2009). Preparation of aminoglycoside-loaded chitosan nanoparticles using dextran sulphate as a counterion. *Journal of Microencapsulation, 26*(4), 346-354. doi:10.1080/02652040802365182

Peppas, N. A., & Mongia, N. K. (1997). Ultrapure poly(vinyl alcohol) hydrogels with mucoadhesive drug delivery characteristics. *European Journal of Pharmaceutics and Biopharmaceutics, 43*(1), 51–58. doi:10.1016/s0939-6411(96)00010-0

Peppas, N. A., & Simmons, R. E. P. (2004). Mechanistic analysis of protein delivery from porous poly(vinyl alcohol) systems. *Journal of Drug Delivery Science and Technology, 14*(4), 285-289.

Price, G., & Patel, D. A. (2020, 10/20/2020). Drug Bioavailability. Retrieved from https://www.ncbi.nlm.nih.gov/books/NBK557852/

Saikia, C., & Gogoi, P. (2015). Chitosan: A Promising Biopolymer in Drug Delivery Applications. *Journal of Molecular and Genetic Medicine, s4*. doi:10.4172/1747-0862.s4-006

Wang, Y., Xing, M., Cao, Q., Ji, A., Liang, H., & Song, S. (2019). Biological Activities of Fucoidan and the Factors Mediating Its Therapeutic Effects: A Review of Recent Studies. *Mar Drugs, 17*(3). doi:10.3390/md17030183

Workman, P., & Collins, I. (2008). Modern cancer drug discovery: integrating targets, technologies and treatments. In S. Neidle & S. Neidle (Eds.), *Cancer Drug Design and Development* (1 ed., pp. 3-33): Academic Press.

Yalkowsky, S. H., Krzyzaniak, J. F., & Ward, G. H. (1998). Formulation-related problems associated with intravenous drug delivery. *J Pharm Sci, 87*(7), 787-796. doi:10.1021/js980051i

Literature Review

Historical progress of drug delivery (DD)

In the quest to "enhance health, lengthen life, and reduce the burdens of illness and disability" (2011), scientists have continued to search for innovative ways to overcome obstacles in drug delivery. Although much progress has been made in drug development from medicinal herbs to synthetic drugs, biological barriers such as metabolism, absorption, excretion, and mode of drug delivery and release can and do affect the drug pharmacokinetics. In order to overcome these barriers, delivery systems have been engineered to control drug release rate and release location in the body.

The oldest recorded controlled delivery system, the pill, dates back to over 1000 years ago in Ancient Persia (Reza Rezaie, Esnaashary, Aref arjmand, & Öchsner, 2018), and its use continued to develop in the nineteenth and twentieth centuries. However, it was not until the late 1940s and early 1950s when the field of drug-delivery technology began to sprout with the development of the first-generation of sustained-release products, followed by a better understanding of drug pharmacokinetics in the 1960s (Rosen & Abribat, 2005). It was also in the 1960s when polymers began to be used in delivery systems (Rosen & Abribat, 2005).

Fast forward a couple of decades (1980-2010), and now we enter the second-generation drug delivery systems (DDSs) with the development of smart polymers, hydrogels, biodegradable microparticles, solid implants, and *in-situ* gel-forming implants (Reza Rezaie et al., 2018). Therefore the third generation of drug delivery systems is left with the task to overcome some of the barriers faced by the previous generations of DDSs, which include delivery of poorly water-soluble drugs, large molecules such as peptides, proteins, and nucleic acids, and better control of nanoparticles for drug delivery (Reza Rezaie et al., 2018).

Routes of drug administration

Oral delivery

When designing a DDS, it is crucial to consider the drug target site to establish the best administration route (Figure 6). Oral delivery is the most used method for delivery into systemic circulation due to its convenient and non-invasive nature. However, most therapeutic peptides and proteins, due to their large size, cannot be transported across the epithelium and become rapidly degraded by the gastrointestinal tract (Alkilani, McCrudden, & Donnelly, 2015). In order to avoid drug breakdown and peak of drug release, systems such as controlled-release oral osmotic (OROS) delivery systems and spheroidal oral absorption systems (SODAS) have been designed to provide a continued release drug profile (Gulledge, Aggen, & Chamberlin, 2003).

Transdermal delivery

Drugs can also enter the systemic circulation by the transdermal route, which avoids the hepatic first-pass metabolism, therefore, improving bioavailability (Rosen & Abribat, 2005). Additionally, dendritic cells (antigen-presenting cells) in the epidermal and dermal layers of the skin make it an ideal vaccination route (Alkilani et al., 2015). While birth control hormones, nicotine, and other small molecular weight molecules (<500Da) have been successfully delivered by transdermal patches since the 1990's the delivery of larger molecules and non-lipophilic drugs remain problematic due to low drug permeation across the skin (Alkilani et al., 2015; Patel & Shah, 2018; Rastogi & Yadav, 2012). Therefore, new techniques have been developed to enhance drug skin permeabilization. These include laser and radiofrequency, iontophoresis, electroporation, microneedles, jet injectors, and ultrasounds (Alkilani et al., 2015).

Transmucosal delivery

The transmucosal route, which includes buccal, nasal, vaginal, rectal, intrauterine, and ocular mucosa, has many advantages (Rosen & Abribat, 2005). Besides being relatively pain-

free, the combination of high membrane permeability and rich blood flow leads to quick systemic circulation uptake (Abhang, Momin, Inamdar, & Kar, 2014). Some common transmucosal drug delivery approaches include tablets, patches, films, gels and ointments, sprays, in-situ gels, microemulsions, liposomes, vaginal ring, drops, powders and microparticles, ophthalmic inserts/films, microspheres & nanoparticles, ion exchange resins, and capsules (Abhang et al., 2014).

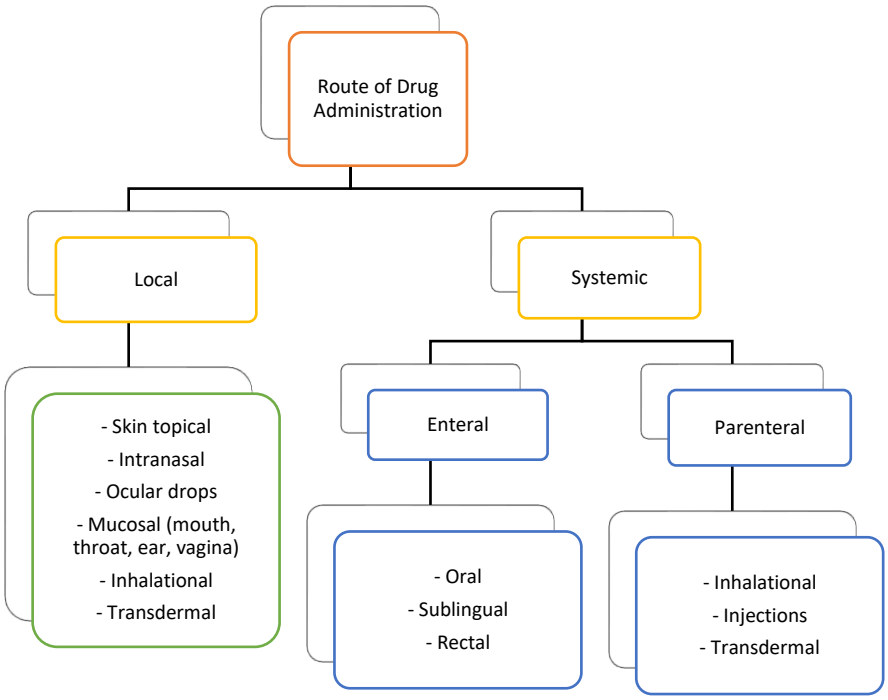

Figure 6 *Routes of Drug Administration.*

Ocular drug delivery

Eye drops are a conventional treatment for anterior eye diseases, and although non-invasive and easily applied, they are often inefficient drug delivery vehicles due to the rapid drug clearance through the canalicular drainage (Maulvi, Soni, & Shah, 2016). Upon contact with the eye, the drug diffuses into the cornea and conjunctiva, the latter being the preferential path due to its larger size and transported into the systemic circulation (Figure 7). Systemic uptake leads to side effects, and less than 5% of the drug reaching the anterior eye (Gaudana, Ananthula,

Parenky, & Mitra, 2010). Thus, requiring multiple applications and variations in drug mass reaching the targeted site, further reducing desired pharmacokinetic drug profiles. Furthermore, studies suggest that multiple applications lead to lower patient compliance, which could compromise treatment outcomes (Mutlu, Shams Es-Haghi, & Cakmak, 2019).

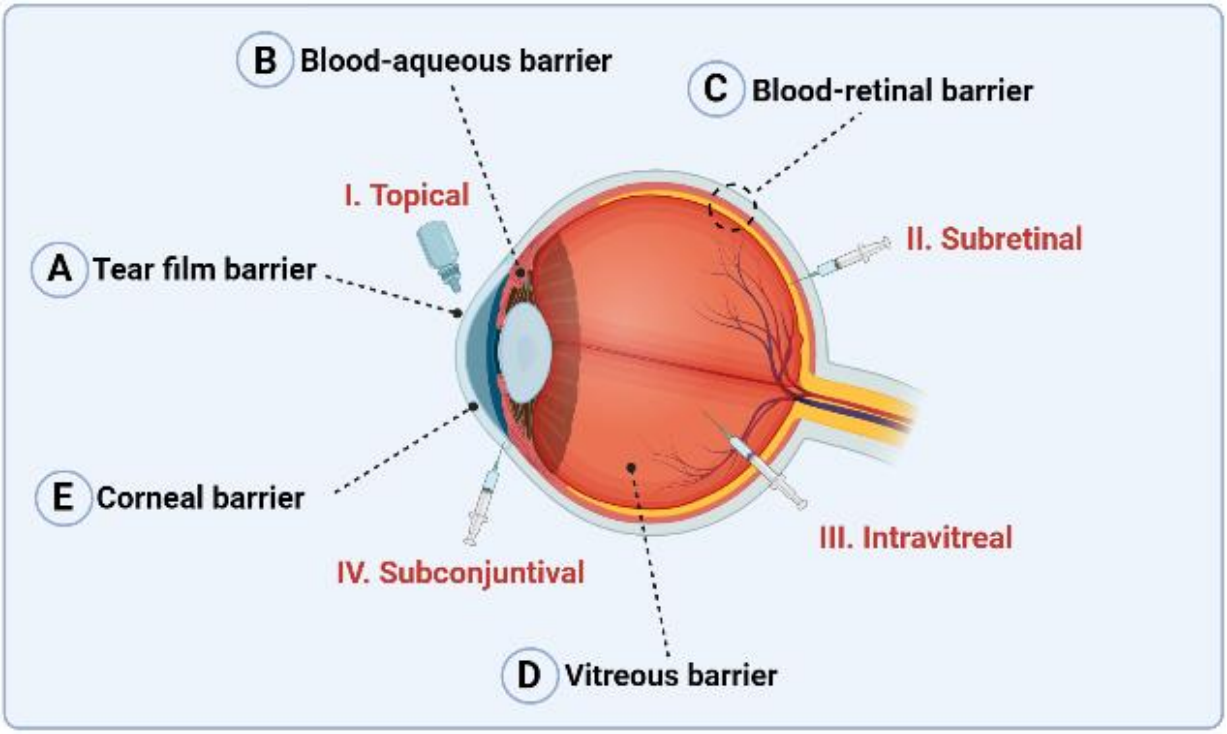

Figure 7 *Anatomical ocular barriers and routes of drug administration.* ***a)*** *ocular barriers and* ***b)*** *methods to drug delivery.*

Developing more effective ocular drug delivery systems remains a challenge, and nanocarriers and therapeutic contact lenses are promising tools in treating anterior eye diseases such as bacterial conjunctivitis. Nanocarriers have been shown to promote sustained and targeted drug release, increase drug bioavailability, lead to fewer applications, and increase patient compliance (Deepthi & Jose, 2019; Gaudana et al., 2010).

Uses of Hydrogels in Drug Delivery

Hydrogels and nanoparticles are incredibly versatile and have been used in all drug administration routes together and individually. Hydrogels were the first materials developed to be used within the human body (Kopecek, 2007; S. C. Lee, Kwon, & Park, 2013; Yahia, 2015). In biological applications, they are often used as matrices in tissue engineering, biosensing, and drug delivery (Choi, Yong, Choi, & Cowie, 2019). Hydrogels are produced by crosslinking water-soluble polymers to form 3D structures that take various physical forms from micro/nanoparticles to films (Hoare & Kohane, 2008). Physical properties such as swelling, tunable pore size for drug loading and release, biodegradability, and biocompatibility have put hydrogels at the forefront of drug delivery materials. Alas, amidst so many benefits, their use in drug delivery remains restricted by large pore sizes and high-water content that lead to rapid drug release.

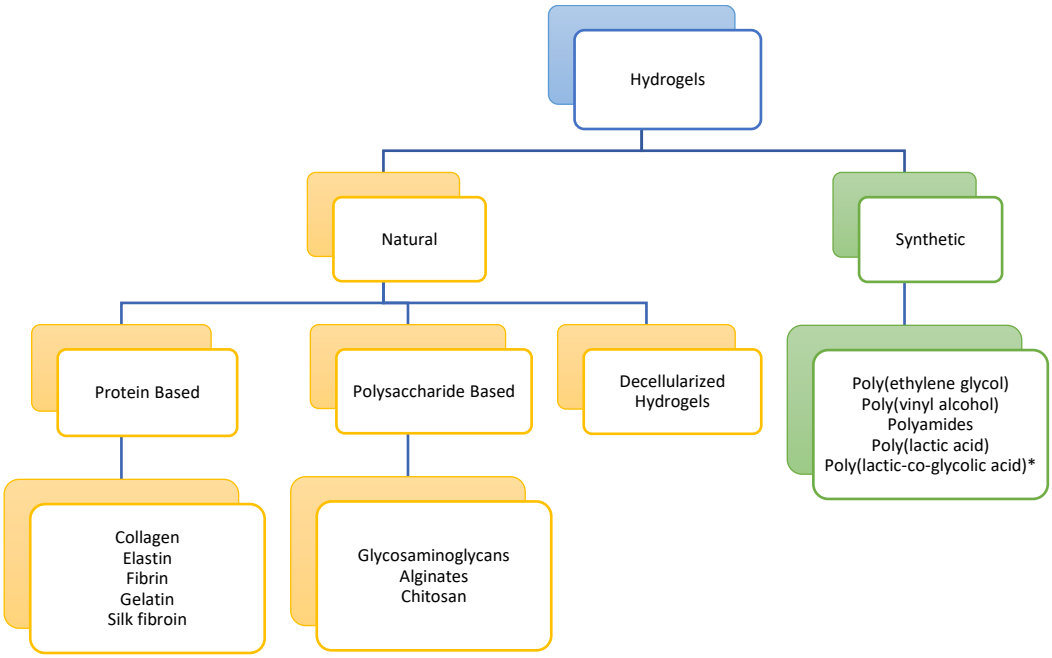

Figure 8 *Materials used in Hydrogel Synthesis.*

Another drawback is the low tensile strength of many hydrogels, which has limited their use in load-bearing applications, such as the development of microneedles (Hoare & Kohane, 2008). An additional desirable characteristic of hydrogels is the ability to be chemically and physically modified to produce smart hydrogels. Smart hydrogel systems (SHS) have been designed to respond to external stimuli, including temperature, pH, ionic concentration, light, magnetic field, electrical fields, and chemicals (Yahia, 2015).

Hydrogels can be produced from natural and synthetic polymers or a hybrid. Natural hydrogels are synthesized from biological molecules that make up the extracellular matrix *in vivo,* such as collagen, hyaluronic acid, chitosan, and alginates (Figure 8). Therefore, natural hydrogels are similar to the physiological environment, which renders them biocompatible (Catoira, Fusaro, Di Francesco, Ramella, & Boccafoschi, 2019; Yahia, 2015). On the other hand, synthetic hydrogels are derived from synthetic polymers such as poly(ethylene glycol) (PEG), poly(ethylene glycol) diacrylate (PEGDA), poly(vinyl alcohol) (PVA), and polyamides (Figure 8). They are hydrophobic and possess greater mechanical strength and durability than natural hydrogels (Gyles, Castro, Silva, & Ribeiro-Costa, 2017). Another benefit of synthetic polymers over natural polymers is reproducibility. Natural polymers vary in composition from one batch to another, which causes reproducibility hard to attain (Yahia, 2015).

Since the first hydrogel development for biological use in 1960 (Wichterle & LÍM, 1960), much has changed. Today's smart hydrogels seek to combine synthetic and natural polymers and materials to produce gels with tunable properties and responsive to stimuli (Yahia, 2015). Unfortunately, as these hydrogel blends emerge, many still require potentially harmful chemicals during synthesis. Hence, developing hydrogels without the use of harsh chemicals remains a necessity.

PEGDA in drug delivery systems

PEGDA properties

In the early 1990s, new methods using mild conditions to crosslink polymers using visible and UV-light were developed (Amsden, 2016), and with it, new photoinducible polymers such as PEGDA. PEGDA is a synthetic polymer derived from PEG (Figure 9). By substituting terminal hydroxyl groups in PEG with acrylates, the molecule can undergo free-radical polymerization in the presence of a photoinitiator (Choi et al., 2019). PEGDA hydrogels have a high molecular weight (MW) ranging from 200-2000Da and are considered non-toxic at MW above 400Da (O'Donnell, Boyd, & Meenan, 2019).

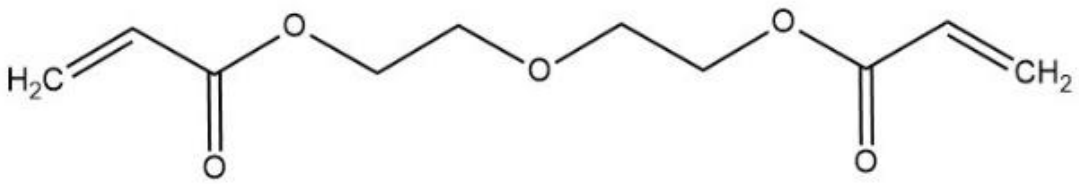

Figure 9 *PEGDA chemical structure.*

Another characteristic inherited from its parent molecule, PEG, is low immunogenicity and low cell attachment due to natural resistance to protein adsorption (Choi et al., 2019; O'Donnell et al., 2019; Tan et al., 2012). PEGDA has been extensively used in long-term controlled drug release because of its good biocompatibility, biodegradability, hydrophilicity, and slow degradation rate (Choi et al., 2019). Additionally, PEGDA can be physically and chemically crosslinked to form hydrogels (O'Donnell et al., 2019), and the presence of two acryl groups also allow for functionalization, as demonstrated by Jia et al. The group produced a PEGDA hydrogel microarray functionalized with peptides for stem cells and tissue engineering (2016).

PEGDA hydrogels

Photocrosslinked PEGDA hydrogels have been successfully used to coat ureteric stents to enhance drug release and transport in ureteric tissue (Lim et al., 2018), in 3D printing for microfluidic structures in tissue engineering (Warr et al., 2020), microneedle patches for antibacterial applications (Gao et al., 2021), ultrasmall nanogels for drug delivery (X. Wang, Peng, Pena, & Xing, 2021) and as a copolymer in the fabrication of programmable nanofiber scaffolds for reduction of inflammation and thrombosis (H. Wang et al., 2020). However, skepticism over the reactivity between the free radicals formed during polymerization with other biological molecules and chemicals such as crosslinking agents, stabilizers, and catalysts leaching into the body, remains a concern (N. A. Peppas & Simmons, 2004).

PEGDA nanoparticles

Although most PEGDA applications revolve around hydrogels, hydrogel nanoparticles (nanogels) (Stillman, Jarai, Raman, Patel, & Fromen, 2020), microbeads (Shikha, Zheng, & Zhang, 2018), and matrix-based nanoparticulate polymeric systems (Thukral, Dumoga, Arora, Chuttani, & Mishra, 2014) have been successfully employed in drug delivery of chemotherapeutic agents, and protein detection.

PEGDA in ocular drug delivery

PEGDA use in ocular delivery is relatively new, with a minimal number of publications as of 2021. Most work in ocular drug delivery has used PEGDA as a photo-induced crosslinker. Swindle-Reilly et al. used a PEGDA crosslinked with poly(ethylene glycol) methacrylate (PEGMA) hydrogel loaded with chitosan nanoparticles containing vitamin C for optical injection to improve drug stability (2020). PEGDA implants, which are less invasive than optical injections, have also been developed but are limited to drug delivery to the eye's anterior surface. Photocrosslinked PEGDA implants have provided a controlled release system for

delivering small and large molecules like triamcinolone acetonide and ova albumin to the ocular surface (McAvoy, Jones, & Thakur, 2018). A combination of PEGDA and PLGA for *in-situ* photocrosslinked implants successfully delivered proteins to the eye for 4-6 months (Thakur, Wang, Soliman, Sonawane, & Jones, 2019). However, safety concerns over free radicals produced by photo-induction remain an issue.

Use of PVA hydrogel in protein delivery

Protein drugs have high clinical potential owing to specificity, low toxicity, and clear biological function. However, difficulties in protein delivery, mainly due to high molecular weight, poor biological membrane penetration, structural instability at low pHs, enzymatic degradation, and low bioavailability in the gastrointestinal environment, restricts the use of most delivery vehicles currently available (Asfour, 2021; Yang et al., 2019). Moreover, proteins have short half-lives, from minutes to several hours, which restricts how they can be administered to the body (Yang et al., 2019). Because of low oral bioavailability, most proteins are administered by the parenteral route, requiring needles (Asfour, 2021). In attempts to minimize patient discomfort, new delivery systems like hydrogel microneedles are being developed, but currently, such vehicles are limited to small molecules and cannot be used to transport large proteins, nucleic acids, and peptides (Reza Rezaie et al., 2018). Therefore, there is a need to fabricate hydrogels to deliver large molecular weight proteins while maintaining protein stability and increasing bioavailability.

Polyvinyl Alcohol (PVA) hydrogel properties

PVA hydrogels have been extensively used in the biomedical field due to their biocompatible, biodegradable, non-carcinogenic, and hydrophilic properties. Although PVA is hydrophilic, once crosslinked, they become insoluble in water. They are also stable at room temperature and swell when immersed in water (N. A. Peppas & Simmons, 2004). Their tissue-

like elasticity and mechanical strength render PVA hydrogels an ideal material for tissue engineering, especially in the fabrication of arterial tissues, artificial grafts, and implants (Nuttelman, Mortisen, Henry, & Anseth, 2001). However, their use in drug delivery is limited to small molecules and by slow drug diffusion (Hoare & Kohane, 2008; N. A. Peppas & Simmons, 2004).

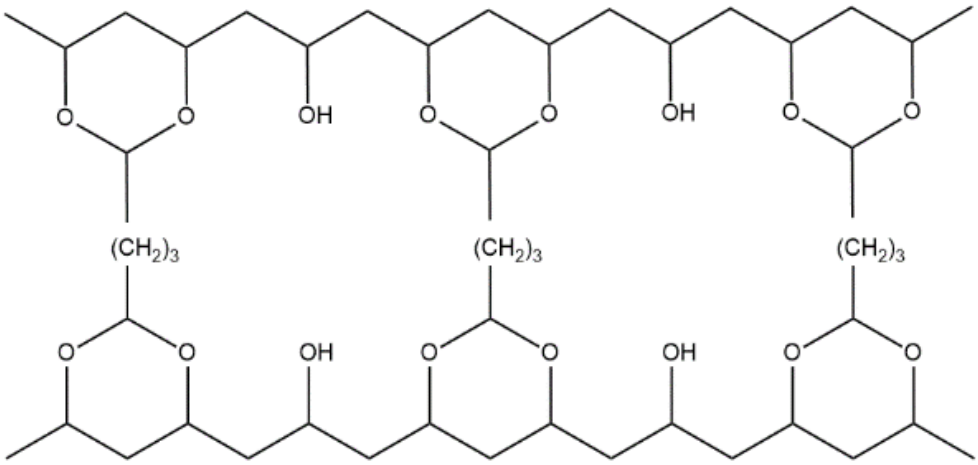

Figure 9 *Chemical structure of PVA crosslinked with glutaraldehyde.*

PVA contains hydroxyl groups that can undergo hydrogen bonding to form hydrogels by physical or chemical interactions. Physical crosslinking can be achieved by cycles of freezing and thawing, while chemical crosslinking involves the use of radiation or crosslinking agents such as glutaraldehyde (Figure 10), methanol, ethanol, propanol, and acetone (Jiang, Liu, & Feng, 2011; Nkhwa, Lauriaga, Kemal, & Deb, 2014). Unfortunately, the toxicity of some chemicals used in chemical crosslinking has posed a barrier to their use in pharmaceutical and biological applications, but crosslinking by freeze-thaw is a safer alternative (N. A. Peppas & Simmons, 2004).

Although PVA hydrogels and nanoparticles have been used to deliver various drugs and proteins, including indomethacin, glucose, insulin, heparin, and albumin; protein stability during long term storage remains a challenge (J. K. Li, Wang, & Wu, 1998; Nikolaos A. Peppas &

Mongia, 1997; Ye, Yu, Wen, Kahkoska, & Gu, 2018). For that reason, to preserve protein stability careful consideration is needed when selecting materials and formulations for hydrogel synthesis. Currently, microneedles are a promising transdermal protein delivery method, and partially dissolving microneedles of polyvinylpyrrolidone (PVP)/polyvinyl alcohol (PVA) have been developed for sustained delivery using bovine serum albumin (BSA) as a protein model (I. C. Lee, He, Tsai, & Lin, 2015).

Chitosan/PEGDA hydrogels use in drug delivery

Minimal research has been done using composite hydrogels made out of chitosan and PEGDA, and the two studies published used such hydrogels for regenerative medicine. Soriente et al. fabricated chitosan/PEGDA scaffolds for implants capable of stimulating neovascularization of tissue-engineered constructs for regenerative medicine (2021), while Sun et al. synthesized halloysites modified PEGDA/thiolated-chitosan hydrogels loaded with bone morphogenic protein-2 for rat skull regeneration (2021).

Chitosan uses in drug delivery

Chitosan properties

Chitosan is a natural linear polysaccharide polymer. Although chitosan is found in limited quantities in nature, most commercially available chitosan is derived from chitin, the second most abundant polysaccharide globally. Chitin is a constituent in the exoskeleton of insects, crustaceans, arthropods, and the cell wall of fungi and some algae. However, chitin's primary source comes from shrimp, crab, and lobster (Whistler, 1993). Chitin is made up of 1-4 linked 2-acetamido-2-deoxy-β-D-glucopyranose units that can become deacetylated by chemical hydrolysis under alkaline conditions or by enzymatic hydrolysis using deacetylase enzymes to produce chitosan.

Chitosan's chemical structure comprises randomly alternating β-(1→4)-linked d-glucosamine and N-acetyl-d-glucosamine units (Figure 11), its molecular weight ranges between 300-1000kDa depending on the chitin source, and its degree of deacetylation varies between 60-100% (Ibrahim & El-Zairy, 2015; Whistler, 1993). Chitosan's molecular weight and degree of deacetylation affect its physicomechanical properties. For example, toxicity increases as molecular weight and degree of deacetylation increase. The same inverse relationship is also observed regarding solubility and degradation relative to molecular weight and degree of acetylation (Garg, Chauhan, Nagaich, & Jain, 2019).

Although insoluble in water, chitosan is a weak acid (pKa 6.5) and can be solubilized in diluted acidic solutions (pH <6) by protonating amino groups (Ahmadi, Oveisi, Samani, & Amoozgar, 2015; Chandra Hembram, Prabha, Chandra, Ahmed, & Nimesh, 2016). This polycationic nature allows chitosan to interact with negative charges in cellular membranes to enhance membrane permeation and mucins to enhance mucoadhesiveness (Eliyahu, Aharon, & Bianco-Peled, 2018; Ibrahim & El-Zairy, 2015). For example, charge interactions between chitosan and clathrin proteins on the surface of cell membranes form clathrin-coated vesicles that lead to chitosan cellular uptake by endocytosis (Salatin & Yari Khosroushahi, 2017).

Additionally, chitosan contains glycosidic bonds that are naturally degraded *in vivo* by proteases. Degradation in the human body requires lysozyme, acid, gastrointestinal enzymes, or colon bacteria. Chitosan can be degraded *in vitro* by β-N-acetylhexosaminidase, chitosanase, chitinase, and chitin deacetylase enzymes (Ahmadi et al., 2015). Moreover, amino and hydroxyl groups in the chitosan structure allow for several reactions, including etherification, esterification, and reductive amination reactions, to form stable covalent bonds (Ibrahim & El-Zairy, 2015).

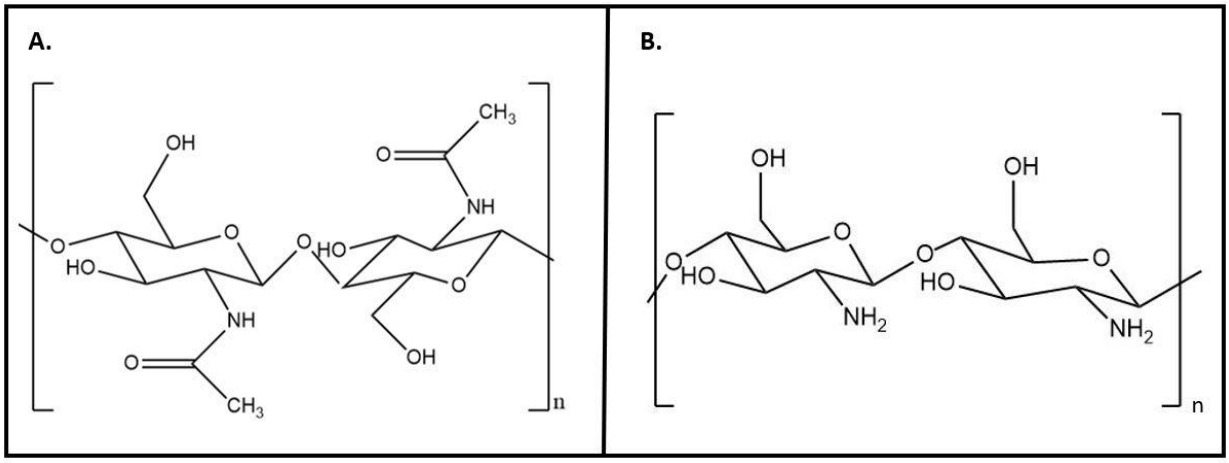

Figure 10 *Chemical structure.* ***a)*** *Chitin is made up of 1-4 linked 2-acetamido-2-deoxy-β-D-glucopyranose.* ***b)*** *Chitosan is made up of randomly alternating β-(1→4)-linked d-glucosamine (deacetylated unit) and N-acetyl-d-glucosamine (acetylated unit).*

Chitosan has many attractive properties for biological applications, including biocompatibility, biodegradability, and non-toxicity. It can be used as an analgesic, antifungal, antimicrobial material, a hemostatic agent, and chelating agent for cholesterol, fats, proteins, and metal ions (Ibrahim & El-Zairy, 2015; Zalloum & Mubarak, 2013). Likewise, chitosan's versatility can be observed in medical, agricultural, food processing, cosmetic industries, and waste and water treatment (Ibrahim & El-Zairy, 2015).

Chitosan applications

Chitosan has been used in agriculture in seed coating to improve germination, leaf coating to enhance leaf growth and fertilizer for soil moisture retention. In the food industry, chitosan has been used in food storage and preservation due to its antimicrobial and antifungal properties. Furthermore, in water treatment to bind and remove metal ions from water. Chitosan's medical applications are vast, including tissue engineering, wound healing, contact lens, and drug delivery (Ibrahim & El-Zairy, 2015).

Chitosan hydrogels

Chitosan hydrogels can be synthesized by chemical or physical crosslinking. Chemically crosslinked chitosan hydrogels are covalently bonded at the amines and hydroxyl groups and form an irreversible bond (Ahmadi et al., 2015). Chemical crosslinking can be achieved using crosslinkers like glutaraldehyde, genipine, dextran sulfate, diisocyanate, and acrylic acid (Anitha, Rejinold, Bumgardner, Nair, & Jayakumar, 2012), or via photopolymerization using a photoinitiator along with visible or UV irradiation. In contrast, physically crosslinked chitosan gels are formed by ionic interactions (Ahmadi et al., 2015).

Because chitosan is a hydrophilic polymer, it can systemically be absorbed and eliminated by renal filtration. Therefore, the appropriate polymer molecular weight must be determined to prevent elimination (Ahmadi et al., 2015). Likewise, chitosan hydrogels' stability is also highly dependent on the polysaccharide molecular weight and ionic strength as chitosan polysaccharide chains can interact with each other by hydrogen, hydrophobic or ionic interactions (Ahmadi et al., 2015).

Chitosan hydrogels have been used in drug delivery to the oral cavity, stomach, intestine, and colon. Smart hydrogels have been developed by combining various polymers and grafting materials to respond to stimuli. Bai et al. recently developed a Thermo/pH-sensitive *N*-succinyl hydroxybutyl chitosan hydrogels with different substitution degrees of succinyl for oral delivery. The group could load and release BSA from their gel successfully at different rates according to local pH (Bai et al., 2018). Pahani et al. designed a stomach-specific chitosan montmorillonite hydrogel for extended drug delivery of clarithromycin, an antibiotic used to treat duodenal ulcers caused by *H. pylori* (2019). A recently developed injectable hydrogel for colon cancer treatment using chitosan-grafted-dihydrocaffeic acid (CS-DA) and oxidized pullulan (OP) was designed with pH sensitivity and tissue adhesiveness for localized delivery of the anticancer drug doxorubicin (Liang et al., 2019).

Chitosan nanoparticles

Nanoparticles (NP) are solid colloidal drug carrier systems composed of natural and synthetic polymers. Sizes can range from 10-1000nm in diameter. However, most biological applications require particles of <200nm due to microcapillaries' width (Divya & Jisha, 2017; Nagpal, Singh, & Mishra, 2010; Singh & Lillard, 2009). The first NP systems were developed in the early 1970s. Since then, they have been widely used in drug encapsulation and delivery (Fattal & Vauthier, 2007), with polymeric nanoparticles at the forefront of drug delivery because of their stability and easy modification (Singh & Lillard, 2009).

Chitosan nanoparticles have many advantages: low toxicity, enhanced biocompatibility, mucoadhesive character, stability, site-specific drug targeting, and enhanced drug therapeutic index. None of the less, some of its limitations include low solubility in neutral and alkaline pH, changes in intrinsic properties due to crosslinking, difficulties in controlling pore size, reduced mechanical resistance, and low encapsulation efficiency of hydrophobic drugs (Garg et al., 2019).

Particle size and size distribution determine the NP *in vivo* distribution, biological fate, toxicity, targeting ability, and drug loading/release efficiency and stability. Smaller NPs have greater cell uptake and faster release due to increased surface-area-to-volume ratio, but they present a greater risk of aggregation during storage, transport, and dispersion. In contrast, larger particles have greater drug encapsulation and slower release (Singh & Lillard, 2009).

NP surface charges determine how quickly they become cleared by the immune system. Coating NPs with hydrophilic polymers such as PEG reduces the surface charge interaction with blood components and increases drug circulation time by preventing opsonization and phagocytosis. The particle's zeta potential characterizes surface charge, and particles with zeta potential above ±30mV show reduced aggregation and greater stability (Singh & Lillard, 2009).

Chitosan NPs can be prepared using the polyelectrolyte complex method, microemulsion, covalent crosslinking, incorporation and incubation, coprecipitation, complex-coacervation, and the most common inotropic gelation (Table 1) (Chandra Hembram et al., 2016).

Table 1 *Methods of preparation of chitosan NPs and particle size. Adapted from (Chandra Hembram et al., 2016)*

Method	Nanoparticle Size
Polyelectrolyte complex	50-700nm
Inotropic gelation	Size can be optimized as required
Microemulsion	<100nm
Covalent crosslinking	Variable sizes can be produced
Incorporation and incubation	100-150nm
Solvent evaporation	50-300nm
Coprecipitation	<10nm
Complex-coacervation	It Varies depending on the anionic coacervate used

Chitosan in ocular delivery

Drug delivery to the eye's anterior surface presents many challenges, one of which is low bioavailability. Only 5% of drugs delivered by eye drops penetrate the corneal epithelium. In recent years, contact lenses have been designed to deliver medication to the eye's anterior surface to increase bioavailability. However, their use in the delivery of highly hydrophilic drugs continues to be a major challenge (Behl, Iqbal, O'Reilly, McLoughlin, & Fitzhenry, 2016). Chitosan nanoparticles have been successfully used to encapsulate highly hydrophilic drugs to increase bioavailability. For example, Behl et al. were able to enhance dexamethasone delivery,

a highly hydrophilic drug used to treat inflammation post-cataract surgery, by incorporating drug-loaded chitosan NPs into pHEMA contact lenses (2016).

Mucoadhesion is another valuable property that chitosan possesses, making it an ideal material for ocular drug delivery. The anterior surface of the eye contains mucins, a type of glycoprotein present in the eye mucosa. Mucins contain negative charges that can interact with the positive charges present in chitosan to increase drug residence time (Yu et al., 2020). Eye drops containing chitosan NPs have been developed to increase the effectiveness of traditional eye drops. Silva et al. investigated the mucoadhesive properties of a novel nanoparticle eye formulation using chitosan-hyaluronic acid for ocular delivery of ceftazidime. Their results indicate that the new formulation is stable, the drug is active after release, and the particles possess greater mucoadhesive properties (2017). Yu et al. were able to produce self-assembling dexamethasone-glycol chitosan NPs with good ocular tolerance and extended pre-corneal duration compared to traditional dexamethasone sodium phosphate formulation (2020). Acrylated chitosan nanoparticles with enhanced mucoadhesion for delivery through the mucosa were produced by grafting PEGDA to chitosan before NP synthesis, but their effectiveness was not tested in an ocular environment (Eliyahu et al., 2018).

As previously mentioned, chitosan contains glycosidic bonds that lysozymes can enzymatically break. Although lysozymes can be found in almost all mammalian secretions, such as milk and saliva, their highest concentration is found in tears (Hankiewicz & Swierczek, 1974; McDermott, 2013; Zahoor, Bahadar, Ayaz, Khan, & Shah, 2018). Lysozymes are produced and secreted by the lacrimal gland acinar cells at 1-3 mg/mL (Hanstock, Edwards, & Walsh, 2019) and can be used to degrade chitosan nanoparticles in the ocular environment for sustained drug release.

NP in cancer treatment

Considerable progress has been made in cancer research in the last decades. Current treatments include surgery, chemotherapy, radiation, cryoablation, hormone therapy, immunotherapy, and targeted drug therapy, with the latter being significantly promising. Although cancer survival has increased overall, many cancers continue to evade even the most advanced treatments (Zugazagoitia et al., 2016). For instance, chemotherapy which is the most used treatment lacks specificity and makes it nearly impossible to distinguish normal cells from cancerous ones. This unwarranted attack on healthy cells often results in patients feeling sicker due to the harsh side effects and sometimes even their demise. Moreover, some cancers are known for developing resistance to the medication over time, thus reducing the treatment's efficacy (Mehta, 2020; Zugazagoitia et al., 2016). Therefore, there is a great need to develop new compounds and delivery systems that are highly effective and target specific, and some promising candidates are fucoidan and nanoparticles.

One of the hallmarks of cancer is an increase in angiogenesis and vascularization at tumor sites. As highly vascularized tumor aggregates begin to form and increased vascular permeability increases, normal fluid transport is disrupted, leading to a phenomenon known as EPR effect, in which small particles accumulate in tumor tissue more than normal tissue (Singh & Lillard, 2009). Because of the EPR effect, NPs tend to accumulate at tumor sites, making them ideal drug vehicles for cancer treatment.

Chitosan in cancer treatment

Chitosan has been widely used in cancer treatment because it has been found to exert anticancer activity with minimal toxicity to normal cells, but its use as a therapeutic agent is hindered by poor solubility (Adhikari & Yadav, 2018). At The Same Time, its anticancerous properties are dependent on molecular weight and degree of deacetylation (Nawaz & Wong,

2020). The increased antitumor activity of low molecular weight chitosan is well established and has been extensively reported in the literature (Maeda & Kimura, 2004; Qin, Du, Xiao, Li, & Gao, 2002). Chitosan has shown cytotoxic activity in a dose-dependent toward hepatocellular carcinoma cells (Hep2), rhabdomyosarcoma (RD), T24 human urinary bladder cancer cell line, and breast cancer cell lines such as MCF-7 and MDA-MB-231 (Nawaz & Wong, 2020).

By chemically modifying chitosan, scientists have synthesized chitosan derivatives with enhanced solubility and biological activity, such as sulfated chitosans and chitosan-metal complexes (Adhikari & Yadav, 2018). Chitosan-metal complexes with enhanced antitumor properties have been developed since the early 2000s, but metals' intrinsic potential to be toxic to humans has hindered their clinical use. None of the less, Zheng et al. were able to synthesize a chitosan-copper complex that selectively inhibits proliferation and enhances cytotoxicity toward 293 and HeLa cells (2006), while Wang et al. used a chitosan-zinc complex to inhibit the growth of SMMC-7721 cell lines in vitro (2009).

In summary, most researchers have focused on using chitosan as a nanoparticle for cancer drug delivery because it combines the inherent chitosan anticancerous properties with the higher selectivity, reduced toxicity, longer clearance times, and increased efficacy of nanoparticles (Nawaz & Wong, 2020). Additionally, chitosan nanoparticles are easily synthesized to yield particles with long blood circulation times and low uptake by the reticuloendothelial system due to their smaller size.

Chitosan in breast cancer treatment

Chitosan derivatives and chitosan-based nanogels have been developed for breast cancer treatment. Chitosan derivatives have been shown to have cytotoxic effects against MCF-7 cells by inhibiting proliferation, inducing apoptosis, blocking ERK phosphorylation, and chitosan oligosaccharides have been shown to suppress metastasis in MDA-MB-231 cells (M.

JIANG et al., 2011; Nam & Shon, 2009). Likewise, chitosan-based nanogel containing hydroxycamptothecin showed greater inhibition to the proliferation of breast cancer cells *in vitro* than the free drug (Guo et al., 2019).

Fucoidan in cancer treatment

In the last couple of decades, there was a surge in research using naturally occurring polysaccharides with anticancer activity and low toxicity to treat breast cancer. The rise in research of polysaccharide derived from algae in cancer treatment is due to their high availability and bioactivity properties (Boisson-vidal et al., 1995; Moussavou et al., 2014; Noda, Amano, Arashima, & Nisizawa, 1990; Reys et al., 2016; Teas, Vena, Cone, & Irhimeh, 2013). For instance, brown seaweed is the second most abundant seaweed (Davis, Volesky, & Mucci, 2003) and contains various fucose components that can be used in cancer drug development and cosmetics, functional food, and other pharmaceutical business (Wijesinghe & Jeon, 2012).

Fucoidan (FU) is a sulfated polysaccharide isolated from the cell wall and intercellular spaces of brown seaweeds (Lu et al., 2018) such as *Fucus vesiculosus*, *Sargassum stenophyllum*, *Chorda filum*, *Ascophyllum nodosum*, *Dictyota menstrualis*, *Fucus evanescens*, *Fucus serratus*, *Fucus distichus*, *Caulerpa racemosa*, *Hizikia fusiforme*, *Padina gymnospora*, *Kjellmaniella crassifolia*, *Analipus japonicus*, *Laminaria hyperborean*, *Ecklonia kurome*, and *Undaria pinnatitinda* (Aisha Abudabbus, 2017; Kim, Lee, & Lee, 2010). The FU structure comprises L-fucose, sulfate groups, and one or more small proportions of xylose, mannose, galactose, rhamnose, arabinose, glucose, glucuronic acid, and acetyl groups in a variety of brown algae (Aisha Abudabbus, 2017).

The structure of FU varies among species and can be classified by two types of homofucose: type (I) contains repeated (1→3)-l-fucopyranose, and type (II) contains alternating and repeated (1→3)- and (1→4)-l-fucopyranose (Figure 12). This variation in the backbone

structure, the degree, and the pattern of sulfated branches result in different bioactivity among various species (Patankar, Oehninger, Barnett, Williams, & Clark, 1993; Zorofchian Moghadamtousi et al., 2014).

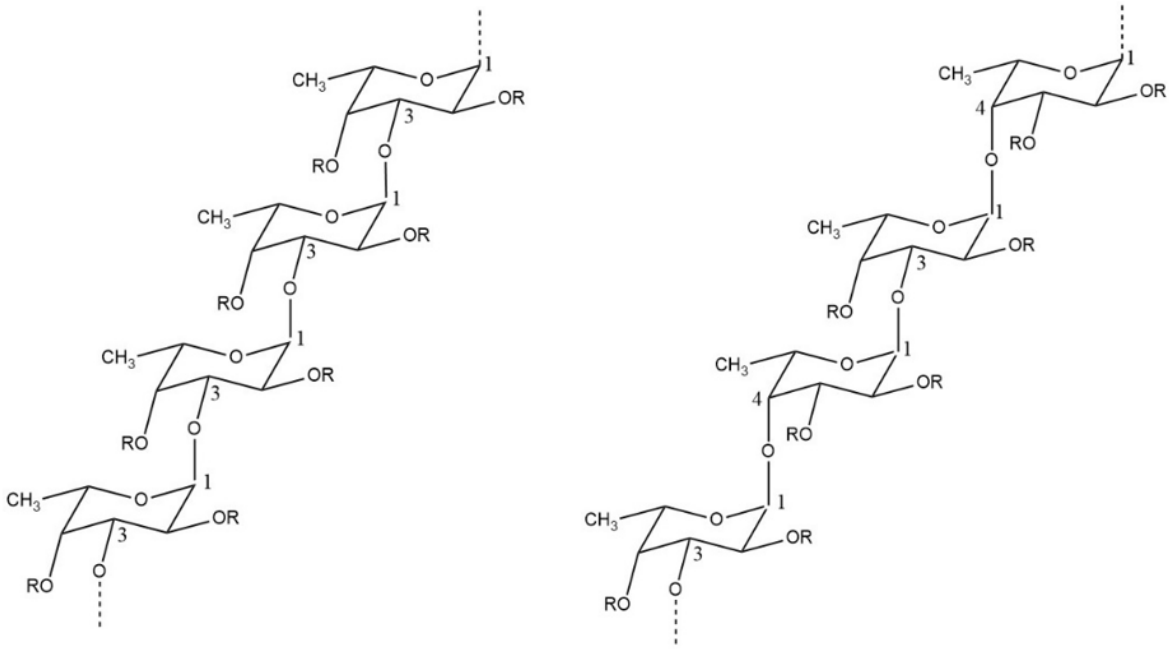

Figure 11 *Fucoidan structure.* ***a)*** *Type I structure and* ***b)*** *Type II structure.*

FU has been shown to have a plethora of medicinal properties, which include anticoagulant, antithrombotic, antitumor, immunomodulation, anticancer, antiproliferative, antivirus, antioxidant, and blood lipid reducing activities (Cumashi et al., 2007; Koyanagi, Tanigawa, Nakagawa, Soeda, & Shimeno, 2003; B. Li, Lu, Wei, & Zhao, 2008; Wijesinghe & Jeon, 2012). FU safety has been assessed *in vitro* and *in vivo*, and no toxic effects were observed regardless of source and acute or chronic exposure (Kim et al., 2010).

Although FU has been successfully used in treating various cancers *in vitro* and *in vivo*, its clinical use has not been approved by the Food and Drug Administration. There are currently three clinical trials using FU. Two clinical trials are assessing its safety as a supplemental therapy for advanced hepatocellular carcinoma (ClinicalTrials.gov, Identifier: NCT04066660)

and as a dietary supplement in addition to chemotherapy on quality of life (ClinicalTrials.gov, Identifier: NCT03130829), and a third one is assessing the safety of radiolabeled fucoidan as a non-invasive imaging agent (ClinicalTrails.gov, Identifier: NCT03422055).

Fucoidan in breast cancer treatment

However, many factors play a role in FU bioactivity toward cancer cells, from structure to purification methods. FU is highly heterogenic, and molecular weight, sulfate content, sugar composition can adversely affect its antitumor properties. Regarding antitumor activity, lower molecular weight, high sulfate content, and structure branching yield greater toxicity toward breast cancer cell lines (Lu et al., 2018; Oliveira et al., 2017). Bioactivity can also be affected depending on the extraction and purification methods used by reducing sulfate content and removing other compounds that enhance activity, such as uronic acid, proteins, and other components found in crude FU (Mak et al., 2014; Zayed et al., 2019). Additionally, other studies also indicate harvest time to play a significant role in antitumor activity (Lu et al., 2018; Skriptsova, Shevchenko, Zvyagintseva, & Imbs, 2009; Zvyagintseva et al., 2003).

In vitro studies using low molecular weight FU has been shown to inhibit the proliferation of breast cancer cell lines MCF-7 and MDA-MB-231 while normal cells remain unaffected (A. Abudabbus, Badmus, Shalaweh, Bauer, & Hiss, 2017; Wu, Yan, Wu, Yuan, & Liu, 2016; Zhang, Teruya, Eto, & Shirahata, 2011). Although there have been no clinical trials examining the safety and efficacy of FU in the treatment of breast cancer in the United States, an Australian study showed no adverse drug interactions when FU is taken concomitantly with letrozole and tamoxifen. In the study, breast cancer patients orally ingested a 500 mg capsule of Maritech extract containing 88.9% FU in the morning and at night after food (Tocaciu et al., 2018).

References

. (2011). Retrieved from https://www.nih.gov/news-events/videos/nih-mission-its-about-life#:~:text=NIH's%20mission%20is%20to%20seek,burdens%20of%20illness%20and%20disability.

Abhang, P., Momin, M., Inamdar, M., & Kar, S. (2014). Transmucosal Drug Delivery- An Overview. *Drug Delivery Letters, 4*(1), 26-37. doi:10.2174/2210303111303999011

Abudabbus, A. (2017). *Effects of Fucoidan and Chemotherapeutic Agent Combinations on Malignant and Non-malignant Breast Cell Lines.* (PhD), University of the Western Cape, South Africa. Retrieved from https://dx.doi.org/10.2174/138920101866617111515112 (3262823)

Abudabbus, A., Badmus, J. A., Shalaweh, S., Bauer, R., & Hiss, D. (2017). Effects of Fucoidan and Chemotherapeutic Agent Combinations on Malignant and Non-malignant Breast Cell Lines. *Curr Pharm Biotechnol, 18*(9), 748-757. doi:10.2174/138920101866617111515112

Adhikari, H. S., & Yadav, P. N. (2018). Anticancer Activity of Chitosan, Chitosan Derivatives, and Their Mechanism of Action. *Int J Biomater, 2018*, 2952085. doi:10.1155/2018/2952085

Ahmadi, F., Oveisi, Z., Samani, S. M., & Amoozgar, Z. (2015). Chitosan based hydrogels: characteristics and pharmaceutical applications. *Res Pharm Sci, 10*(1), 1-16.

Alkilani, A., McCrudden, M. T., & Donnelly, R. (2015). Transdermal Drug Delivery: Innovative Pharmaceutical Developments Based on Disruption of the Barrier Properties of the Stratum Corneum. *Pharmaceutics, 7*(4), 438-470. doi:10.3390/pharmaceutics7040438

Amsden, B. (2016). Photo-Crosslinking Methods to Design Hydrogels. In *Gels Handbook* (pp. 201-218).

Anitha, A., Rejinold, N. S., Bumgardner, J. D., Nair, S. V., & Jayakumar, R. (2012). Approaches for Functional Modification or Cross-linking of Chitosan. In B. Sarmento & J. d. Neves (Eds.), *Chitosan-Based Systems for Biopharmaceuticals*.

Asfour, M. H. (2021). Advanced trends in protein and peptide drug delivery: a special emphasis on aquasomes and microneedles techniques. *Drug Deliv Transl Res, 11*(1), 1-23. doi:10.1007/s13346-020-00746-z

Bai, X., Bao, Z., Bi, S., Li, Y., Yu, X., Hu, S., . . . Chen, X. (2018). Chitosan-Based Thermo/pH Double Sensitive Hydrogel for Controlled Drug Delivery. *Macromol Biosci, 18*(3). doi:10.1002/mabi.201700305

Behl, G., Iqbal, J., O'Reilly, N. J., McLoughlin, P., & Fitzhenry, L. (2016). Synthesis and Characterization of Poly(2-hydroxyethylmethacrylate) Contact Lenses Containing Chitosan Nanoparticles as an Ocular Delivery System for Dexamethasone Sodium Phosphate. *Pharm Res, 33*(7), 1638-1648. doi:10.1007/s11095-016-1903-7

Boisson-vidal, C., Haroun, F., Ellouali, M., Blondin, C., Fischer, A. M., Agostini, A. d., & Jozefonvicz, J. (1995). Biological activities of polysaccharides from marine algae - Review article. *Drugs of the Future, 20*, 1237-1249.

Catoira, M. C., Fusaro, L., Di Francesco, D., Ramella, M., & Boccafoschi, F. (2019). Overview of natural hydrogels for regenerative medicine applications. *Journal of Materials Science: Materials in Medicine, 30*(10). doi:10.1007/s10856-019-6318-7

Chandra Hembram, K., Prabha, S., Chandra, R., Ahmed, B., & Nimesh, S. (2016). Advances in preparation and characterization of chitosan nanoparticles for therapeutics. *Artificial Cells, Nanomedicine, and Biotechnology, 44*(1), 305-314. doi:10.3109/21691401.2014.948548

Choi, J. R., Yong, K. W., Choi, J. Y., & Cowie, A. C. (2019). Recent advances in photo-crosslinkable hydrogels for biomedical applications. *BioTechniques, 66*(1), 40-53. doi:10.2144/btn-2018-0083

Cumashi, A., Ushakova, N. A., Preobrazhenskaya, M. E., D'Incecco, A., Piccoli, A., Totani, L., . . . Nifantiev, N. E. (2007). A comparative study of the anti-inflammatory, anticoagulant, antiangiogenic, and antiadhesive activities of nine different fucoidans from brown seaweeds. *Glycobiology, 17*(5), 541-552. doi:10.1093/glycob/cwm014

Davis, T. A., Volesky, B., & Mucci, A. (2003). A review of the biochemistry of heavy metal biosorption by brown algae. *Water Res, 37*(18), 4311-4330. doi:10.1016/s0043-1354(03)00293-8

Deepthi, S., & Jose, J. (2019). Novel hydrogel-based ocular drug delivery system for the treatment of conjunctivitis. *Int Ophthalmol, 39*(6), 1355-1366. doi:10.1007/s10792-018-0955-6

Divya, K., & Jisha, M. S. (2017). Chitosan nanoparticles preparation and applications. *Environmental Chemistry Letters, 16*(1), 101-112. doi:10.1007/s10311-017-0670-y

Eliyahu, S., Aharon, A., & Bianco-Peled, H. (2018). Acrylated Chitosan Nanoparticles with Enhanced Mucoadhesion. *Polymers (Basel), 10*(2). doi:10.3390/polym10020106

Fattal, E., & Vauthier, C. (2007). Drug delivery: Nanoparticles. In J. Swarbrick (Ed.), *Encyclopedia of Pharmaceutical Technology* (3 ed., Vol. 2, pp. 1183). Pinehurst, North Carolinia, USA: PharmaceuTech, Inc.

Gao, Y., Zhang, W., Cheng, Y. F., Cao, Y., Xu, Z., Xu, L. Q., . . . Xue, P. (2021). Intradermal administration of green synthesized nanosilver (NS) through film-coated PEGDA microneedles for potential antibacterial applications. *Biomaterials science*. doi:10.1039/d0bm02136a

Garg, U., Chauhan, S., Nagaich, U., & Jain, N. (2019). Current Advances in Chitosan Nanoparticles Based Drug Delivery and Targeting. *Advanced Pharmaceutical Bulletin, 9*(2), 195-204. doi:10.15171/apb.2019.023

Gaudana, R., Ananthula, H. K., Parenky, A., & Mitra, A. K. (2010). Ocular drug delivery. *AAPS J, 12*(3), 348-360. doi:10.1208/s12248-010-9183-3

Gulledge, B. M., Aggen, J. B., & Chamberlin, A. R. (2003). Linearized and truncated microcystin analogues as inhibitors of protein phosphatases 1 and 2A. *13*(17), 2903-2906. doi:10.1016/s0960-894x(03)00589-4

Guo, H., Li, F., Qiu, H., Zheng, Q., Yang, C., Tang, C., & Hou, Y. (2019). Chitosan-Based Nanogel Enhances Chemotherapeutic Efficacy of 10-Hydroxycamptothecin against Human Breast Cancer Cells. *International Journal of Polymer Science, 2019*, 1914976. doi:10.1155/2019/1914976

Gyles, D. A., Castro, L. D., Silva, J. O. C., & Ribeiro-Costa, R. M. (2017). A review of the designs and prominent biomedical advances of natural and synthetic hydrogel formulations. *European Polymer Journal, 88*, 373-392. doi:10.1016/j.eurpolymj.2017.01.027

Hankiewicz, J., & Swierczek, E. (1974). Lysozyme in human body fluids. *Clinica Chimica Acta, 57*(3), 205-209. doi:10.1016/0009-8981(74)90398-2

Hanstock, H. G., Edwards, J. P., & Walsh, N. P. (2019). Tear Lactoferrin and Lysozyme as Clinically Relevant Biomarkers of Mucosal Immune Competence. *Frontiers in Immunology, 10*. doi:10.3389/fimmu.2019.01178

Hoare, T. R., & Kohane, D. S. (2008). Hydrogels in drug delivery: Progress and challenges. *Polymer, 49*(8), 1993-2007. doi:10.1016/j.polymer.2008.01.027

Ibrahim, H. M., & El-Zairy, E. M. R. (2015). Chitosan as a Biomaterial — Structure, Properties, and Electrospun Nanofibers. In: InTech.

Jia, J., Coyle, R. C., Richards, D. J., Berry, C. L., Barrs, R. W., Biggs, J., . . . Mei, Y. (2016). Development of peptide-functionalized synthetic hydrogel microarrays for stem cell and tissue engineering applications. *Acta Biomaterialia, 45*, 110-120. doi:10.1016/j.actbio.2016.09.006

JIANG, M., OUYANG, H., RUAN, P., ZHAO, H., PI, Z., HUANG, S., . . . CREPIN, M. (2011). Chitosan Derivatives Inhibit Cell Proliferation and Induce Apoptosis in Breast Cancer Cells. *Anticancer Research, 31*(4), 1321-1328.

Jiang, S., Liu, S., & Feng, W. (2011). PVA hydrogel properties for biomedical application. *J Mech Behav Biomed Mater, 4*(7), 1228-1233. doi:10.1016/j.jmbbm.2011.04.005

Kim, K. J., Lee, O. H., & Lee, B. Y. (2010). Fucoidan, a sulfated polysaccharide, inhibits adipogenesis through the mitogen-activated protein kinase pathway in 3T3-L1 preadipocytes. *Life Sci, 86*(21-22), 791-797. doi:10.1016/j.lfs.2010.03.010

Kopecek, J. (2007). Hydrogel biomaterials: a smart future? *Biomaterials, 28*(34), 5185-5192. doi:10.1016/j.biomaterials.2007.07.044

Koyanagi, S., Tanigawa, N., Nakagawa, H., Soeda, S., & Shimeno, H. (2003). Oversulfation of fucoidan enhances its anti-angiogenic and antitumor activities. *Biochem Pharmacol, 65*(2), 173-179. doi:10.1016/s0006-2952(02)01478-8

Lee, I. C., He, J. S., Tsai, M. T., & Lin, K. C. (2015). Fabrication of a novel partially dissolving polymer microneedle patch for transdermal drug delivery. *J Mater Chem B, 3*(2), 276-285. doi:10.1039/c4tb01555j

Lee, S. C., Kwon, I. K., & Park, K. (2013). Hydrogels for delivery of bioactive agents: A historical perspective. *Advanced Drug Delivery Reviews, 65*(1), 17-20. doi:10.1016/j.addr.2012.07.015

Li, B., Lu, F., Wei, X., & Zhao, R. (2008). Fucoidan: structure and bioactivity. *Molecules, 13*(8), 1671-1695. doi:10.3390/molecules13081671

Li, J. K., Wang, N., & Wu, X. S. (1998). Poly(vinyl alcohol) nanoparticles prepared by freezing–thawing process for protein/peptide drug delivery. *Journal of Controlled Release, 56*(1-3), 117-126. doi:10.1016/s0168-3659(98)00089-3

Liang, Y., Zhao, X., Ma, P. X., Guo, B., Du, Y., & Han, X. (2019). pH-responsive injectable hydrogels with mucosal adhesiveness based on chitosan-grafted-dihydrocaffeic acid and oxidized pullulan for localized drug delivery. *Journal of Colloid and Interface Science, 536*, 224-234. doi:10.1016/j.jcis.2018.10.056

Lim, W. S., Chen, K., Chong, T. W., Xiong, G. M., Birch, W. R., Pan, J., . . . Huang, Y. (2018). A bilayer swellable drug-eluting ureteric stent: Localized drug delivery to treat urothelial diseases. *Biomaterials, 165*, 25-38. doi:10.1016/j.biomaterials.2018.02.035

Lu, J., Shi, K., Chen, S., Wang, J., Hassouna, A., White, L., . . . Nie, S. (2018). Fucoidan Extracted from the New Zealand Undaria pinnatifida—Physicochemical Comparison against Five Other Fucoidans: Unique Low Molecular Weight Fraction Bioactivity in Breast Cancer Cell Lines. *Marine Drugs, 16*(12), 461. doi:10.3390/md16120461

Maeda, Y., & Kimura, Y. (2004). Antitumor effects of various low-molecular-weight chitosans are due to increased natural killer activity of intestinal intraepithelial lymphocytes in sarcoma 180-bearing mice. *J Nutr, 134*(4), 945-950. doi:10.1093/jn/134.4.945

Mak, W., Wang, S. K., Liu, T., Hamid, N., Li, Y., Lu, J., & White, W. L. (2014). Anti-Proliferation Potential and Content of Fucoidan Extracted from Sporophyll of New Zealand Undaria pinnatifida. *Frontiers in Nutrition, 1*. doi:10.3389/fnut.2014.00009

Maulvi, F. A., Soni, T. G., & Shah, D. O. (2016). A review on therapeutic contact lenses for ocular drug delivery. *Drug Deliv, 23*(8), 3017-3026. doi:10.3109/10717544.2016.1138342

McAvoy, K., Jones, D., & Thakur, R. R. S. (2018). Synthesis and Characterisation of Photocrosslinked poly(ethylene glycol) diacrylate Implants for Sustained Ocular Drug Delivery. *Pharm Res, 35*(2), 36. doi:10.1007/s11095-017-2298-9

McDermott, A. M. (2013). Antimicrobial compounds in tears. *Experimental Eye Research, 117*, 53-61. doi:10.1016/j.exer.2013.07.014

Mehta, A. (2020). *Advances in Cyanobacterial Biology*.

Moussavou, G., Kwak, D., Obiang-Obonou, B., Maranguy, C., Dinzouna-Boutamba, S.-D., Lee, D., . . . Choo, Y. (2014). Anticancer Effects of Different Seaweeds on Human Colon and Breast Cancers. *Marine Drugs, 12*(9), 4898-4911. doi:10.3390/md12094898

Mutlu, Z., Shams Es-Haghi, S., & Cakmak, M. (2019). Recent Trends in Advanced Contact Lenses. *Adv Healthc Mater, 8*(10), e1801390. doi:10.1002/adhm.201801390

Nagpal, K., Singh, S. K., & Mishra, D. N. (2010). Chitosan Nanoparticles: A Promising System in Novel Drug Delivery. *Chemical and Pharmaceutical Bulletin, 58*(11), 1423-1430. doi:10.1248/cpb.58.1423

Nam, K. S., & Shon, Y. H. (2009). Suppression of metastasis of human breast cancer cells by chitosan oligosaccharides. *J Microbiol Biotechnol, 19*(6), 629-633. doi:10.4014/jmb.0811.603

Nawaz, A., & Wong, T. W. (2020). Chitosan as Anticancer Compound and Nanoparticulate Matrix for Cancer Therapeutics. In *Encyclopedia of Marine Biotechnology* (pp. 1737-1752).

Nkhwa, S., Lauriaga, K. F., Kemal, E., & Deb, S. (2014). Poly(vinyl alcohol): Physical Approaches to Designing Biomaterials for Biomedical Applications. *Conference Papers in Science, 2014*, 1-7. doi:10.1155/2014/403472

Noda, H., Amano, H., Arashima, K., & Nisizawa, K. (1990). Antitumor activity of marine algae. *Hydrobiologia, 204*(1), 577-584. doi:10.1007/BF00040290

Nuttelman, C. R., Mortisen, D. J., Henry, S. M., & Anseth, K. S. (2001). Attachment of fibronectin to poly(vinyl alcohol) hydrogels promotes NIH3T3 cell adhesion, proliferation, and migration. *Journal of Biomedical Materials Research, 57*(2), 217-223. doi:10.1002/1097-4636(200111)57:2<217::Aid-jbm1161>3.0.Co;2-i

O'Donnell, K., Boyd, A., & Meenan, B. J. (2019). Controlling Fluid Diffusion and Release through Mixed-Molecular-Weight Poly(ethylene) Glycol Diacrylate (PEGDA) Hydrogels. *Materials (Basel), 12*(20). doi:10.3390/ma12203381

Oliveira, C., Ferreira, A. S., Novoa-Carballal, R., Nunes, C., Pashkuleva, I., Neves, N. M., . . . Silva, T. H. (2017). The Key Role of Sulfation and Branching on Fucoidan Antitumor Activity. *Macromolecular Bioscience, 17*(5), 1600340. doi:10.1002/mabi.201600340

Panahi, Y., Gharekhani, A., Hamishehkar, H., Zakeri-Milani, P., & Gharekhani, H. (2019). Stomach-Specific Drug Delivery of Clarithromycin Using aSemi Interpenetrating Polymeric Network Hydrogel Made ofMontmorillonite and Chitosan: Synthesis, Characterization and InVitro Drug Release Study. *Advanced Pharmaceutical Bulletin, 9*(1), 159-173. doi:10.15171/apb.2019.019

Patankar, M. S., Oehninger, S., Barnett, T., Williams, R. L., & Clark, G. F. (1993). A revised structure for fucoidan may explain some of its biological activities. *J Biol Chem, 268*(29), 21770-21776.

Patel, A. V., & Shah, B. N. (2018). Transdermal Drug Delivery System: a Review. *Pharma Science Monitor, 9*(1), 378-390.

Peppas, N. A., & Mongia, N. K. (1997). Ultrapure poly(vinyl alcohol) hydrogels with mucoadhesive drug delivery characteristics. *European Journal of Pharmaceutics and Biopharmaceutics, 43*(1), 51–58. doi:10.1016/s0939-6411(96)00010-0

Peppas, N. A., & Simmons, R. E. P. (2004). Mechanistic analysis of protein delivery from porous poly(vinyl alcohol) systems. *Journal of Drug Delivery Science and Technology, 14*(4), 285-289.

Qin, C., Du, Y., Xiao, L., Li, Z., & Gao, X. (2002). Enzymic preparation of water-soluble chitosan and their antitumor activity. *Int J Biol Macromol, 31*(1-3), 111-117. doi:10.1016/s0141-8130(02)00064-8

Rastogi, V., & Yadav, P. (2012). Transdermal drug delivery system: An overview. *Asian Journal of Pharmaceutics, 6*(3). doi:10.4103/0973-8398.104828

Reys, L. L., Silva, S. S., Soares da Costa, D., Oliveira, N. M., Mano, J. F., Reis, R. L., & Silva, T. H. (2016). Fucoidan Hydrogels Photo-Cross-Linked with Visible Radiation As Matrices for Cell Culture. *ACS Biomaterials Science & Engineering, 2*(7), 1151-1161. doi:10.1021/acsbiomaterials.6b00180

Reza Rezaie, H., Esnaashary, M., Aref arjmand, A., & Öchsner, A. (2018). The History of Drug Delivery Systems. In *A Review of Biomaterials and Their Applications in Drug Delivery* (pp. 1-8).

Rosen, H., & Abribat, T. (2005). The rise and rise of drug delivery. *Nat Rev Drug Discov, 4*(5), 381-385. doi:10.1038/nrd1721

Salatin, S., & Yari Khosroushahi, A. (2017). Overviews on the cellular uptake mechanism of polysaccharide colloidal nanoparticles. *Journal of Cellular and Molecular Medicine, 21*(9), 1668-1686. doi:10.1111/jcmm.13110

Shikha, S., Zheng, X., & Zhang, Y. (2018). Upconversion Nanoparticles-Encoded Hydrogel Microbeads-Based Multiplexed Protein Detection. *Nano-Micro Letters, 10*(2). doi:10.1007/s40820-017-0184-y

Silva, M., Calado, R., Marto, J., Bettencourt, A., Almeida, A., & Gonçalves, L. (2017). Chitosan Nanoparticles as a Mucoadhesive Drug Delivery System for Ocular Administration. *Marine Drugs, 15*(12), 370. doi:10.3390/md15120370

Singh, R., & Lillard, J. W., Jr. (2009). Nanoparticle-based targeted drug delivery. *Exp Mol Pathol, 86*(3), 215-223. doi:10.1016/j.yexmp.2008.12.004

Skriptsova, A. V., Shevchenko, N. M., Zvyagintseva, T. N., & Imbs, T. I. (2009). Monthly changes in the content and monosaccharide composition of fucoidan from Undaria pinnatifida (Laminariales, Phaeophyta). *Journal of Applied Phycology, 22*(1), 79-86. doi:10.1007/s10811-009-9438-5

Soriente, A., Amodio, S. P., Fasolino, I., Raucci, M. G., Demitri, C., Engel, E., & Ambrosio, L. (2021). Chitosan/PEGDA based scaffolds as bioinspired materials to control in vitro angiogenesis. *Mater Sci Eng C Mater Biol Appl, 118*, 111420. doi:10.1016/j.msec.2020.111420

Stillman, Z., Jarai, B. M., Raman, N., Patel, P., & Fromen, C. A. (2020). Degradation profiles of poly(ethylene glycol)diacrylate (PEGDA)-based hydrogel nanoparticles. *Polymer Chemistry, 11*(2), 568-580. doi:10.1039/c9py01206k

Sun, Q.-B., Xu, C.-P., Li, W.-Q., Meng, Q.-J., & Qu, H.-Z. (2021). Halloysites modified polyethylene glycol diacrylate/thiolated chitosan double network hydrogel combined with BMP-2 for rat skull regeneration. *Artificial Cells, Nanomedicine, and Biotechnology, 49*(1), 71-82. doi:10.1080/21691401.2020.1858845

Swindle-Reilly, K., McLean, R. M., Jiang, P., Torres Flores, T. C., Jacobs, K. M., Reilly, M. A., . . . Tram, N. K. (2020). Methods to Improve Vitamin C Stability in Hydrogel Vitreous Substitutes to Prevent Cataract. *Investigative Ophthalmology & Visual Science, 61*, 3726-3726.

Tan, F., Xu, X., Deng, T., Yin, M., Zhang, X., & Wang, J. (2012). Fabrication of positively charged poly(ethylene glycol)-diacrylate hydrogel as a bone tissue engineering scaffold. *Biomed Mater, 7*(5), 055009. doi:10.1088/1748-6041/7/5/055009

Teas, J., Vena, S., Cone, D. L., & Irhimeh, M. (2013). The consumption of seaweed as a protective factor in the etiology of breast cancer: proof of principle. *Journal of Applied Phycology, 25*(3), 771-779. doi:10.1007/s10811-012-9931-0

Thakur, R. R., Wang, Y., Soliman, K., Sonawane, R., & Jones, D. (2019). In situ forming photocrosslinked biodegradable implants for sustained delivery of proteins. *Investigative Ophthalmology & Visual Science, 60*(9), 3376-3376.

Thukral, D. K., Dumoga, S., Arora, S., Chuttani, K., & Mishra, A. K. (2014). Potential carriers of chemotherapeutic drugs: matrix based nanoparticulate polymeric systems. *Cancer Nanotechnol, 5*(1), 3. doi:10.1186/s12645-014-0003-9

Tocaciu, S., Oliver, L. J., Lowenthal, R. M., Peterson, G. M., Patel, R., Shastri, M., . . . Fitton, J. H. (2018). The Effect of Undaria pinnatifida Fucoidan on the Pharmacokinetics of Letrozole and Tamoxifen in Patients With Breast Cancer. *Integrative Cancer Therapies, 17*(1), 99-105. doi:10.1177/1534735416684014

Wang, H., Xia, Y., Liu, J., Ma, Z., Shi, Q., & Yin, J. (2020). Programmable release of 2-O-d-glucopyranosyl-l-ascorbic acid and heparin from PCL-based nanofiber scaffold for reduction of inflammation and thrombosis. *Materials Today Chemistry, 17*. doi:10.1016/j.mtchem.2020.100303

Wang, R.-M., He, N.-P., Song, P.-F., He, Y.-F., Ding, L., & Lei, Z.-Q. (2009). Preparation of nano-chitosan Schiff-base copper complexes and their anticancer activity. *Polymers for Advanced Technologies, 20*(12), 959-964. doi:https://doi.org/10.1002/pat.1348

Wang, X., Peng, Y., Pena, J., & Xing, J. (2021). Preparation of ultrasmall nanogels by facile emulsion-free photopolymerization at 532 nm. *Journal of Colloid and Interface Science, 582*, 711-719. doi:10.1016/j.jcis.2020.08.056

Warr, C., Valdoz, J. C., Bickham, B. P., Knight, C. J., Franks, N. A., Chartrand, N., . . . Cook, A. D. (2020). Biocompatible PEGDA Resin for 3D Printing. *ACS Appl Bio Mater, 3*(4), 2239-2244. doi:10.1021/acsabm.0c00055

Whistler, R. L. (1993). Chitin. In *Industrial Gums* (pp. 601-604).

Wichterle, O., & LÍM, D. (1960). Hydrophilic Gels for Biological Use. *Nature, 185*(4706), 117-118. doi:10.1038/185117a0

Wijesinghe, W. A., & Jeon, Y. J. (2012). Enzyme-assistant extraction (EAE) of bioactive components: a useful approach for recovery of industrially important metabolites from seaweeds: a review. *Fitoterapia, 83*(1), 6-12. doi:10.1016/j.fitote.2011.10.016

Wu, S.-Y., Yan, M.-D., Wu, A. T. H., Yuan, K. S.-P., & Liu, S. H. (2016). Brown Seaweed Fucoidan Inhibits Cancer Progression by Dual Regulation of mir-29c/ADAM12 and miR-17-5p/PTEN Axes in Human Breast Cancer Cells. *Journal of Cancer, 7*(15), 2408-2419. doi:10.7150/jca.15703

Yahia, L. (2015). History and Applications of Hydrogels. *Journal of Biomedical Sciencies, 04*(02). doi:10.4172/2254-609x.100013

Yang, Y., Chen, Q., Lin, J., Cai, Z., Liao, G., Wang, K., . . . Yu, Z. (2019). Recent Advance in Polymer Based Microspheric Systems for Controlled Protein and Peptide Delivery. *Curr Med Chem, 26*(13), 2285-2296. doi:10.2174/0929867326666190409130207

Ye, Y., Yu, J., Wen, D., Kahkoska, A. R., & Gu, Z. (2018). Polymeric microneedles for transdermal protein delivery. *Advanced Drug Delivery Reviews, 127*, 106-118. doi:10.1016/j.addr.2018.01.015

Yu, A., Shi, H., Liu, H., Bao, Z., Dai, M., Lin, D., . . . Wang, Y. (2020). Mucoadhesive dexamethasone-glycol chitosan nanoparticles for ophthalmic drug delivery. *Int J Pharm, 575*, 118943. doi:10.1016/j.ijpharm.2019.118943

Zahoor, M., Bahadar, H., Ayaz, M., Khan, A., & Shah, M. J. (2018). In vitro Study on the Antimicrobial Activity of Human Tears with Respect to Age. *Korean J Clin Lab Sci, 50*(2), 93-99.

Zalloum, H. M., & Mubarak, M. S. (2013). Chitosan and Chitosan Derivatives as Chelating Agents. In S. Thomas, N. Ninan, S. Mohan, & E. Francis (Eds.), *Advances in Materials Science* (Vol. 2, pp. 2-9): Apple Academic Press.

Zayed, A., Hahn, T., Finkelmeier, D., Burger-Kentischer, A., Rupp, S., Krämer, R., & Ulber, R. (2019). Phenomenological investigation of the cytotoxic activity of fucoidan isolated from Fucus vesiculosus. *Process Biochemistry, 81*, 182-187. doi:10.1016/j.procbio.2019.03.026

Zhang, Z., Teruya, K., Eto, H., & Shirahata, S. (2011). Fucoidan Extract Induces Apoptosis in MCF-7 Cells via a Mechanism Involving the ROS-Dependent JNK Activation and Mitochondria-Mediated Pathways. *PLoS One, 6*(11), e27441. doi:10.1371/journal.pone.0027441

Zheng, Y., Yi, Y., Qi, Y., Wang, Y., Zhang, W., & Du, M. (2006). Preparation of chitosan-copper complexes and their antitumor activity. *Bioorganic & Medicinal Chemistry Letters, 16*(15), 4127-4129. doi:10.1016/j.bmcl.2006.04.077

Zorofchian Moghadamtousi, S., Karimian, H., Khanabdali, R., Razavi, M., Firoozinia, M., Zandi, K., & Abdul Kadir, H. (2014). Anticancer and antitumor potential of fucoidan and fucoxanthin, two main metabolites isolated from brown algae. *ScientificWorldJournal, 2014*, 768323. doi:10.1155/2014/768323

Zugazagoitia, J., Guedes, C., Ponce, S., Ferrer, I., Molina-Pinelo, S., & Paz-Ares, L. (2016). Current Challenges in Cancer Treatment. *Clinical Therapeutics, 38*(7), 1551-1566. doi:10.1016/j.clinthera.2016.03.026

Zvyagintseva, T. N., Shevchenko, N. M., Chizhov, A. O., Krupnova, T. N., Sundukova, E. V., & Isakov, V. V. (2003). Water-soluble polysaccharides of some far-eastern brown seaweeds. Distribution, structure, and their dependence on the developmental conditions. *Journal of Experimental Marine Biology and Ecology, 294*(1), 1-13. doi:10.1016/s0022-0981(03)00244-2

Chapter 1

Chitosan-PEGDA nanoparticle for ocular delivery of gentamicin

Introduction

Bacterial infections of the eye affect approximately 6 million people and account for 1% of all primary care office visits in the US yearly (Shields & Sloane, 1991; Udeh, Schneider, & Ohsfeldt, 2008). The treatment often consists of ophthalmic antibiotic eyedrops or ointments (Azari & Barney, 2013; Morrow & Abbott, 1998). Although easily applied and convenient, eye drops are often inefficient drug delivery vehicles due to the rapid drug clearance through the canalicular drainage (Lanier et al., 2021). Upon contact with the eye, the drug diffuses into the cornea and conjunctiva, the latter being the preferential path due to its larger size and transported into the systemic circulation. Systemic uptake leads to side effects, and less than 5% of the drug reaching the anterior eye (Gaudana, Ananthula, Parenky, & Mitra, 2010; Nayak & Misra, 2018). Thus, requiring multiple applications and variations in drug mass reaching the targeted site, further reducing desired pharmacokinetic drug profiles.

Nanoparticle systems for targeted drug delivery have been shown to improve bioavailability by increasing drug residence time and sustained release. Chitosan nanoparticles are very promising because of their biocompatibility, low immunogenicity, low toxicity, antimicrobial, mucoadhesive properties, and ability to spontaneously form nanoparticles in the presence of tripolyphosphate (TPP) (Anand, Sathyapriya, Maruthupandy, & Hameedha Beevi, 2018; Barbosa, Coutinho, Costa Lima, & Reis, 2019; Chandra Hembram, Prabha, Chandra, Ahmed, & Nimesh, 2016; Desai, 2016; Monteiro et al., 2015). However, what makes chitosan an ideal polymer for sustained drug delivery at the eye's surface is its ability to form nanoparticles that the ocular enzyme lysozyme can degrade (Han, Nwe, Furuike, Tokura, & Tamura, 2012; Kim et al., 2018; Lončarević, Ivanković, Rogina, & Ye, 2017; Pangburn, Trescony, & Heller,

1982; Stokke, Varum, Holme, Hjerde, & Smidsrsd, 1995). Lysozymes are present in various body fluids, but their highest concentrations are found in human tears and range between ~1-3 mg/mL (Hankiewicz & Swierczek, 1974; McDermott, 2013). The enzyme can catalyze the hydrolysis of the β-(1→4)- glycosidic bonds of chitosan to release the contents stored inside the nanoparticle (Stokke et al., 1995). Furthermore, chitosan cationic nature can be used to increase drug residence time at the ocular surface by interacting with ocular mucins, negatively charged proteins present at the ocular surface epithelia (Abhang, Momin, Inamdar, & Kar, 2014; Collado-Gonzalez, Gonzalez Espinosa, & Goycoolea, 2019; Mantelli & Argüeso, 2008).

Unfortunately, gentamicin, an aminoglycoside antibiotic used to treat conjunctivitis, has low encapsulation efficiency into chitosan nanoparticles due to charge repellence between the positive charges of gentamicin and chitosan. Lu et al. successfully increased encapsulation of aminoglycosides into chitosan nanoparticles using counterions (2009). However, various poly(ethylene glycol) diacrylate (PEGDA) properties make it a better candidate for ocular delivery, including low immunogenicity, low toxicity, and biocompatibility (L. Huang et al., 2019; Y. C. Huang, Li, Chen, & Chen, 2016). Furthermore, PEGDA shares many of the same characteristics of its parent molecule poly(ethylene glycol) (PEG), which has been extensively used as a lubricating agent and main component in the treatment of dry eyes, a common symptom of conjunctivitis (Azari & Barney, 2013; Cohen, Martin, & Sall, 2013). Therefore PEGDA can be used as a non-ionic dispersing agent to increase drug encapsulation by shielding the charge interactions of chitosan and gentamicin while providing eye lubrication.

Methodology

Synthesis of chitosan nanoparticles

Prepared chitosan stock solution by diluting 50 mg of chitosan in 50 mL of 0.05% acetic acid (1mg/mL) stirred for two hours at 1000 rpm; tripolyphosphate (TPP) stock solution by

diluting 50 mg of TPP into 50 mL of DI water; and PEGDA stock solution by diluting 6.7 mL of PEGDA in 18.3 mL of DI water.

Chitosan nanoparticles (Cs NP)

Added 5 mL of 1 mg/mL chitosan into 2 mL of 1 mg/mL of TPP dropwise using a syringe pump set to 0.083 mL/min while stirring (1000 rpm) at room temperature. The solution continued to stir for an hour, followed by dialysis overnight. Next, the solution was centrifuged for one hour at 3750 rpm and four °C, and the opalescent top layer was collected.

Chitosan-Gentamicin nanoparticles (Cs-GtS NP)

Added 5 mg of gentamicin to 5 mL of 1 mg/mL chitosan dissolved in 0.05% acetic acid. Next, the solution was added into 2 mL of 1 mg/mL of TPP dropwise using a syringe pump set to 0.083 mL/min while stirring (1000 rpm) at room temperature. The solution continued to stir for an hour, followed by overnight dialysis. Next, the solution was centrifuged for one hour at 3750 rpm and 4°C, and the opalescent top layer was collected.

Chitosan-PEGDA-Gentamicin nanoparticles (Cs-PEGDA-GtS NP)

Added 5 mg of gentamicin to 5 mL of 1 mg/mL chitosan dissolved in 0.05% acetic acid, followed by adding 0.5 mL of PEGDA stock solution. Next, the PEGDA-Cs-GtS mixture was added dropwise using a syringe pump set to 0.083 mL/min with stirring to 2 mL of 1 mg/mL TPP. The solution was allowed to stir at room temperature for one hour before dialyzing overnight. Next, the solution was centrifuged for one hour at 3750 rpm and 4°C, and the opalescent top layer was collected.

Characterization of chitosan nanoparticles

FTIR of chitosan nanoparticles

Fourier-Transform Infrared Spectroscopy (FTIR) was used to identify the functional groups present in the nanoparticles after synthesis. One microliter of nanoparticle solution was

placed on the crystal and dried using nitrogen gas before the analysis. The samples' FTIR spectra were recorded in the 4000-400 cm^{-1} region with a spectra resolution of $4cm^{-1}$.

Morphology of chitosan nanoparticles

The scanning electron microscope (SEM) images were captured using a Philips XL30 environmental scanning electron microscope. Samples were placed on an SEM stub and sputter-coated with titanium for 120 seconds.

Transmission electron microscope (TEM) images were captures using a Titan 80-3000 TEM. Samples were dipped onto a TEM copper grid and allowed to dry at room temperature for 72 hours before analysis.

Dynamic light scattering (DLS) and zeta potential

DLS was used to establish particle size, zeta potential, and polydispersity index (PDI). Samples were sonicated for 5 min, followed by a 100X dilution (10 mL in 1000 mL aqueous solution of 10 mM NaCl). Diluted samples were sonicated again for 15 min immediately before analysis.

Encapsulation efficiency

UV-vis was used to detect the gentamicin concentration post-synthesis to determine the encapsulation efficiency. Ninhydrin can be used as a colorimetric reagent to detect the absorption of gentamicin. Colorimetric reagent stock was made by diluting 50 mg of ninhydrin in 10 mL of phosphate-buffered saline. Samples were centrifuged for 2 minutes at 1300 rpm. The supernatant was collected, and an equal amount of colorimetric reagent was added to the solution. The sample was incubated at 95°C for 15 minutes, followed by 10 minutes in an ice-cold water bath. Absorption was taken using Shimadzu's UV-vis spectrophotometer at 418 nm wavelength. Encapsulation efficiency was determined using the following Equation:

$$EE\ (\%) = \frac{GtS_{initial\ concentration} - GtS_{non-encapsulated}}{GtS_{initial\ concentration}}\ X\ 100$$

In vitro degradation studies

Chitosan nanoparticle lysozyme degradation

Chitosan nanoparticles were resuspended in 1 mL of 2 mg/mL lysozyme solution 24 hours with stirring at 37°C.

FTIR of chitosan nanoparticles post lysozyme degradation

Fourier Transform-Infrared spectroscopy (FTIR) was used to identify the functional groups present in the nanoparticles after lysozyme degradation. One microliter of the nanoparticle-lysozyme solution was placed on the crystal and dried using nitrogen gas before the analysis. The samples' FT-IR spectra were recorded in the 4000-400 cm^{-1} region with a spectra resolution of 4cm^{-1}.

Antimicrobial assay to assess gentamicin activity post-release

A single colony of *E. coli* was inoculated in 10 mL of LB media containing 10 µL of ampicillin overnight. Agar plates were coated with 100 µL of bacterial growth, and 200 µL of NP solution was dropped in the center of the plate and incubated overnight at 37°C.

ELISA assay to assess gentamicin activity post-release

MaxSignal® Gentamicin ELISA kit purchased from PerkinElmer, USA, was used to determine the gentamicin concentration post-release.

Results and Discussion

Nanoparticle characterization results

Nanoparticle FTIR

Fourier-transform infrared spectroscopy (FTIR) of chitosan nanoparticles was performed to establish the interactions between chitosan and PEGDA. Characteristic peaks of chitosan are also present in all three nanoparticles, including a broad band between 3250 and 3361 cm^{-1} due

to the stretching vibrations of O−H or N−H groups. The band at 1639 cm^{-1} is related to the vibrations of carbonyl bonds (C=O) (amide I) of O=C-NHR, while the peak at 1571 cm^{-1} corresponds to the bending of N−H bonds (amide II) (NH_2). Two peaks corresponding to the saccharide structure are seen at 895 cm^{-1} and 1150 cm^{-1}, the latter relating to the asymmetric C-O-C stretching associated with the glycosidic bonds, while the two broad peaks at 1030 and 1073 cm^{-1} relate to the C-O stretching vibrations in chitosan. The peak at 1530 cm^{-1} corresponds to C-H vibrations of the alkyl group and the peak at 1650 cm^{-1} to the C-N stretching from amide II.

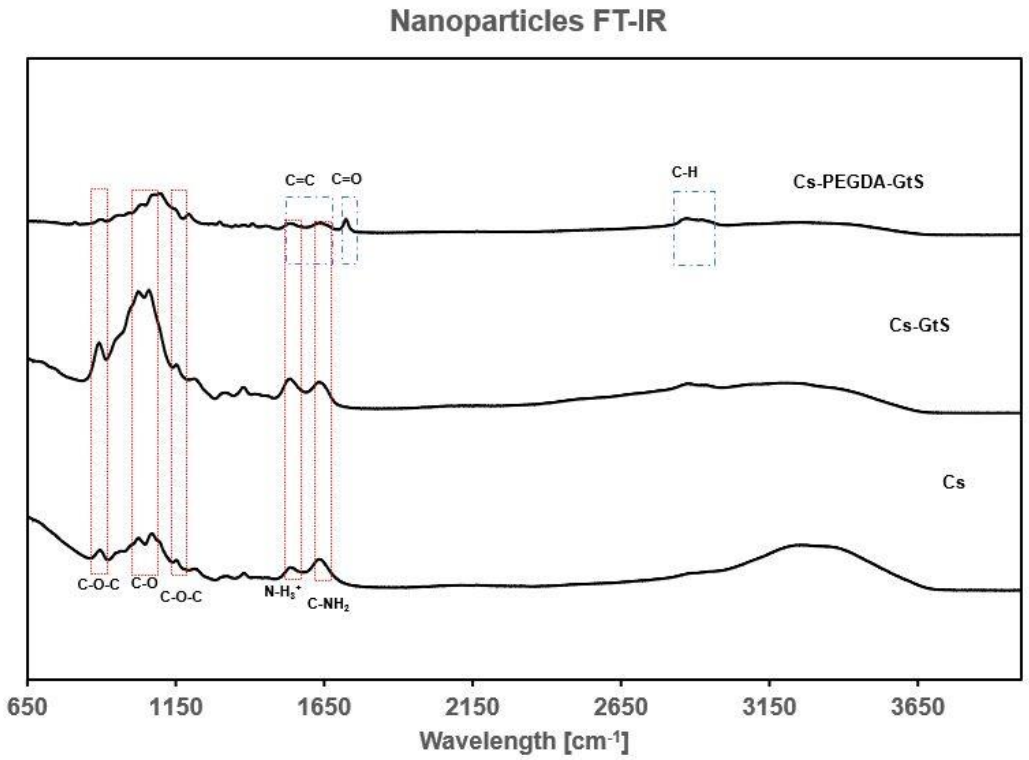

Figure 1.1 *FTIR spectrum region between 4000 and 650 cm^{-1}. Red chitosan associated peaks: peak 829 cm^{-1} C-O-C from the saccharide structure, two broad bands at 1030 and 1073 cm^{-1} due to C-O stretching, 1150 cm^{-1} peak from asymmetric C-O-C stretching of the glycosidic bonds, peak at 1571 cm^{-1} from N-H bending (amine) and 1650 cm^{-1} from C-N stretching (amide II). Blue PEGDA peaks: 1617 and 1641 cm^{-1} C=C asymmetric and symmetric stretching, respectively. Peak 1725 cm^{-1} C=O carbonyl group symmetric stretching and 2879 and 2931 cm^{-1}due to C-H stretching.*

PEGDA contains four characteristic peaks, one at 1725 cm^{-1} attributed to asymmetric stretching of C=O, two bands around 2879 and 2931 cm^{-1} due to C-H stretching, and vibrational bands at 1641 cm^{-1} (C=C symmetric stretching) and 1617 cm^{-1} (C=C asymmetric stretching). All characteristic peaks of PEGDA were present on the Cs-PEGDA-GtS spectra. However, most Cs-PEGDA-GtS peaks overlap with peaks present on chitosan except for the peak 1725 cm^{-1} which corresponds to a carbonyl group (C=O) symmetric stretching found in Cs-PEGDA-GtS and PEGDA spectra (Figure 1.1).

Morphological characterization

Transmission electron microscopy (TEM) was used for the morphological characterization of the nanoparticles (Figure 1.2). Cs-PEGDA-GtS particles were overall smaller, 4.5-7.3nm in size, and more homogeneous than Cs and Cs-GtS NPs. Cs-GtS showed the largest particles ranging from 4.9-14.9 nm.

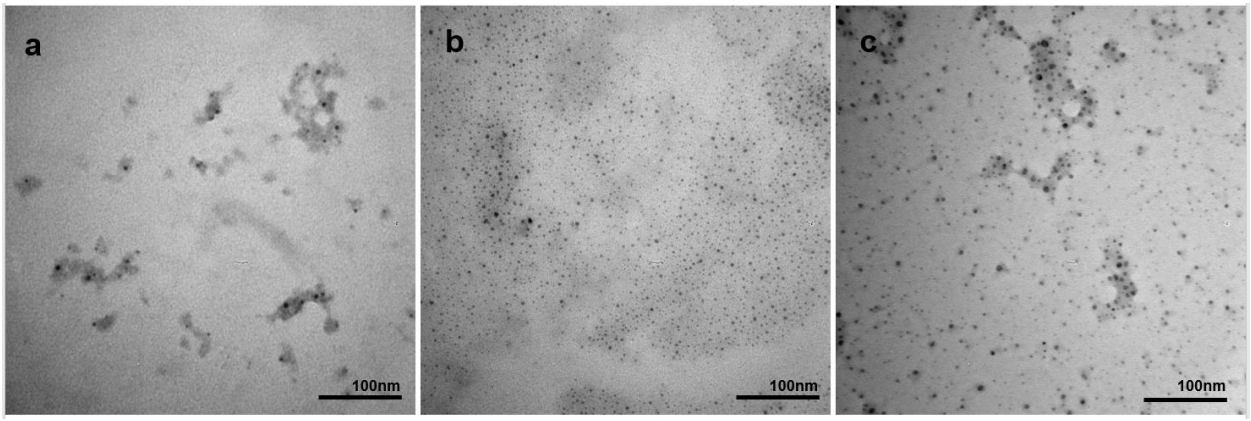

Figure 1.2 *TEM images of nanoparticles.* ***a)*** *chitosan* ***b)*** *Cs-PEGDA-GtS* ***c)*** *Cs-GtS nanoparticles at 300000X magnification.*

Dynamic Light Scattering (DLS)

DLS was used to determine particle size distribution, a zeta potential (ZP) analyzer to measure particle surface charge, and polydispersity index (PDI) to measure particle size distribution. ZP is used to estimate the surface charge of nanoparticles, which is indicative of the

particle's physical stability. Small ZP can result in particle aggregation due to van der Waals interparticle attraction. In general, NPs with ZP ranging from +30 mV to -30 mV display a high degree of stability. Perfectly uniform samples have a PDI of zero, while moderate polydisperse samples range from 0.1-0.4, and highly disperse samples have PDI's >0.4.

All particles had acceptable ZP, with Cs-PEGDA-GtS NP and Cs-GtS NP having a greater ZP than Cs NP. The increase in ZP can be explained by the encapsulation of GtS, which is positively charged in neutral pH, therefore increasing the positive overall surface charge of the cationic Cs NP. The addition of PEGDA increased the ZP by 0.34 mV compared to Cs-GtS, making the NP slightly more stable and more homogeneous with a PDI of 0.35±0.11. Even Though Cs-GtS NPs produced the smallest particles, the particles were highly polydisperse with sizes ranging from 225.54 to 404.58 nm (Table 1.1).

Altogether, the data shows that adding PEGDA during C-GtS NP synthesis produces more stable and homogeneous particles.

Table 1.1 *Dynamic light scattering was used to determine particle size distribution, zeta potential analyzer to measure particle surface charge, and PDI to measure sample size heterogeneity. All samples were analyzed in triplicates, and the averages were reported.*

	Z-average (nm)	Zeta Potential (mV)	Polydispersity Index
Cs-PEGDA-GtS NP	370.89 ± 44.68	20.14 ± 4.56	0.35 ± 0.11
Cs-GtS NP	315.06 ± 89.52	19.8 ± 2.9	0.48 ± 0.09
Cs NP	421.57 ± 18.83	16.06 ± 1.12	0.46 ± 0.08

Nanoparticle encapsulation efficiency

UV-vis spectroscopy was used for the detection of gentamicin post-NP synthesis to determine the drug encapsulation efficiency. Ninhydrin reacts with amines present in gentamicin to give Ruhemann's purple (Figure 1.3b).

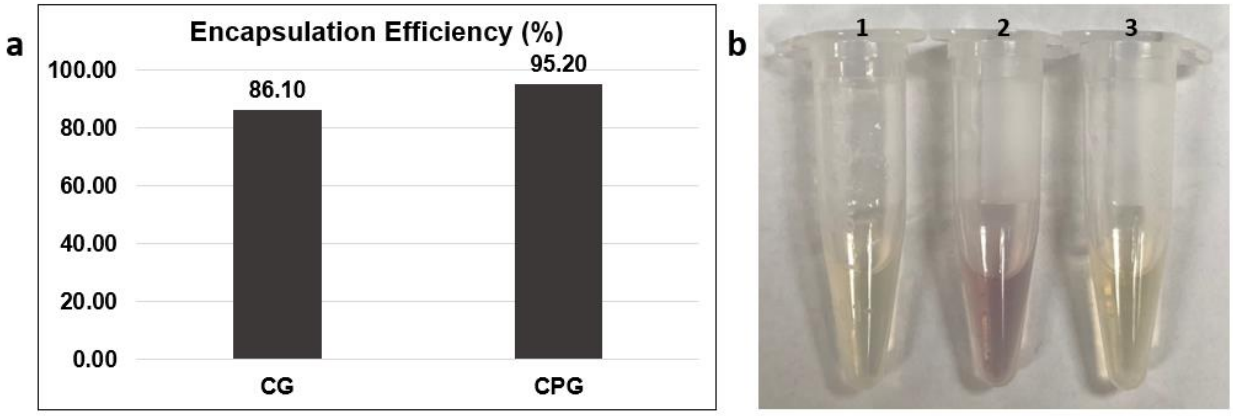

Figure 1.3 *Gentamicin encapsulation efficiency.* ***a)*** *Chitosan-PEGDA nanoparticles had 9.1% greater gentamicin encapsulation compared to chitosan alone.* ***b)*** *Colorimetric test using ninhydrin for the detection of gentamicin.* ***b1)*** *chitosan,* ***b2)*** *chitosan-gentamicin and* ***b3)*** *chitosan-PEGDA-gentamicin. All assays were done in triplets, and the averages were used to determine the encapsulation efficiency.*

Figure 1.3a shows Cs-PEGDA-GtS NPs had 9.1% greater encapsulation efficiency than Cs. The better encapsulation efficiency observed in Cs-PEGDA-GtS NPs can be explained by PEGDA's ability to shield the repelling forces between the positive charges of chitosan and gentamicin. Figure 1.3b shows a stronger purple hue indicative of greater GtS concentration in the post-encapsulation solution of the CG sample.

Enzymatic degradation results

Nanoparticle degradation by lysozyme

NPs were incubated with lysozymes to determine if the addition of PEGDA affected the activity of lysozymes on particle degradation. FTIR was used on particles before and after degradation to determine changes in sample composition. Polysaccharides with 1-4 glycosidic

linkage are characterized by absorption bands in the 1175-1140 cm^{-1} range due to the C-O-C bridge between monomers. Figure 1.4 shows sharp peaks associated with glycosidic bonds before digestion for all three samples. Lysozymes catalyze the hydrolysis of glycosidic bonds in chitosan. Considering the characteristic peaks of lysozyme are found at 1655 cm^{-1} (amide I), 1542 cm^{-1} (amide II), and 1453 cm^{-1} (amide III), and the disappearance of the sharp peak associated with the glycosidic bridge is no longer present post-degradation in all samples, the data indicates that the addition of PEGDA to Cs-NPs does not affect lysozyme activity.

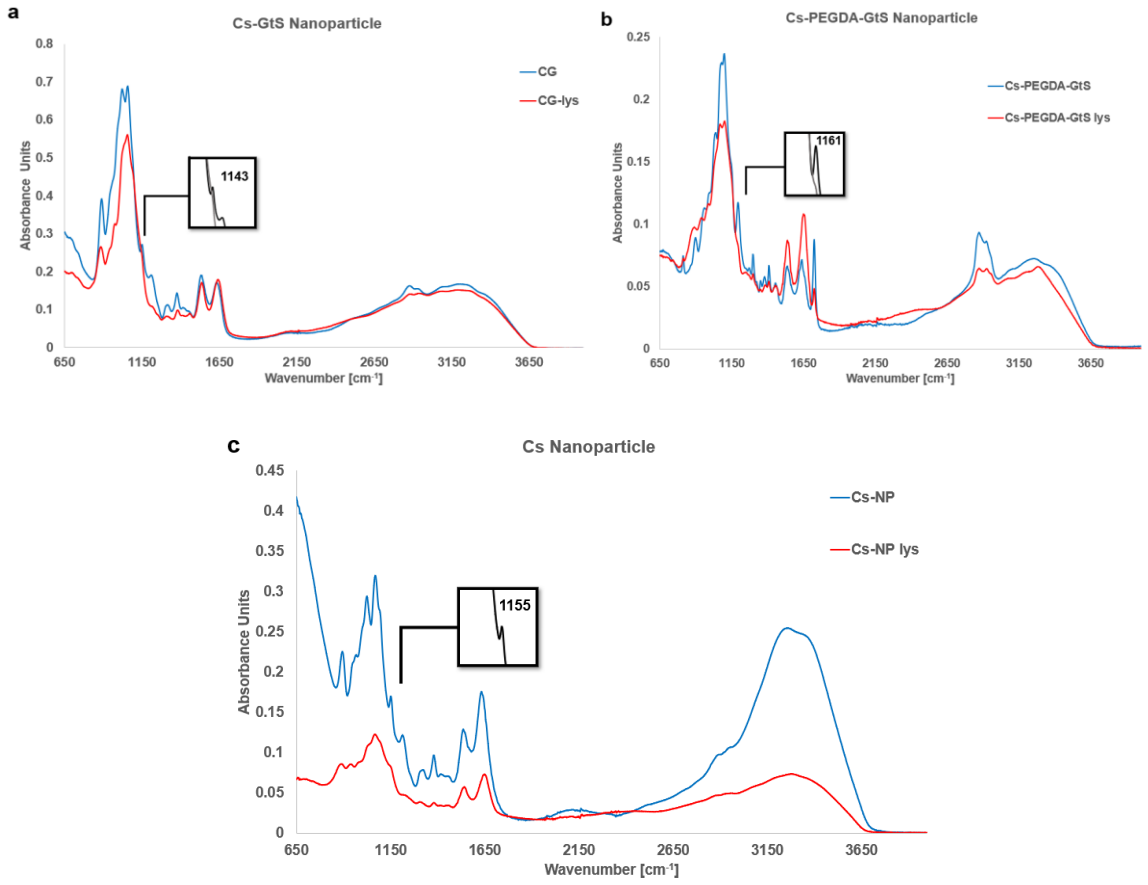

Figure 1.4 *FTIR of nanoparticles post-degradation highlighting the peaks associated with the C-O-C bridge of chitosan.* ***a)*** *chitosan-gentamicin* ***b)*** *chitosan-PEGDA-gentamicin, and* ***c)*** *chitosan nanoparticles spectra.*

Antimicrobial activity results

Nanoparticle antimicrobial activity

To further confirm lysozyme's ability to degrade the chitosan nanoparticles, the particles were incubated with buffer and lysozyme for 24 hours, and the solution was added to an agar plate containing *E. coli*. The antimicrobial assay was also used to determine the capacity of gentamicin to inhibit bacterial growth post-release.

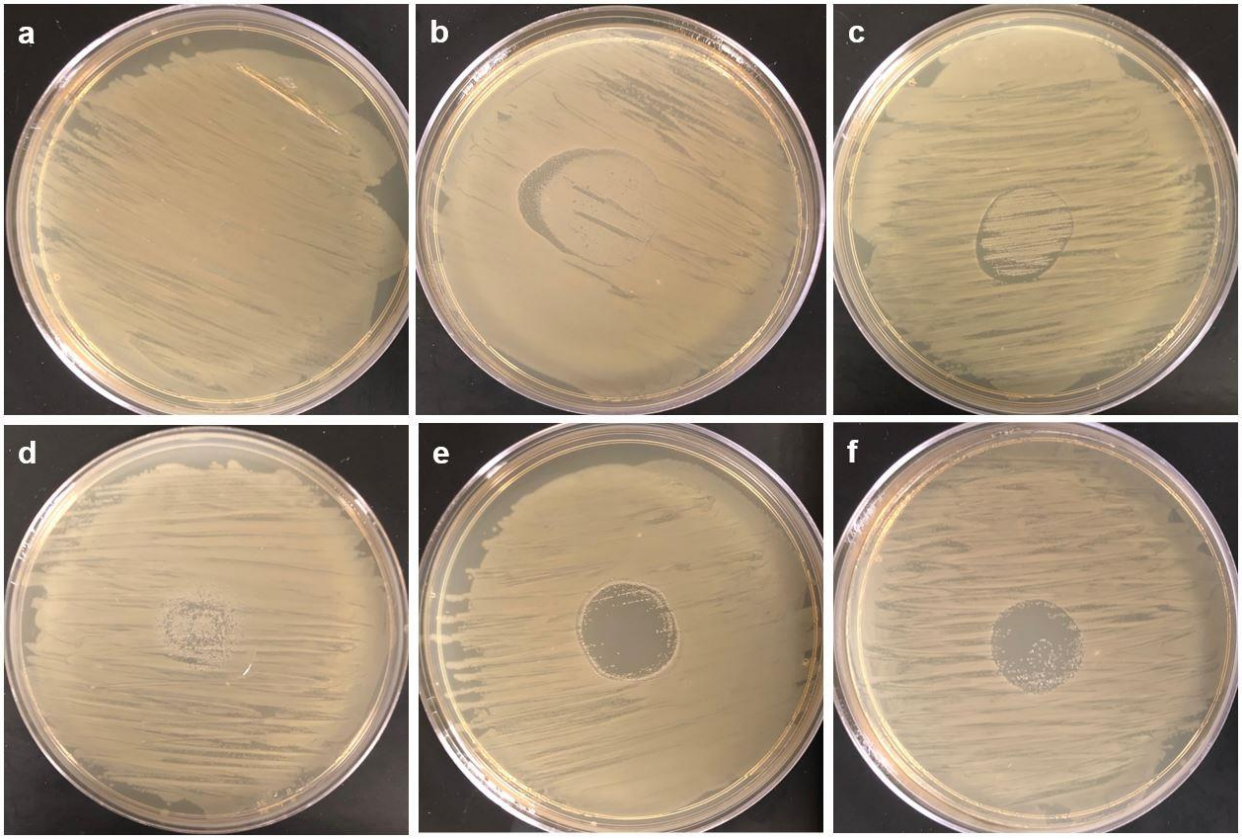

Figure 1.5 *Agar plates of E. coli BL-21 for antibacterial assay of chitosan nanoparticles to assess gentamicin activity. Top row: nanoparticle antimicrobial activity pre-enzymatic degradation. Bottom row: nanoparticle activity post-enzymatic degradation by lysozyme.* ***a & d)*** *Chitosan-NP* ***b & e)*** *Chitosan-PEGDA-Gentamicin NP* ***c & d)*** *Chitosan-Gentamicin NP.*

Cs NPs showed no antimicrobial activity when incubated with buffer, but Cs NPs incubated with lysozymes did show some growth inhibition (Figure 1.5 a & d). Although chitosan is known for possessing antimicrobial properties, its antibacterial ability depends on chitosan's

molecular weight and degree of deacetylation, explaining the difference in results considering control plates (lysozyme only) did not prevent bacterial growth. Cs-PEGDA-GtS NPs and Cs-GtS NPs incubated in buffer solution showed some inhibition indicating that NPs can degrade and release GtS in buffer (Figure 1.5 b & c). However, compared to the NPs incubated in lysozyme solution, the inhibition was significantly smaller, which suggests GtS was released at a much slower rate (Figure 1.5 e & f). This finding supports other reports of Cs NP releasing loaded drugs without chemical and enzymatic hydrolysis (Islam, Dmour, & Taha, 2019; Mohammed, Syeda, Wasan, & Wasan, 2017). Although both Cs-PEGDA-GtS NPs and Cs-GtS NPs showed significant inhibition, Cs-PEGDA had a larger zone of inhibition (Figure 1.5 e & f). The greater inhibition of Cs-PEGDA-GtS can be best explained by the 9.1% increase in encapsulation efficiency compared to Cs-GtS NP.

ELISA of nanoparticle release

ELISA was used for the detection and quantification of gentamicin after release from the nanoparticles. In this competitive ELISA assay, GtS present in the sample competes for the primary antibodies, preventing the binding of the primary antibodies to the GtS coated plate. Once the secondary antibody tagged with peroxidase enzyme is added, it targets the primary antibody complexed to the GtS coated plate resulting in a color change when TMB substrate is added. Therefore, as the concentration on the sample increases, the intensity of the dye decreases. Cs nanoparticles did not contain gentamicin, resulting in an intense yellow signal due to primary antibodies binding to the plate. As a result, the coloration was like that of the negative control (Figure 1.6 1A-B and 4A-B). Meanwhile, GtS in the solution of Cs-PEGDA-GtS and C-GtS samples resulted in a reduction of primary antibodies binding to the plate, causing the dye's intensity to diminish, confirming the presence of GtS in both samples (Figure 1.6 3A-B and 5A-B).

The gentamicin concentration of each sample was calculated using a gentamicin standard curve with a detection range of 2.7-0.05 ng/mL. Cs-PEGDA-GtS concentration was ~1.4 mg/mL and Cs-PEGDA ~1.7 mg/mL after accounting for the sample dilution.

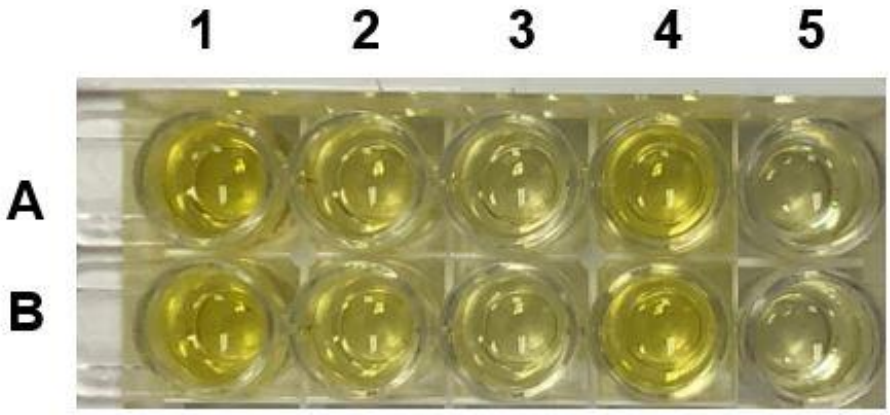

Figure 1.6 1A-B: *negative control,* ***2A-B:*** *positive control (2.7ng/mL gentamicin),* ***3A-B:*** *Cs-PEGDA-GtS,* ***4A-B:*** *Cs and* ***5A-B:*** *Cs-GtS. There is an inverse relationship between gentamicin concentration and the intensity of the dye.*

Conclusion

This study aimed to assess the ability of Cs-NP and Cs-PEGDA NPs to be enzymatically degraded by lysozymes at an ocular concentration to provide a targeted drug delivery system for the anterior surface of the eye. The model drug in this study, gentamicin, has a low encapsulation efficiency into Cs-NPs due to charge repulsion between the positive charges of chitosan and gentamicin. PEGDA was added as a copolymer to mitigate chitosan and gentamicin's charge interactions to increase gentamicin's encapsulation efficiency. The results show that the addition of PEGDA did not affect lysozyme activity, and NPs incubated with lysozymes had greater gentamicin release than those in buffer solution. The addition of PEGDA increased encapsulation by 9.1%, further supporting the use of PEGDA as a non-ionic dispersing agent to stabilize the charge interactions between chitosan and gentamicin. The increased encapsulation efficiency of Cs-PEGDA-GtS NPs caused the particles to be slightly larger. However, Cs-PEGDA-GtS NPs had the best PDI and ZP values of all three NPs,

indicating that adding PEGDA helps produce more stable and homogeneous particles. Altogether the data indicates that Cs-PEGDA NPs is a better drug delivery system for aminoglycosides and a viable system for ocular targeted drug delivery.

Future works

It is important to assess the effects of PEGDA on particle residence time and chitosan's ability to interact with ocular mucins. It is also necessary to establish the system's safety and efficacy through tissue culture experiments using corneal epithelial cells and animal models that closely resemble the human system.

References

Abhang, P., Momin, M., Inamdar, M., & Kar, S. (2014). Transmucosal Drug Delivery- An Overview. *Drug Delivery Letters, 4*(1), 26-37. doi:10.2174/2210303111303999011

Anand, M., Sathyapriya, P., Maruthupandy, M., & Hameedha Beevi, A. (2018). Synthesis of chitosan nanoparticles by TPP and their potential mosquito larvicidal application. *Frontiers in Laboratory Medicine, 2*(2), 72-78. doi:10.1016/j.flm.2018.07.003

Azari, A. A., & Barney, N. P. (2013). Conjunctivitis. *JAMA, 310*(16), 1721. doi:10.1001/jama.2013.280318

Barbosa, A. I., Coutinho, A. J., Costa Lima, S. A., & Reis, S. (2019). Marine Polysaccharides in Pharmaceutical Applications: Fucoidan and Chitosan as Key Players in the Drug Delivery Match Field. *Marine Drugs, 17*(12), 654. doi:10.3390/md17120654

Chandra Hembram, K., Prabha, S., Chandra, R., Ahmed, B., & Nimesh, S. (2016). Advances in preparation and characterization of chitosan nanoparticles for therapeutics. *Artificial Cells, Nanomedicine, and Biotechnology, 44*(1), 305-314. doi:10.3109/21691401.2014.948548

Cohen, S., Martin, A., & Sall, K. (2013). Evaluation of clinical outcomes in patients with dry eye disease using lubricant eye drops containing polyethylene glycol or carboxymethylcellulose. *Clinical Ophthalmology*, 157. doi:10.2147/opth.s53822

Collado-Gonzalez, M., Gonzalez Espinosa, Y., & Goycoolea, F. M. (2019). Interaction Between Chitosan and Mucin: Fundamentals and Applications. *Biomimetics (Basel), 4*(2). doi:10.3390/biomimetics4020032

Desai, K. G. H. (2016). Chitosan Nanoparticles Prepared by Ionotropic Gelation: An Overview of Recent Advances. *Critical Reviews™ in Therapeutic Drug Carrier Systems, 33*(2), 107–158.

Gaudana, R., Ananthula, H. K., Parenky, A., & Mitra, A. K. (2010). Ocular drug delivery. *AAPS J, 12*(3), 348-360. doi:10.1208/s12248-010-9183-3

Han, T., Nwe, N., Furuike, T., Tokura, S., & Tamura, H. (2012). Methods of N-acetylated chitosan scaffolds and its In-vitro biodegradation by lysozyme. *Journal of Biomedical Science and Engineering, 05*(01), 15-23. doi:10.4236/jbise.2012.51003

Hankiewicz, J., & Swierczek, E. (1974). Lysozyme in human body fluids. *Clinica Chimica Acta, 57*(3), 205-209. doi:10.1016/0009-8981(74)90398-2

Huang, L., Zhu, Z., Wu, D., Gan, W., Zhu, S., Li, W., . . . Lu, L. (2019). Antibacterial poly (ethylene glycol) diacrylate/chitosan hydrogels enhance mechanical adhesiveness and promote skin regeneration. *Carbohydr Polym, 225*, 115110. doi:10.1016/j.carbpol.2019.115110

Huang, Y. C., Li, R. Y., Chen, J. Y., & Chen, J. K. (2016). Biphasic release of gentamicin from chitosan/fucoidan nanoparticles for pulmonary delivery. *Carbohydr Polym, 138*, 114-122. doi:10.1016/j.carbpol.2015.11.072

Islam, N., Dmour, I., & Taha, M. O. (2019). Degradability of chitosan micro/nanoparticles for pulmonary drug delivery. *Heliyon, 5*(5), e01684. doi:10.1016/j.heliyon.2019.e01684

Kim, S., Cui, Z. K., Koo, B., Zheng, J., Aghaloo, T., & Lee, M. (2018). Chitosan-Lysozyme Conjugates for Enzyme-Triggered Hydrogel Degradation in Tissue Engineering Applications. *ACS Appl Mater Interfaces, 10*(48), 41138-41145. doi:10.1021/acsami.8b15591

Lanier, O. L., Manfre, M. G., Bailey, C., Liu, Z., Sparks, Z., Kulkarni, S., & Chauhan, A. (2021). Review of Approaches for Increasing Ophthalmic Bioavailability for Eye Drop Formulations. *AAPS PharmSciTech, 22*(3), 107. doi:10.1208/s12249-021-01977-0

Lončarević, A., Ivanković, M., Rogina, A., & Ye, L. (2017). Lysozyme-Induced Degradation of Chitosan: The Characterisation of Degraded Chitosan Scaffolds. *Journal of Tissue Repair and Regeneration, 1*(1), 12-22. doi:10.14302/issn.2640-6403.jtrr-17-1840

Lu, E. X., Franzblau, S., Onyuksel, H., & Popescu, C. (2009). Preparation of aminoglycoside-loaded chitosan nanoparticles using dextran sulphate as a counterion. *Journal of Microencapsulation, 26*(4), 346-354. doi:10.1080/02652040802365182

Mantelli, F., & Argüeso, P. (2008). Functions of ocular surface mucins in health and disease. *Current Opinion in Allergy & Clinical Immunology, 8*(5), 477-483. doi:10.1097/aci.0b013e32830e6b04

McDermott, A. M. (2013). Antimicrobial compounds in tears. *Experimental Eye Research, 117*, 53-61. doi:10.1016/j.exer.2013.07.014

Mohammed, M., Syeda, J., Wasan, K., & Wasan, E. (2017). An Overview of Chitosan Nanoparticles and Its Application in Non-Parenteral Drug Delivery. *Pharmaceutics, 9*(4), 53. doi:10.3390/pharmaceutics9040053

Monteiro, N., Martins, M., Martins, A., Fonseca, N. A., Moreira, J. N., Reis, R. L., & Neves, N. M. (2015). Antibacterial activity of chitosan nanofiber meshes with liposomes immobilized releasing gentamicin. *Acta Biomater, 18*, 196-205. doi:10.1016/j.actbio.2015.02.018

Morrow, G. L., & Abbott, R. L. (1998). Conjunctivitis. *Am Fam Physician, 57*(4), 735-746.

Nayak, K., & Misra, M. (2018). A review on recent drug delivery systems for posterior segment of eye. *Biomed Pharmacother, 107*, 1564-1582. doi:10.1016/j.biopha.2018.08.138

Pangburn, S. H., Trescony, P. V., & Heller, J. (1982). Lysozyme degradation of partially deacetylated chitin, its films and hydrogels. *Biomaterials, 3*(2), 105-108. doi:10.1016/0142-9612(82)90043-6

Shields, T., & Sloane, P. D. (1991). A comparison of eye problems in primary care and ophthalmology practices. *Fam Med, 23*(7), 544-546.

Stokke, B. T., Varum, K. M., Holme, H. K., Hjerde, R. J. N., & Smidsrsd, O. (1995). Sequence specificities for lysozyme depolymerization of partially N-acetylated chitosans. *Canadian Journal of Chemistry, 73*, 1972-1981.

Udeh, B. L., Schneider, J. E., & Ohsfeldt, R. L. (2008). Cost effectiveness of a point-of-care test for adenoviral conjunctivitis. *Am J Med Sci, 336*(3), 254-264. doi:10.1097/MAJ.0b013e3181637417

Chapter 2

Chitosan film and derivatives methodology

Introduction

Nanoparticles have greatly improved ocular drug delivery. However, major physical barriers such as blinking and high tear turnover rate remain a challenge when nanocarriers are delivered by eye drops and ointments, leading to low drug bioavailability, requiring higher drug concentrations to reach the desired effects and daily recurring applications (Dubey, Prabhu, Parth, & Ghate, 2015; Hu et al., 2011; Maulvi, Lakdawala, et al., 2016). Therapeutic contact lenses have been employed to mitigate some of these issues by entrapping nanoparticles within hydrogel matrixes, but storage can lead to drug leaching before reaching the target site (Maulvi, Soni, & Shah, 2016; Mutlu, Shams Es-Haghi, & Cakmak, 2019). Because lysozymes present in tears degrade chitosan nanoparticles, chitosan nanoparticles can be used for drug encapsulation and further chemically attached to contact lenses to prevent premature drug release (Han, Nwe, Furuike, Tokura, & Tamura, 2012; Islam, Wang, Maqbool, & Ferro, 2019; Kim et al., 2018; Lončarević, Ivanković, Rogina, & Ye, 2017; Pangburn, Trescony, & Heller, 1982).

Poly(ethylene glycol diacrylate) (PEGDA) is a synthetic polymer derived from poly(ethylene glycol) (PEG), a common polymer used in the synthesis of contact lenses. PEGDA contains two acryl groups that can covalently bond with the amine groups of chitosan and chitosan nanoparticles in the presence of a strong base by Michael's reaction, and further be crosslinked by freeze-thaw to produce a film (Al-Matar, Khalil, Meier, Kolshorn, & Elnagdi, 2008; Ma, Zhang, Han, Song, & Nie, 2009; Sashiwa, Yamamori, Ichinose, Sunamoto, & Aiba, 2003). Once the film containing the loaded nanoparticles becomes in contact with the eye, they are exposed to lysozymes secreted by the lacrimal glands. Lysozyme can cleave the β-(1→4)-

glycosidic bonds of chitosan nanoparticles, slowly releasing the drug at the ocular surface. (McDermott, 2013; Zahoor, Bahadar, Ayaz, Khan, & Shah, 2018).

Methodology

Film synthesis

Synthesis of chitosan (Cs) film

Cs film was made by dissolving 0.25 g of chitosan in 12.5 mL of 1% acetic acid with stirring at 50°C. Next, the sample was dialyzed overnight for 48 hours. The sample was cast in between two glass plates following 3 cycles of 20-hour freezing and 4 hours thaw to make the film.

Synthesis of chitosan-PEGDA film

Cs-PEGDA films were synthesized by Michael's addition reaction. Cs-PEGDA was made by dissolving 0.25g of chitosan in 12.5 mL of 1% acetic acid with stirring at 50°C. Next, 267 µL of $PEGDA_{400}$ was added to the solution, and the pH was adjusted to 8.5 using sodium bicarbonate powder. Samples were dialyzed overnight for 48 hours. The samples were cast in between two glass plates following 3 cycles of 20-hour freezing and 4 hours thaw to make the films.

Synthesis of chitosan-PEGDA-CGNP film

Cs-PEGDA-CG(NP) films were synthesized by Michael's addition. Cs-PEGDA-CGNP was made by dissolving 0.25g of chitosan in 12.5 mL of 1% acetic acid with stirring at 50°C. Next, 267 µL of $PEGDA_{400}$ and 70 mg of chitosan nanoparticles containing gentamicin were added to the solution, and the pH was adjusted to 8.5 using sodium bicarbonate powder. The sample was dialyzed overnight for 48 hours. The sample was cast in between two glass plates following 3 cycles of 20-hour freezing and 4 hours thaw to make the film.

Synthesis of chitosan-PEGDA film

Cs-PEGDA-GtS films were made by dissolving 0.25 g of chitosan in 12.5 mL of 1% acetic acid with stirring at 50°C. Next, 267 µL of $PEGDA_{400}$ and 63.8 mg of gentamicin were added to the solution, and the pH was adjusted to 8.5 using sodium bicarbonate powder. The sample was dialyzed overnight for 48 hours. The sample was cast in between two glass plates following 3 cycles of 20-hour freezing and 4 hours thaw to make the film.

Cs-PEGDA film characterization

FTIR of Cs-PEGDA films

Fourier-Transform Infrared Spectroscopy was used to identify the functional groups present in the film after synthesis. Membranes were placed in a covered petri dish and allowed to air dry for 72 hours. The samples' FT-IR spectra were recorded in the 4000-400 cm^{-1} region with a spectra resolution of $4cm^{-1}$.

Morphology of CS-PEGDA films

The scanning electron microscope (SEM) images were captured using a Philips XL30 environmental scanning electron microscope. Samples were placed on an SEM stub and sputter-coated with titanium for 120 seconds.

CS-PEGDA film swelling studies

2 mg/mL of Lysozyme stock solution was made by dissolving 100 mg of lysozyme in 50 mL of 20mM phosphate buffer at pH 7.4. 5 mg of membranes were cut off and placed inside individual glass vials containing 5 ml of lysozyme solution and incubated with a cap on and stirring for 2 hours at 37°C. After two hours, the membranes were removed from the lysozyme solution and dried at 37°C. The samples were weighed before (W_{wet}) and after drying (W_{dry}). The equilibrium solution content (ESC) was determined using the following equation:

$$ESC(\%) = \frac{W_{wet} - W_{dry}}{W_{wet}} x100$$

In vitro degradation studies

Cs-PEGDA film in vitro lysozyme degradation

2 mg/mL of Lysozyme stock solution was made by dissolving 100 mg of lysozyme in 50 mL of 20mM phosphate buffer at pH 7.4. 5 mg of membranes were cut off and placed inside individual glass vials containing 5 ml of lysozyme solution and incubated with a cap on and stirring for 2 hours at 37°C. After two hours, the membranes were removed from the lysozyme solution, rinsed with DI water, and gently pat dried using a Kimwipe and allowed to dry at 37°C before FTIR and SEM images.

Morphology of Cs-PEGDA films post lysozyme degradation

The scanning electron microscope (SEM) images were captured using a Philips XL30 environmental scanning electron microscope. Samples were placed on an SEM stub and sputter-coated with titanium for 120 seconds.

FTIR of Cs-PEGDA films post lysozyme degradation

Fourier-Transform Infrared Spectroscopy (FTIR) was used to identify the functional groups present in the film after lysozyme degradation. Membranes were placed in a covered petri dish and allowed to air dry for 72 hours. The samples' FTIR spectra were recorded in the 4000-400 cm^{-1} region with a spectra resolution of 4 cm^{-1}.

Antimicrobial assay to test gentamicin activity post-release

A single colony of *E. coli* was inoculated in 10 mL of LB media containing 10 µL of ampicillin overnight. Agar plates were coated with 100 µL of bacterial growth, and 200 µL of NP solution was dropped in the center of the plate and incubated overnight at 37°C.

Results and Discussion

Film characterization results

Morphological characterization of Cs-PEGDA and Cs-PEGDA-CG(NP) films

Scanning electron microscopy (SEM) was used to obtain images of the films to confirm the presence of chitosan-gentamicin nanoparticles (CGNPs) at the surface. Cs-PEGDA film images show a smooth surface with no visible particles at the surface (Figure 2.1a). As expected, Cs-PEGDA-CGNP films contain particles in the nano range at the surface of the film, confirming the presence of CGNPs (Figure 2.1b). Cs-PEGDA film images were taken at 80x, 500x magnification, and Cs-PEGDA-CGNP images were taken at 3500x and 10000x.

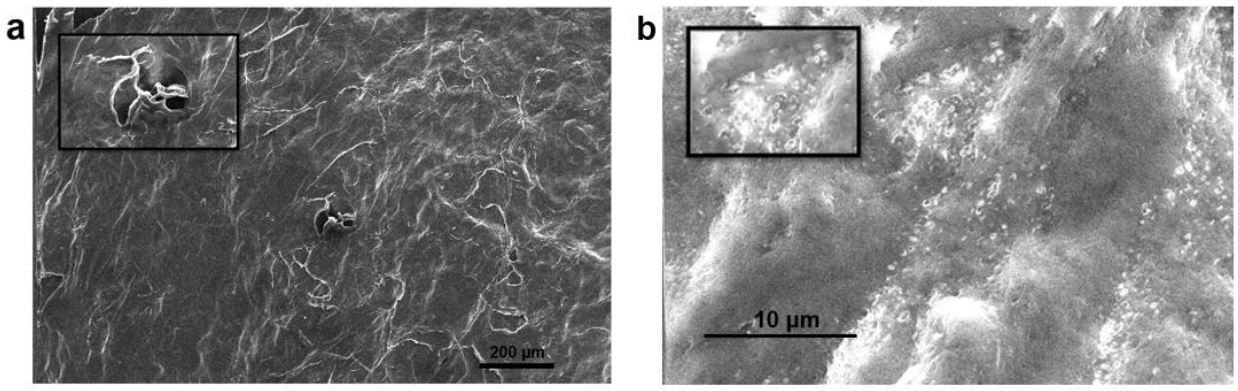

Figure 2.1 *SEM film characterization.* ***a)*** *CS-PEGDA film and* ***b)*** *Cs-PEGDA-CGNP. SEM image was taken at 80x and 500x magnification.*

Cs-PEGDA and Cs-PEGDA-CGNP Film FTIR

Fourier-transform infrared spectroscopy (FTIR) of chitosan films was performed to establish the interactions between chitosan and PEGDA. Characteristic peaks of chitosan are also present in the chitosan film FTIR, including an N-H bending at 1560 cm^{-1} indicative of amine, another peak at 1650 cm^{-1} C-N stretching from amide II, and a peak at 1150 cm^{-1} of the asymmetric C-O-C stretching. The Cs-PEGDA film spectrum is similar to the Cs film, with the added ester pattern of three peaks 1727, 1202, and 1150 cm^{-1} found in PEGDA. The Cs-

PEGDA spectrum also shows a shoulder at 1641 cm^{-1} in the range of monosubstituted alkenes (1648-1638 cm^{-1}) not present in the Cs film (Figure 2.2a).

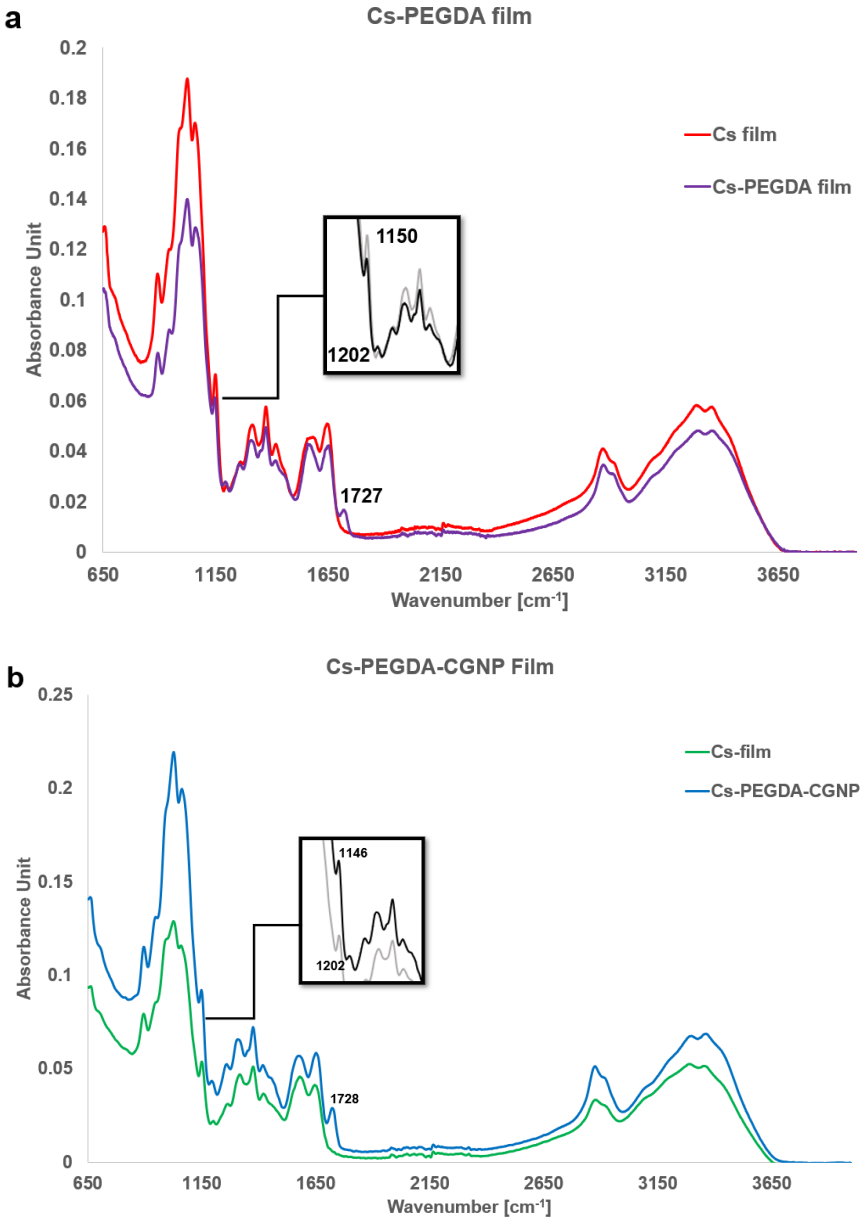

Figure 2.2 *FTIR characterization.* ***a)*** *Cs-PEGDA film spectra show a new peak at 1720 cm^{-1} attributed to the ester functional group of PEGDA.* ***b)*** *Cs-PEGDA-CGNP film spectra showing a new peak at 1722 cm^{-1} attributed to the ester functional group of PEGDA.*

Although the FTIR confirms the presence of PEGDA, it cannot confirm the chemical attachment of PEGDA and Cs due to overlapping peaks. Meanwhile, Cs-PEGDA-CGNP also

contains the characteristic ester peaks at 1728, 1202, and 1146 $cm^{-1,}$ but no shoulder at 1640 cm^{-1} is present (Figure 2.2b).

Swelling behavior of Cs films

Equilibrium solution content (ESC) was calculated to investigate the effect of adding PEGDA to Cs film swelling. The addition of PEGDA did not significantly alter the film's swelling properties. However, adding GtS to the film increased the ESC by 9.3% and doubled the swelling ratio compared to the Cs-film (Figure 2.3).

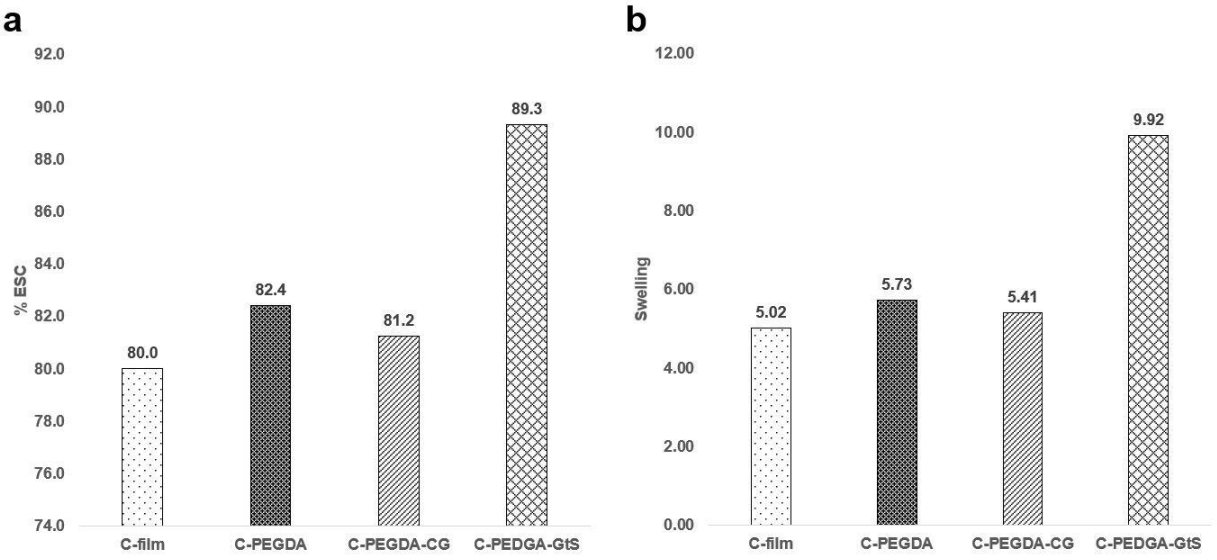

Figure 2.3 *Swelling behavior of films.* ***a)*** *Equilibrium solution content and* ***b)*** *swelling ratio of chitosan films and derivatives. Adding PEGDA to chitosan did not significantly affect the films swelling properties. However, adding GtS to the Cs-PEGDA film increased the ESC by 9.3%, and the swelling ratio nearly doubled compared to the Cs film.*

The data indicate that adding GtS causes the pore size to increase, which can be explained by GtS being physically entrapped within the film's pores during crosslinking, consequently increasing the ESC and swelling ratio. The larger pore also explains the quicker degradation of Cs-PEGDA-GtS films than the other films (Figure 2.4). On the other hand, the similar swelling behavior between Cs-PEGDA-CGNP and the Cs films suggests that CGNPs were not entrapped in the pores but were involved in the crosslinking process.

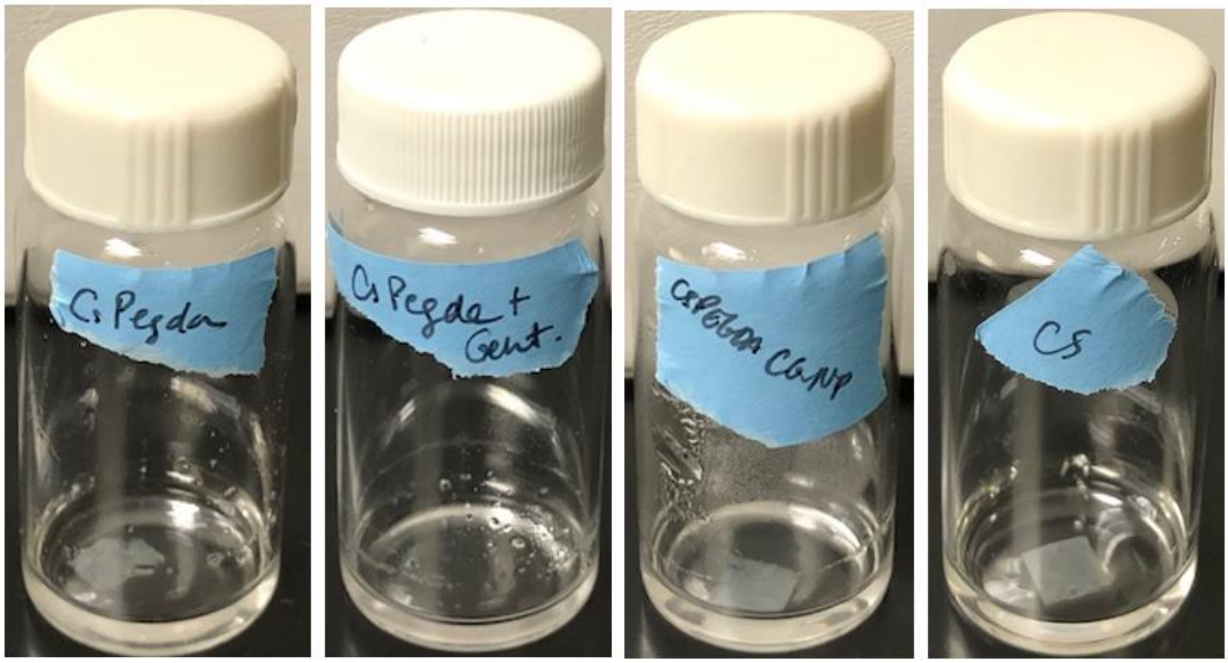

Figure 2.4 *Vials containing films incubated with 2mg/mL lysozyme for one week. Cs-PEGDA-GtS film was completely degraded after one week. Chitosan film was the most stable.* ***a)*** *Chitosan-PEGDA film* ***b****) Chitosan-PEGDA-GtS film* ***c)*** *Chitosan-PEGDA-CsGtSNP film* ***d)*** *Chitosan.*

Film enzymatic degradation results

SEM images of films post degradation

Cs-PEGDA film was incubated with 1mL of 2 mg/mL of lysozyme pH 7.4 for 24 hours to test lysozyme's ability to degrade the film. Lysozyme enzymatically degrades Cs by hydrolysis of β-(1→4) N-acetylglucosamine units. The SEM images were taken before and after incubation with lysozyme (Figure 2.5a and b, respectively). Before incubation with lysozymes, no pores were visible on the film's surface (Figure 2.5a). However, visible signs of degradation were observed after incubation, as evident by the various pores on the film's surface in agreement with other reports of chitosan hydrogel degradation (Tanuma et al., 2010). The SEM images indicate that adding PEGDA to chitosan did not prevent lysozyme activity.

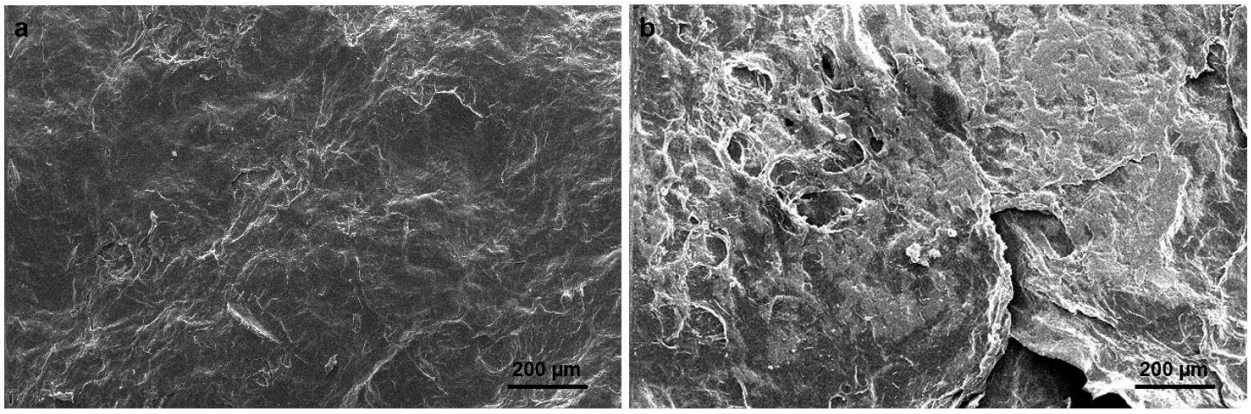

Figure 2.5 *SEM images of Cs-PEGDA films* ***a)*** *before and* ***b)*** *post degradation with lysozymes. SEM image b shows signs of degradation after being incubated with lysozyme for 24 hours.*

FTIR of films post degradation

FTIR was used to further determine changes to the film post-incubation with lysozyme. Figure 2.6a shows the spectra for Cs-PEGDA film before and after incubation with lysozyme. Figure 2.6b highlights the symmetric and asymmetric glucoside C-O-C stretching bands. Deconvolution of the peaks and area under the peaks showed no significant changes between films before and after incubation.

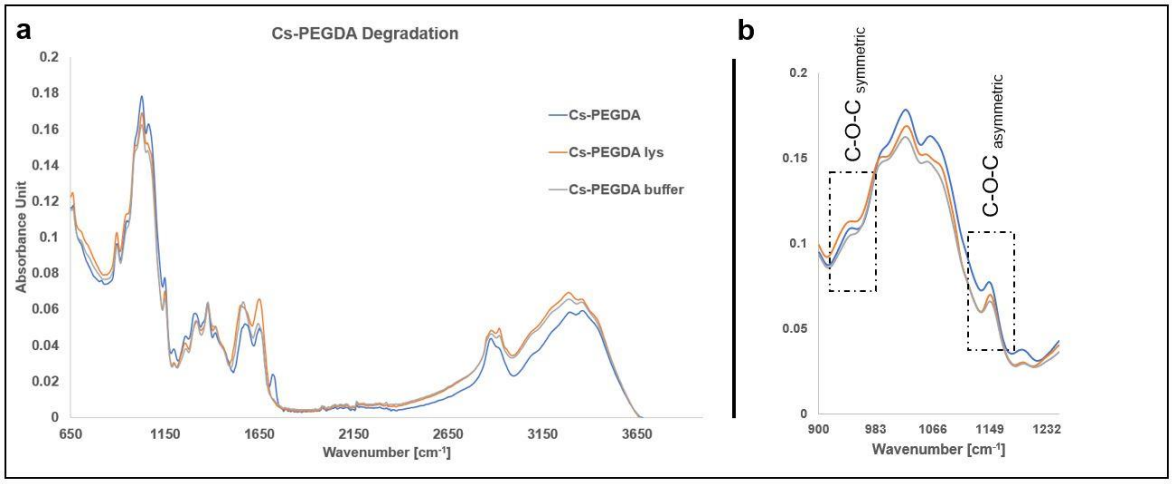

Figure 2.6 *FTIR of Cs-PEGDA films.* ***a)*** *Cs-PEGDA film spectra before and after enzymatic degradation.* ***b)*** *Magnified spectra highlighting the absorbance changes for the symmetric and asymmetric C-O-C glycosidic bridge, 908 and 1147 cm^{-1}, respectively.*

Antimicrobial results

Film antimicrobial properties

Individual films were dipped into an overnight bacterial growth and incubated for 24 hours to determine if bacteria could grow on the films. The results show that bacteria were unable to grow on Cs-PEGDA, Cs-PEGDA-CGNP, and Cs-PEGDA-GtS films. Of the three, Cs-PEGDA-GtS showed the most antimicrobial activity by further preventing bacteria from growing on the agar plate on the films' edges. However, few bacterial colonies were visible on Cs film (Figure 2.7e). The results indicate that adding PEGDA did not reduce chitosan's inherent antimicrobial activity but indeed enhanced it.

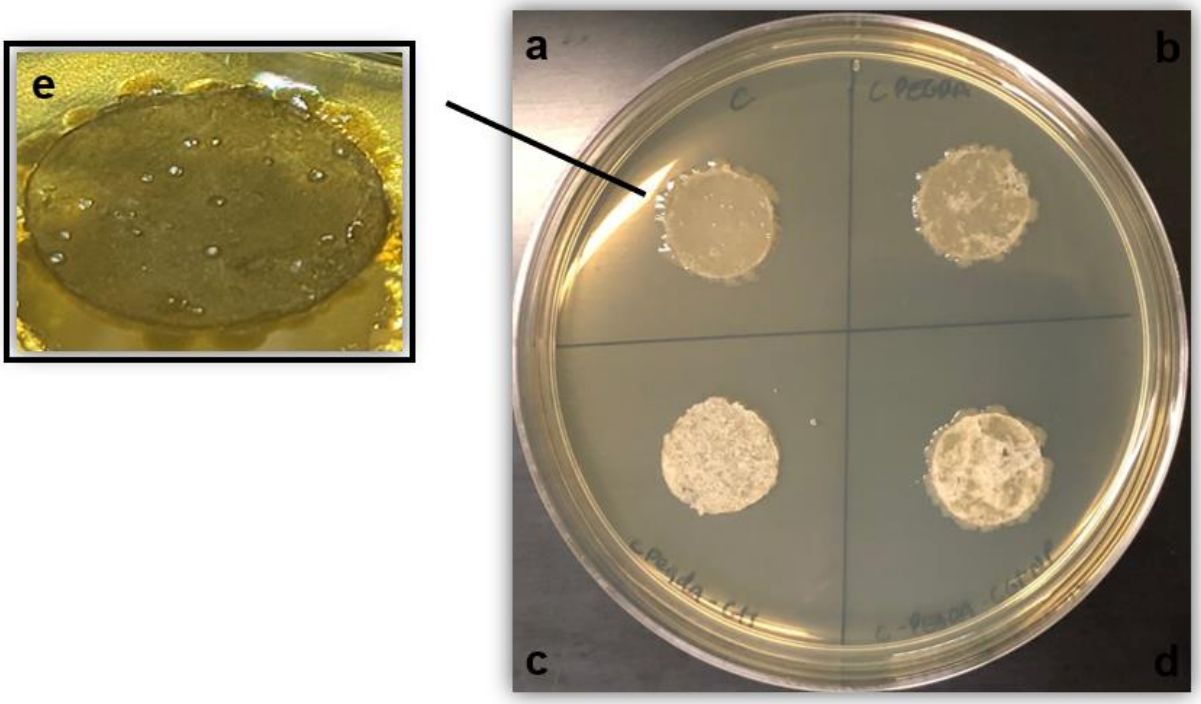

Figure 2.7 *Cs films inoculated with liquid bacterial growth.* ***a)*** *chitosan film,* ***b)*** *Cs-PEGDA,* ***c)*** *Cs-PEGDA-GtS,* ***d)*** *Cs-PEGDA-CGNP, and* ***e)*** *magnified image of the chitosan film in which bacterial colonies can be seen.*

Antimicrobial properties of post lysozyme incubation solution

Individual films were incubated in 1 mL of 2 mg/mL lysozyme solution to determine the effects of crosslinking PEGDA to chitosan on lysozyme activity. Next, 100 µL of the solution was added to agar plates inoculated with *E. coli* BL-21 to determine gentamicin's presence and activity in the solution.

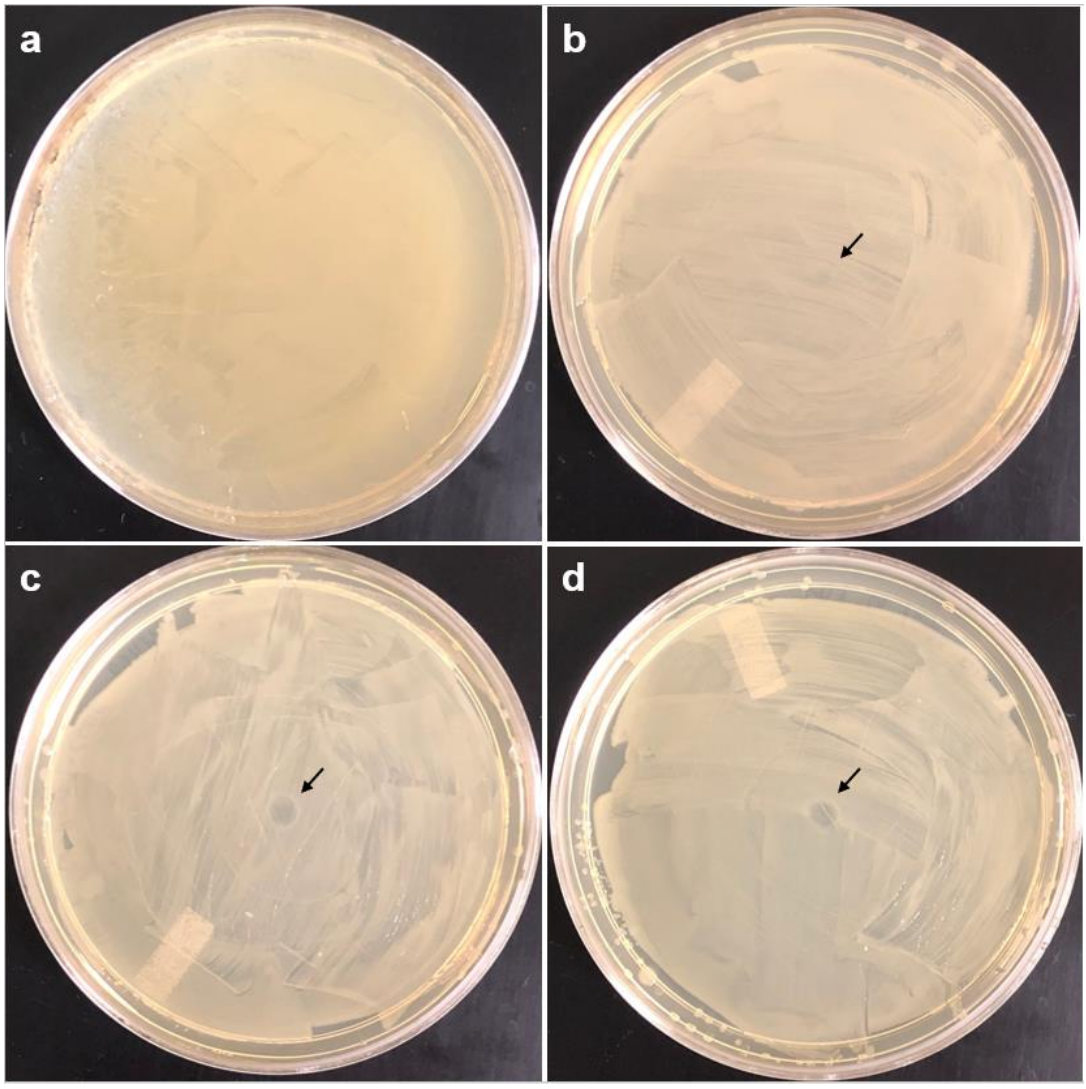

Figure 2.8 *Cs films and derivatives were incubated in 1 mL of 2 mg/mL lysozyme solution for six days to determine if the addition of PEGDA affected lysozyme activity. The post-incubation solution was plated on agar plates inoculated with E. coli BL-21 to assess gentamicin's presence and activity in the solution.* ***a)*** *chitosan film,* ***b)*** *cs-PEGDA film,* ***c)*** *chitosan-PEGDA-CGNP, and* ***d)*** *Cs-PEGDA-GtS.*

No inhibition was observed from the Cs-film solution, and a very small area of inhibition was present from the Cs-PEGDA film solution. Chitosan is known for having antimicrobial properties dependent on the degree of acetylation, which could explain the lack of inhibition for the Cs film and the small area of inhibition on the Cs-PEGDA solution. An obvious area of no bacterial growth of approximately similar size was present on both Cs-PEGDA-CGNP and Cs-PEGDA-GtS film solutions indicating that GtS was released from CGNPs and Cs-PEGDA-GtS films during incubation (Figure 2.8).

Conclusion

FTIR spectra of Cs-PEGDA and Cs-PEGDA-CGNP films show the presence of the three peaks characteristic of unsaturated ester bonds at 1727, 1200, and 1150 cm^{-1} for Cs-PEGDA and 1728, 1202, and 1146 cm^{-1} for Cs-PEGDA-CGNP. The FTIR data alone cannot confirm PEGDA and Cs' chemical attachment by Michael's addition, but preliminary H-NMR data indicates that the reaction was successful. Furthermore, the addition of PEGDA did not hinder the film enzymatic degradation by lysozyme, as confirmed by the SEM images; however, no significant changes were observed on the FTIR of degraded films to indicate hydrolysis of the glycosidic bonds. Similar antimicrobial activity of Cs-PEGDA-CGNP film and Cs-PEGDA indicates that NPs could release gentamicin after incubation with lysozyme, providing more evidence that enzymatic degradation took place. Lastly, adding PEGDA does not significantly alter chitosan's antimicrobial activity, as evidenced by the lack of bacterial colonies on Cs-PEGDA, Cs-PEGDA-CGNP, and Cs-PEGDA-GtS films dipped in bacterial growth.

Future works

To determine if the Cs-PEGDA-CGNP film is a viable candidate material for therapeutic contact lenses studies to determine the film's optical transparency, mechanical properties, and oxygen permeability are needed.

References

Al-Matar, H. M., Khalil, K. D., Meier, H., Kolshorn, H., & Elnagdi, M. H. (2008). Chitosan as heterogeneous catalyst in Michael additions: the reaction of cinnamonitriles with active methylene moieties and phenols. *ARKIVOC*(xvi), 288-301.

Dubey, A., Prabhu, P., Parth, V., & Ghate, V. (2015). Investigation of hydrogel membranes containing combination of gentamicin and dexamethasone for ocular delivery. *International Journal of Pharmaceutical Investigation, 5*(4), 214. doi:10.4103/2230-973x.167684

Han, T., Nwe, N., Furuike, T., Tokura, S., & Tamura, H. (2012). Methods of N-acetylated chitosan scaffolds and its In-vitro biodegradation by lysozyme. *Journal of Biomedical Science and Engineering, 05*(01), 15-23. doi:10.4236/jbise.2012.51003

Hu, X., Hao, L., Wang, H., Yang, X., Zhang, G., Wang, G., & Zhang, X. (2011). Hydrogel Contact Lens for Extended Delivery of Ophthalmic Drugs. *International Journal of Polymer Science, 2011*, 1-9. doi:10.1155/2011/814163

Islam, N., Wang, H., Maqbool, F., & Ferro, V. (2019). In Vitro Enzymatic Digestibility of Glutaraldehyde-Crosslinked Chitosan Nanoparticles in Lysozyme Solution and Their Applicability in Pulmonary Drug Delivery. *Molecules, 24*(7). doi:10.3390/molecules24071271

Kim, S., Cui, Z. K., Koo, B., Zheng, J., Aghaloo, T., & Lee, M. (2018). Chitosan-Lysozyme Conjugates for Enzyme-Triggered Hydrogel Degradation in Tissue Engineering Applications. *ACS Appl Mater Interfaces, 10*(48), 41138-41145. doi:10.1021/acsami.8b15591

Lončarević, A., Ivanković, M., Rogina, A., & Ye, L. (2017). Lysozyme-Induced Degradation of Chitosan: The Characterisation of Degraded Chitosan Scaffolds. *Journal of Tissue Repair and Regeneration, 1*(1), 12-22. doi:10.14302/issn.2640-6403.jtrr-17-1840

Ma, G., Zhang, X., Han, J., Song, G., & Nie, J. (2009). Photo-polymeriable chitosan derivative prepared by Michael reaction of chitosan and polyethylene glycol diacrylate (PEGDA). *Int J Biol Macromol, 45*(5), 499-503. doi:10.1016/j.ijbiomac.2009.08.007

Maulvi, F. A., Lakdawala, D. H., Shaikh, A. A., Desai, A. R., Choksi, H. H., Vaidya, R. J., . . . Shah, D. O. (2016). In vitro and in vivo evaluation of novel implantation technology in hydrogel contact lenses for controlled drug delivery. *J Control Release, 226*, 47-56. doi:10.1016/j.jconrel.2016.02.012

Maulvi, F. A., Soni, T. G., & Shah, D. O. (2016). A review on therapeutic contact lenses for ocular drug delivery. *Drug Deliv, 23*(8), 3017-3026. doi:10.3109/10717544.2016.1138342

McDermott, A. M. (2013). Antimicrobial compounds in tears. *Experimental Eye Research, 117*, 53-61. doi:10.1016/j.exer.2013.07.014

Mutlu, Z., Shams Es-Haghi, S., & Cakmak, M. (2019). Recent Trends in Advanced Contact Lenses. *Adv Healthc Mater, 8*(10), e1801390. doi:10.1002/adhm.201801390

Pangburn, S. H., Trescony, P. V., & Heller, J. (1982). Lysozyme degradation of partially deacetylated chitin, its films and hydrogels. *Biomaterials, 3*(2), 105-108. doi:10.1016/0142-9612(82)90043-6

Sashiwa, H., Yamamori, N., Ichinose, Y., Sunamoto, J., & Aiba, S. (2003). Michael reaction of chitosan with various acryl reagents in water. *Biomacromolecules, 4*(5), 1250-1254. doi:10.1021/bm030022o

Tanuma, H., Saito, T., Nishikawa, K., Dong, T., Yazawa, K., & Inoue, Y. (2010). Preparation and characterization of PEG-cross-linked chitosan hydrogel films with controllable swelling and enzymatic degradation behavior. *Carbohydrate Polymers, 80*(1), 260-265. doi:10.1016/j.carbpol.2009.11.022

Zahoor, M., Bahadar, H., Ayaz, M., Khan, A., & Shah, M. J. (2018). In vitro Study on the Antimicrobial Activity of Human Tears with Respect to Age. *Korean J Clin Lab Sci, 50*(2), 93-99.

Chapter 3

Chitosan-Fucoidan nanoparticles for the treatment of breast cancer

Introduction

Breast cancer (BC) is the second leading cause of cancer death among women, and although the incidence rate has slightly increased between 2012-2016, the death rate has steadily declined (Desantis et al., 2019). Early intervention and effective drug therapies have radically altered the outcome of BCs, but unfortunately, the outcome is not quite as bright when it comes to triple-negative breast cancers. Triple-negative BCs have high molecular heterogeneity, and the lack of estrogen receptor, progesterone receptor, and HER2 overexpression makes it extremely difficult to develop targeted therapies (Lee & Djamgoz, 2018).

Fucoidan (FU), a natural sulfonated polysaccharide derived from brown seaweed, is known to inhibit tumor growth and metastasis *in vitro* and *in vivo* while displaying low human toxicity. Moreover, *in vitro* studies using low molecular weight FU has been shown to inhibit the proliferation of the receptors positive MCF-7 and the triple-negative MDA-MB-231 BC cell lines while normal cells remain unaffected (Abudabbus, Badmus, Shalaweh, Bauer, & Hiss, 2017; Wu, Yan, Wu, Yuan, & Liu, 2016; Zhang, Teruya, Eto, & Shirahata, 2011). Although variation in the polysaccharide backbone structure, the degree, and the pattern of sulfated branches result in different bioactivity among various species (Patankar, Oehninger, Barnett, Williams, & Clark, 1993; Zorofchian Moghadamtousi et al., 2014), multiple studies have reported FU to exert greater toxicity toward MCF-7 cells than MDA-MB-231 which further supports the difficulty in treating triple-negative BC (Lu et al., 2018; Zhang et al., 2011). However, no studies reported on the cytotoxicity of FU delivered to MCF-7 and MDA-MB-231 cells using chitosan nanoparticles as of the time of this publication. Chitosan nanoparticles enter the cell via endocytosis, providing

an alternative cellular entry for FU into MDA-MB-231 cells to increase cytotoxicity (Salatin & Yari Khosroushahi, 2017).

Methodology

Synthesis of Chitosan-Fucoidan Nanoparticles

Preparation of low molecular weight fucoidan

500 mg of fucoidan was diluted in 4 mL of DMSO and 6 mL of DI water. Once the sample was completely dissolved, the sample was further diluted with 10 mL of DI water. Fucoidan was separated using 300k, 100k, and 30k centrifuge filters and stored at -20°C.

Preparation of stock solutions

Prepared chitosan stock solution by diluting 50 mg of chitosan in 50 mL of 0.05% acetic acid (1 mg/mL) stirred for two hours at 1000 rpm and TPP stock solution diluting 50 mg of TPP into 50 mL of DI water.

Chitosan nanoparticles

Added 5 mL of 1 mg/mL chitosan into 2 mL of 1 mg/mL TPP dropwise using a syringe pump set to 0.083 mL/min while stirring (1000 rpm) at room temperature. Let the solution continue to stir for an hour after all the content has been mixed before dialyzing overnight. Next, the solution was centrifuged for one hour at 3750 rpm and 4°C, and the opalescent top layer was collected.

Chitosan-Fucoidan nanoparticles

Added 1.05 mL of 10 mg/mL fucoidan into 5 mL of 1 mg/mL chitosan. Next, the solution was added into 2 mL of 1 mg/mL of TPP dropwise using a syringe pump set to 0.083 mL/min while stirring (1000 rpm) at room temperature. Let the solution continue to stir for an hour after

all the content has been mixed before dialyzing overnight. The solution was centrifuged for one hour at 3750 rpm at 4°C, and the opalescent top layer was collected.

Chitosan-Fucoidan nanoparticle characterization

Morphology of chitosan nanoparticles

Transmission electron microscope (TEM) images were captures using a Titan 80-3000 TEM. Samples were dipped onto a TEM copper grid and allowed to dry at room temperature for 72 hours before analysis.

Dynamic light scattering (DLS) and zeta potential

DLS was used to establish particle size, zeta potential, and polydispersity index (PDI). Samples were sonicated for 5 minutes, followed by a 100X dilution (10 mL in 1000 mL aqueous solution of 10 mM NaCl). Diluted samples were sonicated again for 15 min immediately before analysis.

Encapsulation efficiency

UV-vis was used to detect the fucoidan concentration post-synthesis to determine the encapsulation efficiency. Phenol sulfuric method was used to measure the total carbohydrate content post encapsulation. 0.5 mL of 5% phenol solution was added to 0.5 mL of the sample, followed by the immediate addition of 2.5 mL concentrated sulfuric acid. The sample was incubated at 95°C for 15 minutes, followed by 10 minutes in an ice-cold water bath. Absorption was taken using Shimadzu's UV-vis spectrophotometer at 490 nm wavelength. Encapsulation efficiency was determined using the following Equation:

$$EE\ (\%) = \frac{Fucoidan_{initial\ concentration} - Fucoidan_{non-encapsulated}}{Fucoidan_{initial\ concentration}}\ X\ 100$$

Cytotoxicity Assay

Cell culture

MCF-7 and MDA-MD-231 were grown in DMEM medium supplemented with 5% FBS and 1% penicillin/streptomycin.

MTT assay

Cells were grown to 90% confluence. Cells were dissociated by adding 0.05% trypsin to the flasks and quenched with 5 mL of complete media. Next, one hundred microliters of cell solution were seeded in 96 well plates at the density 5×10^4 cell/mL and incubated at 37 ºC in 5% CO_2 for 24 h. The next day each well was treated with 100 µL of serial dilutions of fucoidan, chitosan-fucoidan nanoparticle, and chitosan-nanoparticle starting at 1600 µg/mL concentration, in triplicates, and incubated for 48 h. Tetrazolium dye was used to determine the cell viability by measuring the fluorescent absorbance at 580 and 620 nm wavelength using a microplate reader.

Results and Discussion

CFU Nanoparticle characterization results

Dynamic Light Scattering (DLS)

DLS was used to determine particle size distribution, a zeta potential (ZP) analyzer to measure particle surface charge, and polydispersity index (PDI) to measure particle size distribution. ZP is used to estimate the surface charge of nanoparticles, which is indicative of the particle's physical stability. Small ZP can result in particle aggregation due to van der Waals interparticle attraction. In general, NPs with ZP ranging from +30 mV to -30 mV display a high degree of stability. Perfectly uniform samples have a PDI of zero, while moderate polydisperse samples range from 0.1-0.4, and highly disperse samples have PDI's >0.4. CFU particle size was on average 366.27 ± 39.75 nm, which is ~55.3 nm smaller than Cs NP, 421.57 ± 18.83.

According to the ZP data, both samples have values in the stable range, although CFU NP was slightly more stable as indicated by the greater ZP than Cs NP, 17.79 and 16.06, respectively. The variance in particle size and ZP can be best explained by chitosan's molecular weight as various reports in the literature indicate that as molecular weight increases, particle size increases and zeta potential decreases (Nguyen, Nguyen, Wang, Vo, & Nguyen, 2016). Although both samples were moderately dispersed, CFU NP had slightly lower PDI, 0.40, than Cs NP, 0.46 (Table 3.1). However, a PDI of <0.3 is considered ideal for nanoparticles for cancer treatment, and both particles have greater PDI than that (Danaei et al., 2018).

Table 3.1 *Dynamic light scattering was used to determine particle size distribution, zeta potential analyzer to measure particle surface charge, and PDI to measure sample size heterogeneity. All samples were analyzed in triplicates, and the averages were reported.*

	Z-average (nm)	**Polydispersity Index**	**Zeta Potential (mV)**
CFU NP	366.27 ± 39.75	0.40 ± 0.05	17.79 ± 2.22
Cs NP	421.57 ± 18.83	0.46 ± 0.08	16.06 ± 1.12

Morphological characterization of nanoparticles

Transmission electron microscopy (TEM) was used for the morphological characterization of the nanoparticles (Figure 3.1). CFU NP displayed greater size variation, but particle morphology is similar to Cs NP. Images were taken at 100k magnification.

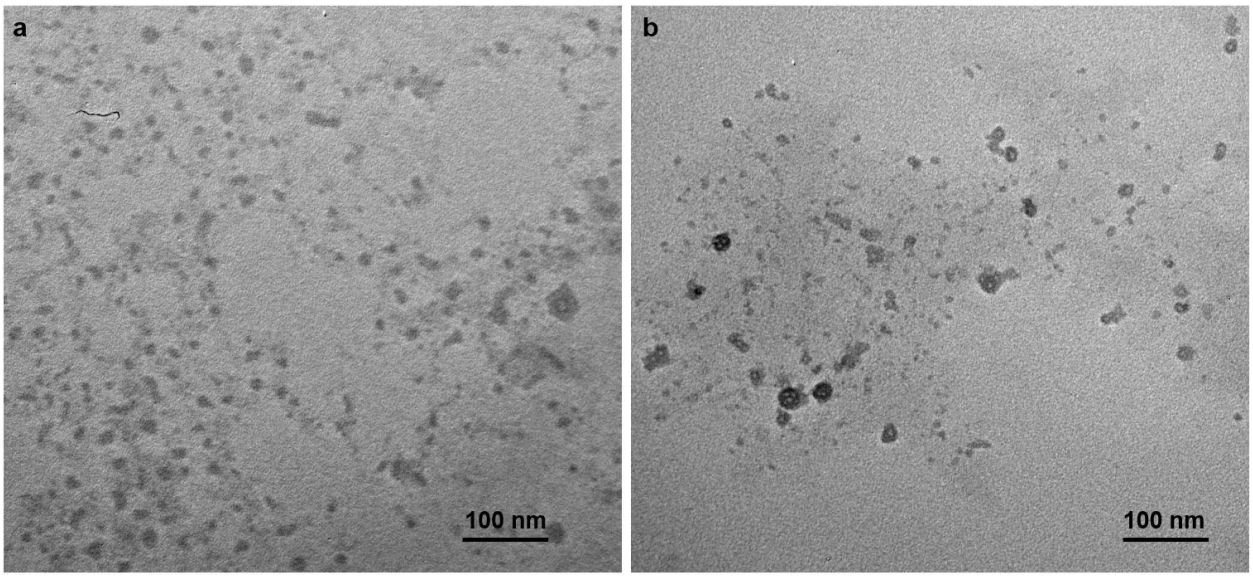

Figure 3.1 *TEM images of* ***a)*** *chitosan np and* ***b)*** *CFU np at 100000x magnification.*

Cytotoxicity assay

MTT assay was used to establish the cytotoxicity of CFU NP, Cs NP, and low molecular weight free-FU on the triple-negative breast cancer cell line MDA-MB-231, the estrogen receptor-containing breast cancer cell line MCF-7. MDA-MB-231 cells were mostly unaffected by free-FU at all concentrations tested. The lowest viability to MDA-MB-231 cells was 93% at 2.4 mg/mL. On the other hand, MCF-7 cells showed a significant decrease in cell viability when treated with free-FU. At 1.2 mg/mL, viability decreased by 31% and at 2.4 mg/mL by 26%. The results are congruent to what has been reported in the literature, in which FU is cytotoxic to MCF-7 cells but not MDA-MB-231 (Figure 3.2).

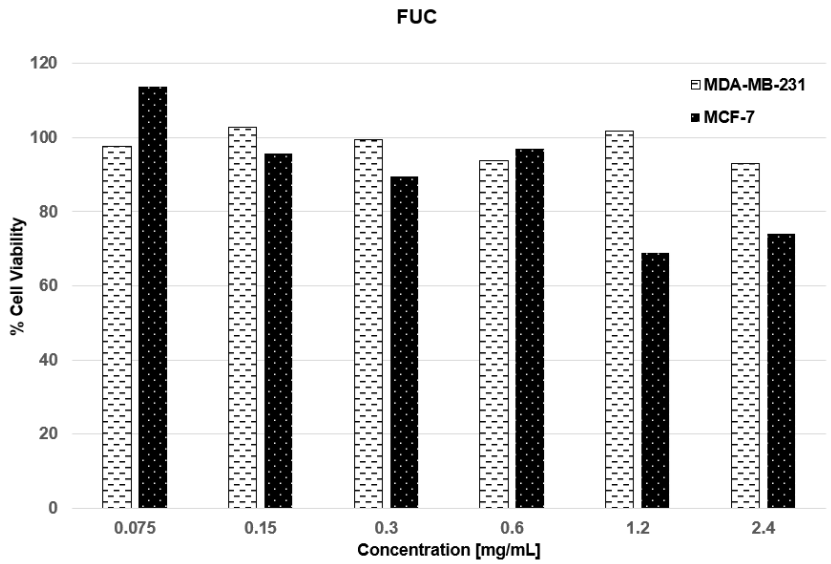

Figure 3.2 *Fucoidan cytotoxicity to MDA-MB-231 and MCF-7 cells. MCF-7 cells viability decreased by 31% at 1.2 mg/mL and 26% at 2.4 mg/mL. MDA-MB-231 remained mostly unaffected.*

Interestingly, encapsulating FU into Cs NPs increased FU's toxicity toward MDA-MB-231 cells. Cell viability for MDA-MB-231 steadily decreased in a dose-dependent manner from 92.87%, 87.41% and 82.08% cell viability at 0.6, 1.2 and 2.4 mg/mL, respectively. MCF-7 cells also displayed a dose-dependent response to CFU NP, and at 0.6 mg/mL viability was 89.82%, at 1.2 mg/mL 85.41%, and at 2.4 mg/mL 73.86%. CFU and free-FU presented similar cytotoxicity toward MCF-7 except for 1.2 mg/mL concentration, in which free-FU 16.43% more cytotoxic than CFU (Figure 3.4). The MDA-MB-231 lack of receptors can best explain the discrepancy in FU's cytotoxicity between cancer cell lines. Chitosan nanoparticles enter the cell via endocytosis, and the data indicates that this delivery system is suitable for the cellular uptake of FU into MDA-MB-231 cells to increase toxicity to triple-negative BC cells.

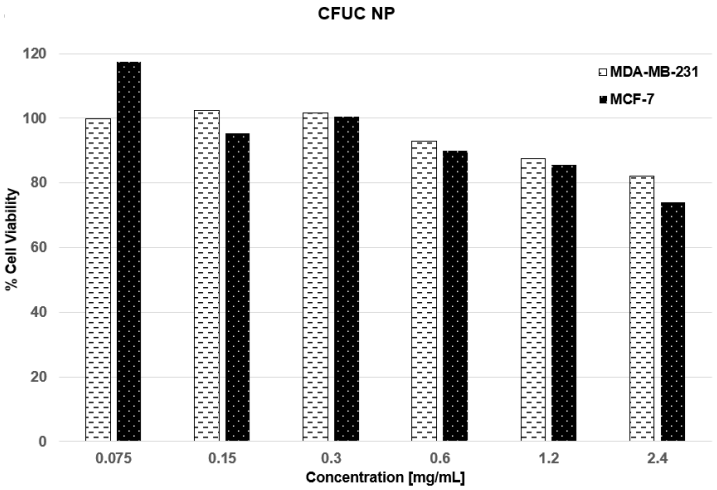

Figure 3.3 *Chitosan-fucoidan nanoparticle cytotoxicity to MDA-MB-231 and MCF-7 cells.*

To determine if the cytotoxicity observed was due to Cs NP or encapsulated FU, the cells were also treated with Cs NPs. MDA-MB-231 cells were not significantly affected by Cs NPs, and cell viability remained above 95.7% for all concentrations. The same was true for MCF-7 cells, although viability slightly decreased to 91.63% at 0.15 mg/mL and 85.11% at 2.4 mg/mL (Figure 3.5). The result supports the use of CFU as a delivery system to enhance FU's toxicity against MDA-MB-231 cells.

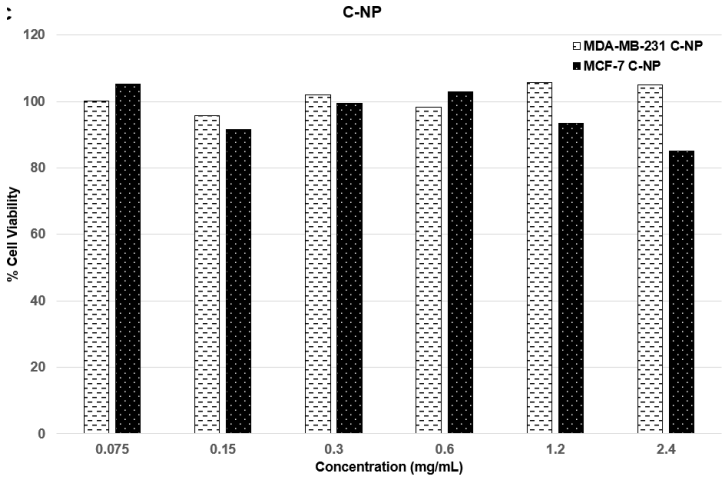

Figure 3.4 *Chitosan nanoparticle cytotoxicity to MDA-MB-231 and MCF-7 cells. Cs-NPs did not affect the cell viability of MDA-MB-231 cells. However, the cell viability of MCF-7 cells treated with Cs-NPs started to decrease at 1.2 mg/mL..*

Conclusion

The data further supports the findings of other published works in which FU shows greater cytotoxicity toward MCF-7 cells than MDA-MB-231. The different effects of FU on both cell lines are best explained by FU's ability to interact with BC receptors at the surface of MCF-7 cells to enter the cell. MDA-MB-231 and MCF-7 cells showed dose-dependent cytotoxicity when treated with CFU starting at 0.6 mg/mL. However, no significant difference in toxicity was observed on MCF-7 cells treated with FU and CFU. Cs NPs, on the other hand, enter the cells via endocytosis, and the data shows it to be a viable delivery system to increase the cytotoxicity of FU toward MDA-MB-231. This finding is important considering triple-negative breast cancers are hard to treat, and drug resistance is common. Furthermore, blank Cs-NPs did not affect cell viability of MDA-MB-231 cells, while MCF-7 cells had viability reduced by 15% at 2.4 mg/mL.

Future works

Various FU species have been shown to possess different anticancerous properties, and as described in this study, cell lines can respond differently to FU treatment. In the future, testing the effects of various species of FU using multiple breast cancer cell lines may shed light on which species and cancer cell lines are better suited for FU treatment and their mechanism of action.

References

Abudabbus, A., Badmus, J. A., Shalaweh, S., Bauer, R., & Hiss, D. (2017). Effects of Fucoidan and Chemotherapeutic Agent Combinations on Malignant and Non-malignant Breast Cell Lines. *Curr Pharm Biotechnol, 18*(9), 748-757. doi:10.2174/1389201018666171115115112

Danaei, M., Dehghankhold, M., Ataei, S., Hasanzadeh Davarani, F., Javanmard, R., Dokhani, A., . . . Mozafari, M. (2018). Impact of Particle Size and Polydispersity Index on the Clinical Applications of Lipidic Nanocarrier Systems. *Pharmaceutics, 10*(2), 57. doi:10.3390/pharmaceutics10020057

Desantis, C. E., Ma, J., Gaudet, M. M., Newman, L. A., Miller, K. D., Goding Sauer, A., . . . Siegel, R. L. (2019). Breast cancer statistics, 2019. *CA: A Cancer Journal for Clinicians, 69*(6), 438-451. doi:10.3322/caac.21583

Lee, A., & Djamgoz, M. B. A. (2018). Triple negative breast cancer: Emerging therapeutic modalities and novel combination therapies. *Cancer Treat Rev, 62*, 110-122. doi:10.1016/j.ctrv.2017.11.003

Lu, J., Shi, K., Chen, S., Wang, J., Hassouna, A., White, L., . . . Nie, S. (2018). Fucoidan Extracted from the New Zealand Undaria pinnatifida—Physicochemical Comparison against Five Other Fucoidans: Unique Low Molecular Weight Fraction Bioactivity in Breast Cancer Cell Lines. *Marine Drugs, 16*(12), 461. doi:10.3390/md16120461

Nguyen, T. V., Nguyen, T. T. H., Wang, S.-L., Vo, T. P. K., & Nguyen, A. D. (2016). Preparation of chitosan nanoparticles by TPP ionic gelation combined with spray drying, and the antibacterial activity of chitosan nanoparticles and a chitosan nanoparticle–amoxicillin complex. *Research on Chemical Intermediates, 43*(6), 3527-3537. doi:10.1007/s11164-016-2428-8

Patankar, M. S., Oehninger, S., Barnett, T., Williams, R. L., & Clark, G. F. (1993). A revised structure for fucoidan may explain some of its biological activities. *J Biol Chem, 268*(29), 21770-21776.

Salatin, S., & Yari Khosroushahi, A. (2017). Overviews on the cellular uptake mechanism of polysaccharide colloidal nanoparticles. *Journal of Cellular and Molecular Medicine, 21*(9), 1668-1686. doi:10.1111/jcmm.13110

Wu, S.-Y., Yan, M.-D., Wu, A. T. H., Yuan, K. S.-P., & Liu, S. H. (2016). Brown Seaweed Fucoidan Inhibits Cancer Progression by Dual Regulation of mir-29c/ADAM12 and miR-17-5p/PTEN Axes in Human Breast Cancer Cells. *Journal of Cancer, 7*(15), 2408-2419. doi:10.7150/jca.15703

Zhang, Z., Teruya, K., Eto, H., & Shirahata, S. (2011). Fucoidan Extract Induces Apoptosis in MCF-7 Cells via a Mechanism Involving the ROS-Dependent JNK Activation and Mitochondria-Mediated Pathways. *PLoS One, 6*(11), e27441. doi:10.1371/journal.pone.0027441

Zorofchian Moghadamtousi, S., Karimian, H., Khanabdali, R., Razavi, M., Firoozinia, M., Zandi, K., & Abdul Kadir, H. (2014). Anticancer and antitumor potential of fucoidan and fucoxanthin, two main metabolites isolated from brown algae. *ScientificWorldJournal, 2014*, 768323. doi:10.1155/2014/768323

Chapter 4

Study of Pneumococcal Surface Protein, PspA, Incorporated in Poly(Vinyl Alcohol) Hydrogel Membranes

Introduction

Despite research and advances in the use of therapeutic proteins, delivery vehicles have limited their use (Bruno, Miller, & Lim, 2013; Craik, Fairlie, Liras, & Price, 2013). Therapeutic protein delivery has been explored via hydrogel membrane systems to avoid degradation and restrictive gastrointestinal absorption, intravenous (Bruno et al., 2013; Craik et al., 2013; Park, 2014). The use of membranes will potentially decrease the use of needles for vaccines and, consequently, increasing patient comfort and compliance. Controlled drug delivery has progressed over the years and is improving with the use of different types of hydrogel membranes. Understanding polymers, protein release mechanisms, and molecular interactions are necessary for efficient design and fabrication (Bruno et al., 2013; Park, 2014). Desired protein drug release kinetics requires an understanding of the proposed mechanism and delivery material (Ahmed, 2015; Barzegar-Jalali et al., 2012).

Streptococcus pneumoniae (pneumococcus) is a gram-positive, alpha-hemolytic bacterium with 91 serotypes. *S. pneumoniae* is known for causing human diseases such as osteomyelitis, keratitis, septic arthritis, endocarditis, peritonitis, cellulitis, brain abscesses, and otitis media. It is a primary cause of morbidity and mortality; therefore, a vaccine has been administered since the 1970s (Briles et al., 1998). Studies have shown a reduction in the prevalence of the disease as a result of the various vaccines (M. R. Moore et al., 2015). This study investigates the interaction, release rates, and diffusion efficiency of different proteins from a hydrogel membrane.

A surface protein of *S. pneumoniae*, PspA (Pneumococcal Surface Protein A), elicits protection against pneumococci. PspA contains four distinctive domains, which include the N-terminal domain, alpha-helical domain, a proline-rich domain, and a choline-binding (Norcross, Sanders, Moore, & Marquart, 2011). The alpha-helical domain contains protection-eliciting epitopes. It has a high degree of serological variability with a size ranging from 67 to 99 kDa, however, this study uses a truncated version (the alpha helix), 38 kDa (Jedrzejas, 2001). The truncated PspA has been proven to elicit immunity (Q. C. Moore, Bosarge, Quin, & McDaniel, 2006). PspA is highly electrostatic with an elongated rod-like shaped, coiled-coil structure (Jedrzejas, 2001), and the functional N-terminal end is electronegative. Regarding PspA virulence, studies have shown that the presence of PspA protects pneumococci from clearance in the blood of infected mice (Jedrzejas, Lamani, & Becker, 2001; Q. C. Moore, Johnson, Repka, & McDaniel, 2007). The evidence demonstrated that PspA incorporated into a poly(ethylene oxide) matrix inhibits complement activation through the interference with the deposition of C3b; this inhibition can occur in classical and alternative pathways (Briles et al., 1998; Q. C. Moore et al., 2007). Studies on PspA reported that it is a promising vaccine candidate (Briles et al., 1998; Q. C. Moore et al., 2007; Yatim et al., 2013).

Poly(vinyl alcohol) (PVA) cross-linked with glutaraldehyde (GA), a prolonged-release micrometrics, is useful for drug delivery (Chaouat et al., 2008; Kamoun, Chen, Mohy Eldin, & Kenawy, 2015). PVA swells and absorbs water to create a swelling-controlled delivery system, and various studies are being conducted worldwide for the application of hydrogels as controlled released drug delivery systems (Kamoun et al., 2015; Prabhu, Dubey, Parth, & Ghate, 2015; Sittiwong, Niamlang, Paradee, & Sirivat, 2012). We are studying the PVA membrane for its use and ability to deliver a large protein into the desired environment (Censi, Di Martino, Vermonden, & Hennink, 2012; Kamoun et al., 2015). Furthermore, the use of PVA increases the bioavailability of drugs (Sittiwong et al., 2012) and decreases drug loss due to the increase in

viscosity (Ibrahim, 2010; Kiani, Shahbazi, & Asempour, 2012; Kulkarni, Sreedhar, Mutalik, Setty, & Sa, 2010). PVA membranes are non-biodegradable, and the retained structure allows the space for drug release (Juntanon, Niamlang, Rujiravanit, & Sirivat, 2008; Sirousazar, Kokabi, & Hassan, 2012; Thompson, Nguyen, & Nave, 2013). A saturated solution of the drug is entrapped within the PVA membrane structure, and the drug diffuses across the hydrogel matrix when the surface of the PVA hydrogel encounters hydrophilic solution (Barbara, 2008; Juntanon et al., 2008; Kulkarni et al., 2010; Mishra, Majeed, & Banthia, 2011). Therefore, the PVA crystalline-like structure can be modified to control the diffusion rate of the drug via the cross-linking ratio (Figueiredo, Alves, & Borges, 2009; Thompson et al., 2013; Varshosaz & Hajian, 2004).

With the isolation of a truncated fragment of PspA from *E. coli*, this study investigates the release of PspA from the open-mesh of hydrogel membranes cross-linked with glutaraldehyde. Many characteristics play a part in this study, including testing protein release and diffusion at pH 7.4 (which represents any biological environment), calculating the Equilibrium Solution Constant, and determining protein presence in the gel after incorporation using ATR-FTIR. This study also investigated the release mechanism of PspA and how a sufficient amount of protein is released from a membrane over time. With the characterization of the PspA filled thin film hydrogel membrane, it provides the necessary information to develop a drug delivery system. This system represents a proof of concept for a large protein. The mechanism of hydrogel formation allows modifications that control protein entrapment and release.

Materials and Methods

Materials

The hydrogels used for this study were prepared using poly(vinyl alcohol) PVA (98% hydrolyzed, the molecular weight of 70,000 - 100,000 g/mol−1), acetic acid (AA), and glutaraldehyde (GA) (50% aqueous solution). All materials for the formation of membranes were purchased from Sigma-Aldrich chemical company (St. Louis, MO, USA). Nitrogen gas was purchased from Airgas, USA. Ampicillin was also purchased from Sigma-Aldrich chemical company. Sodium phosphate and Luria broth were purchased from Fisher Scientific. All chemicals were used without further purification and were of analytical grade. The alpha-helical domain of PspA was purified from the E. coli clone. Anti-6x His tag antibody was purchased from Abcam, USA. Anti-PspA mouse monoclonal antibody XiR278 (IgG) was gifted from Dr. Larry McDaniel at the University of Mississippi Medical Center. Secondary antibody Alkaline Phosphatase-conjugated AffinPure Goat Anti-Mouse IgG (H + L) was purchased from Jackson ImmunoResearch Laboratories, USA.

Growth and Purification of Pneumococcal Surface Protein A(PspA)

PspA is highly expressed in *E. coli*. 5 ml of *E. coli* overnight growth was inserted into a flask containing 1 liter of Luria Broth (LB) and 75 µg/ml of ampicillin. The starter culture was then incubated in a shaker for 2.5 hours with an RPM of 200 at 37˚C. Cells were grown to an OD600 of 0.6 - 0.9 at 37˚C, and 1 mM IPTG was added for the expression of PspA. Cells were allowed to continue growing for 4 hours after induction. Cells were harvested and sonicated. The lysate was subjected to purification using the Fast Protein Liquid Chromatography (FPLC) system from ÄKTA Amersham Pharmacia was used to purify PspA. Recombinant PspA was designed with His-tag on the C-terminal to facilitate the purification steps using IMAC nickel

loaded HiTrap IMAC FF column (Ni-NTA). Sodium dodecyl polyacrylamide gel electrophoresis (SDS-PAGE) and Western Blot was used to confirm the isolation, purity, and activity of PspA.

Preparation of PspA-Loaded Poly(Vinyl) Alcohol (PVA) Hydrogels

The hydrogels were made by dissolving 5 g of high molecular weight PVA in 40 ml of boiling deionized water, allow the solution to cool to room temperature. Mix 250 µl of PspA (final concentration, 0.12 mg/ml or 0.7 mg/ml) and 960 µl of PVA solution with 108.75 µl of 10% (v/v) sulfuric acid (catalyst), 36.25 µl of 10% (v/v) acetic acid (buffer), 36.25 µl of 50% (v/v) methanol (quencher) and 108.75 µl of 1% (v/v) Glutaraldehyde (cross-linker). The solution was poured on a glass plate to form a membrane. The membrane was cross-linked overnight at room temperature inside a nitrogen gas chamber to control humidity.

$$(0.12 \text{ or } 0.7 \text{ mg ml PSA})(1.5 \text{ ml PVA}) = (C_O|)(250 \text{ ul PspA})$$

C_O = Concentration of PspA stock.

Equation (1) Equation for Constitutional formula of PspA, Poly(vinyl alcohol).

Diffusion Cell Experiments (DC)

Hydrogel membranes were placed between two adjacent diffusion cells to perform drug diffusion experiments. One chamber was vacant, and the other contained 5 mL of 20 mmol sodium phosphate buffer solution exposing only one face of the membrane to a concentration gradient. The solution is stirred continuously using a stirring rod and maintained at 37˚C by circulating heated water through the jacketed diffusion cells. A UV spectrophotometer is used to calculate the concentration of protein diffused into the buffer solution. Samples are taken periodically over 48 hours, and absorbance is recorded at 277 nm for PspA. The protein concentration was calculated using Beer's Law, A = εlc.

Equilibrium Solution Content (ESC) of Protein-loaded PVA Hydrogel

The equilibrium solution content was calculated to determine the characterization of the porous structure of the hydrogel for the drug delivery system of PspA. This measurement provides the relative measure of swelling to approximate the mesh size of the hydrogel. The ESC was determined by placing the hydrogel in buffer solutions ranging at pH 7.4 for this study. ESC, swelling ratio, and mesh size were calculated using Equations (2)-(4) (Matsuyama, Teramoto, & Urano, 1997).

$$ESC = \left(\frac{W_{wet} - W_{dry}}{W_{wet}}\right) \times 100\%$$

Equation 2. Equation for ESC.

$$Swelling\ ratio = \frac{Wwet}{Wdry}$$

Equation 3. Equation for the swelling ratio.

$$\xi_S = l_c \left(\frac{M_c}{M_r}\right)^{\frac{1}{2}} C_n{}^{\frac{1}{2}} v_2^{\frac{1}{3}}$$

Equation 4. Equation for the mesh size.

C_n is the rigidity coefficient, M_c is the number of average molecular weight between junction, M_r is the molar mass of repeating units of PVA, lc is the C-C bond length (0.154 nm), v_2 is the swollen polymer volume fraction after equilibrium.

Application of Mass Transport Equations

Higuchi's Equation can be applied because the experimental system follows the same basic principles from the original derivation. Higuchi's equation assumes a pseudo-steady-state

in which the initial drug concentration is at least ten times greater in magnitude than the drug solubility (Siepmann & Peppas, 2011).

$$k_H = \frac{M_t}{\sqrt{t}}, D = \frac{\pi}{t}\left(\frac{M_t}{2M_0 A}\right)^2$$

Equation (5) Higuchi K Constant and Equation (6) Diffusion Coefficient.

M_t = the mass [mg] diffused at time t, √t = square root of time [seconds];

M_t = the mass [mg] diffused at time t;

M_0 = initial mass [mg] diffused at time 0, t = time [seconds];

A = the exposed surface area of hydrogel.

Protein Release Study (PR)

PspA hydrogel membranes were submerged in 5 mL of 20 mmol sodium phosphate buffer of pH 7.4. The tubes are incubated at 37˚C with agitation. UV spectrophotometer was used to measure PspA concentration by recording absorbance at 277 nm. The aliquot was returned to the sample. SDS-PAGE and native gel electrophoresis were used to confirm PspA diffusion from the PVA membranes. Western blot was used to validate that the released protein was active.

Fourier Transform Infrared Spectroscopy (FTIR).

Membranes with and without protein were dried at 90˚C, and ATR-FTIR (IR-Affinity) was used to analyze the surface of the membrane. This technique was used to determine functional groups, such as hydroxyl groups present within the cross-linked membrane matrix, and peaks associated with the presence of protein.

Human Corneal Epithelial Cells

Human Corneal Epithelial Cells (HCEC) were purchased from Invitrogen and maintained in Keratinocyte media supplemented with 0.2% v/v Bovine pituitary extract (BPE), 1 µg/mL Recombinant human insulin-like growth factor-I, 0.18 µg/mL Hydrocortisone, 5 µg/mL Bovine transferrin and 0.2 ng/ml human epidermal growth factor. HCEC were grown to confluency and were introduced to the hydrogel with or without the protein (PspA), for 24 hours in separate experiments. The supernatant was collected to use in both Cytokine Arrays and Enzyme-linked immunosorbent assay (ELISA). The assay's protocol was performed according to the manufacturer's guidelines.

Cytokine Assays

Supernatants from Human Corneal Epithelial Cells (HCEC) exposed to growth media, and PspA hydrogel was collected 18 - 20 hours following exposure. Homogenates were analyzed with human cytokine antibody array 7 (Ray Biotech) according to the manufacturer's specifications. Briefly, antibody array membranes 7 were placed into eight-well trays and blocked with 2 ml of blocking buffer for 30 minutes. Blocking buffer was decanted, and membranes were incubated at 25˚C for 2 hours with l ml of supernatants. Samples were decanted, and membranes were washed three times with 1x wash buffer I followed by 2x wash buffer II at 25˚C with shaking. Diluted biotin-conjugated antibodies (1 ml) were added to each membrane and allowed to incubate at 4˚C overnight. Membranes were again washed with 1x wash buffers I and II prior to being incubated at 25˚C for 2 h with diluted horseradish peroxidase-conjugated streptavidin. Following a final wash, the membranes were incubated with detection buffers C and D. The chemiluminescent signal was then detected by exposure to film, and intensity was determined by densitometry. Signal intensities were quantitated using the Gel Doc system (BioRad), and the increased levels of cytokines from the exposure were compared.

ELISA

HCEC exposed supernatants were analyzed with specific ELISA Kits Interleukin-6 (IL6), Interleukin-8 (IL8), Interferon gamma (IFN-γ), Tumor necrosis factor alpha (TNF-α), Interleukin-12 (IL-12) P40, Interleukin-12 (IL-12) P70, Interleukin-16 (IL-16) and GRO-α (Ray Biotech). The homogenates were incubated in the ELISA plate at 4˚C overnight, which was followed by wash according to the wash solutions in the kit. Diluted biotin-conjugated antibodies specific to the cytokine being evaluated was added to each well and allowed to incubate at 4˚C overnight. Wells were washed and incubated at 25˚C for 45 min with diluted horseradish peroxidase-conjugated streptavidin. The wells were washed, and 100 µl of TMB One-Step Substrate Reagent was added to each well and allowed to incubate at room temperature for 30 min. The reaction was stopped solution and read at 450 nm immediately with the Biotech plate reader at 450 nm for ELISA analysis.

Statistical Analysis: Multi-way ANOVA and post-hoc Tukey HSD tests were performed using GraphPad Prism 8 software. Significance was defined by $\alpha = 0.05$.

All experiments were carried out at the University of Arkansas except the Cytokine Assays and ELISAs.

Results and Discussion

Recombinant PspA Purification

E. coli BL21 cloned with PspA plasmid lysate was purified using Ni-NTA. The SDS-page stained with Coomassie Brilliant Blue shows a strong band at 38kD for 32.25 mM and 62.5 mM fractions (Figure 4.1(a)). The 32.25 mM imidazole fraction (lanes 4 - 6) shows some impurities while the 62.5 mM imidazole fractions (lanes 7 - 9) show a pure 38 kD band, which represents recombinant PspA. Western blot result confirmed the 38 kD fraction has a His-tag protein signal

related to the recombinant PspA (Figure 4.1(b)). Purified PspA from 62.5 mM imidazole fraction was used for future experiments and application.

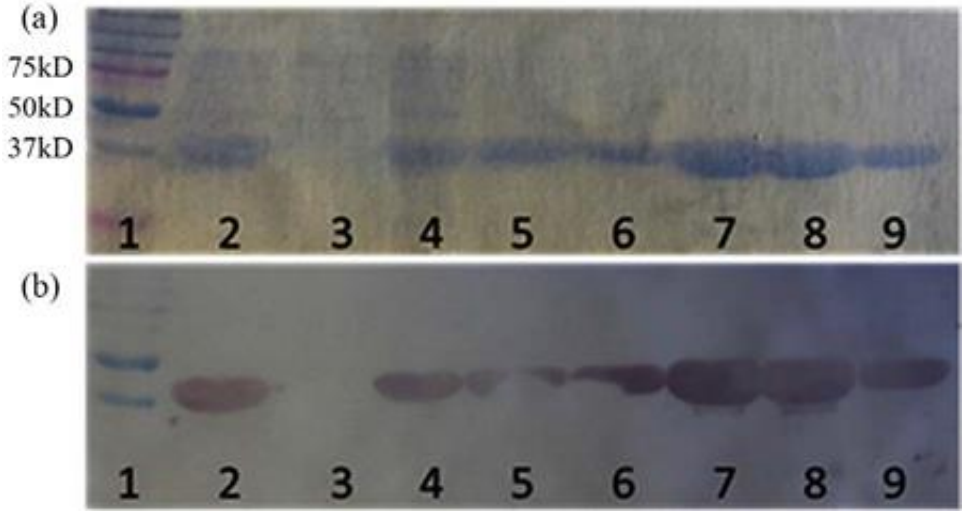

Figure 4.1 *Coomassie Brilliant Blue staining and Western blot using Anti-6x His-tag antibody of a riveting IMAC fraction of recombinant PspA. For both methods;* ***a.*** *CBB and* ***b.*** *WB. Lanes 1—molecular weight marker; 2—lysate; 3—flow through; 4 - 6—fraction 9 to 11 respectively; 7 - 9—fraction 18 to 20, respectively.*

The results of the PspA diffusion cell experiments are presented in Figure 4.2. At the neutral pH of 7.4, the maximum diffusion experienced was ~60%. The “initial burst effect” is experienced, and the diffusion profile demonstrates a constant release until equilibrium is reached (Figure 4.2(a)) (Huang, Chestang, & Brazel, 2002; Zu et al., 2012). After 12 hours, the rate appears to decline. The calculated Diffusion coefficient [cm^2/s] in Figure 4. 2(b), correlates with the release percentage data. The rate is initially faster and plateaus around 18 hours in the experiment.

Swelling Behavior of the Protein-Loaded PVA Hydrogel

The equilibrium solution content was calculated to characterize the porous structure of the hydrogel for the drug delivery system of PspA. The results show that swelling of 1% GA membranes is close and above 80% after 24 hours of swelling and above 90% after 48 hours of swelling (Figure 4.3(a)). The equilibrium solution results from release experiments illustrate a

similar ESC value between 0.12 mg/ml drug-loaded membranes and its respective controls (Figure 4.3(a)). However, the data shows that at the higher concentration, 0.7 mg/ml, PspA membranes at 24 h have a 12.5% larger ESC compared to 24 h control ($p \leq 0.0001$). The ESC value for 0.7 mg/ml has less than 1% increase at 48 hours, suggesting that 0.7 mg/ml membranes are near equilibrium at 24 hours, while 0.12 mg/ml membranes may take over 48 hours to do the same. At 0.12 mg/ml concentration, the protein molecules are more dispersed, making it more difficult for collisions between molecules to happen, therefore slowing down the diffusion out of the membrane. The results demonstrate that protein concentration affects the swelling and mesh size of the hydrogel (Huang et al., 2002; Nave, Luo, & Coleman, 2008). The higher protein concentration produces a greater concentration gradient that leads to a rapid increase in swelling and pore size (Å) until equilibrium is reached (Sirousazar et al., 2012).

There were no significant changes in swelling properties between 0.12 mg/ml PspA membranes with corresponding controls at 24 and 48 hours (Figure 4.1(b)). Both membranes nearly double in the swelling ratio at 48 hours. However, at 24 hours, the 0.7 mg/ml PspA membrane had three times the swelling ratio of its respective control ($p \leq 0.0001$). While the control membrane had a significant increase in swelling with time ($p = 0.0029$) (Jensen, Dávila, & Zelikin, 2016; Sirousazar et al., 2012), the 0.7 mg/ml PspA membrane did not. The results indicate that the 0.7 mg/ml hydrogel was already swollen to near its maximum capacity with the more significant protein concentration, while the control and 0.12 mg/ml PspA membranes expanded with the influx of buffer at 48 hours.

An evaluation of the hydrogel pore structure shows that mesh size increases with the protein concentration of the hydrogel (Figure 4.3(c)). The mesh size for 0.12 mg/ml PspA membranes relative to its controls is not significantly different, signifying that 0.12 mg/ml is such a low concentration that the gel mesh size is virtually unaltered (Nave et al., 2008; Thompson et al., 2013). However, increasing the concentration to 0.7 mg/ml of PspA causes the mesh size to rise by 335 Å relative to 24 hr control (p≤ 0.0001). While the control and 0.12 mg/ml membrane continued to increase in mesh size at 48 hours, the 0.7 mg/ml membrane only showed a neglectable increase.

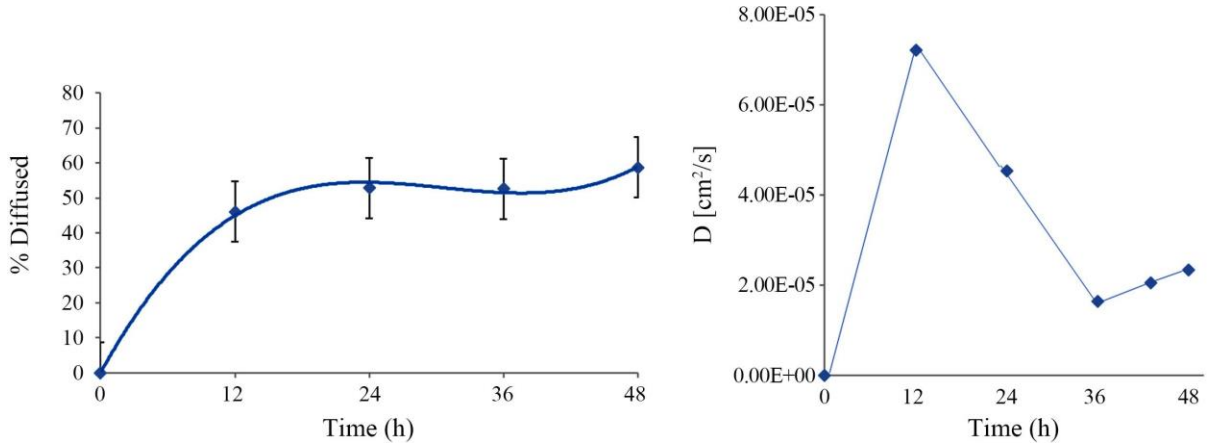

Figure 4.2 (a) *The percentage of PspA released in 5 mL Sodium Phosphate, pH 7.4* ***(b)*** *Calculated Diffusion Coefficient [cm^2/s].*

The higher protein concentration causes the mesh to be so stretched that as proteins is released and buffer diffuses in, the size remains nearly the same. At lower protein concentration, however, the membrane pores are not fully stretched, so as the buffer moves into the hydrogel, the pore increases in size, and the membrane swells.

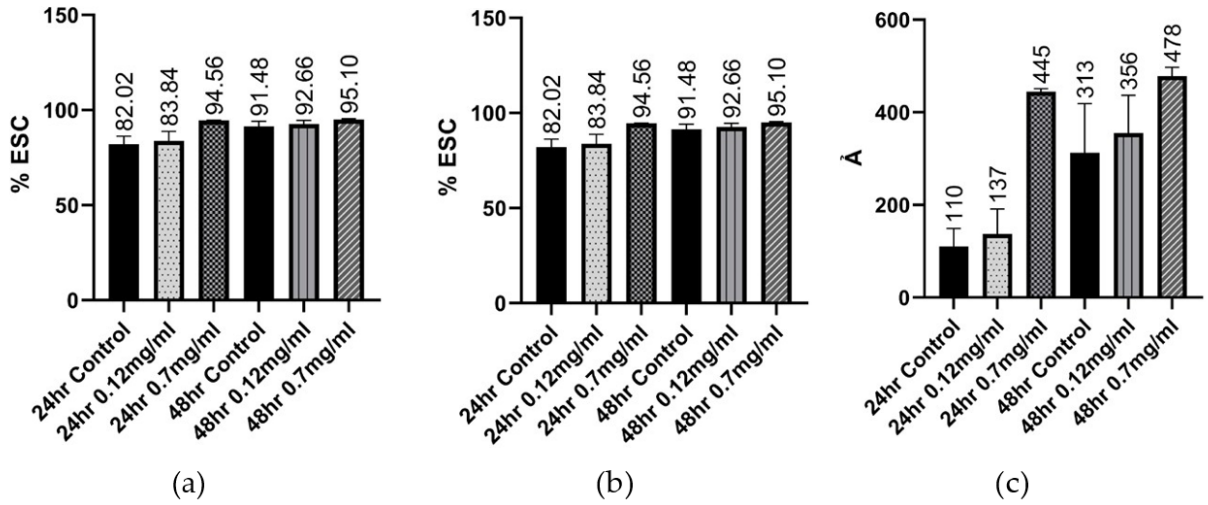

Figure 4.3 (a) *Equilibrium Solution Content of protein-loaded PVA hydrogel at 0.12 mg/ml and 0.7 mg/ml PspA concentrations.* ***(b)*** *Swelling ratio of hydrogels from 0.12 mg/ml and 0.7 mg/ml PspA membranes at 24-hours and 48-hours.* ***(c)*** *Mesh size in Å of hydrogels from0.12 mg/ml and 0.7 mg/ml PspA membranes at 24-hours and 48-hours.*

Two different methods were used to confirm protein release. The UV-vis result shows no significant changes in the amount of protein released from 24 hours to 48 hours for 0.7 mg/ml membranes and 0.12 mg/ml membranes, indicating that all the protein within the hydrogels is released at 24 hours. The 24-hour membranes had 5% less release than 48-hour most likely due to the increased space between the molecules, and the random motion of proteins in and out of the membrane, which explains the larger standard deviation for the 0.12 mg/ml membranes (Figure 4.4(a)). Native gel confirmed that encapsulating the protein within the hydrogel does not lead to protein aggregation and that the protein integrity is not affected after release (Figure 4.4(b)). Recombinant PspA was designed with 6x His-tag in C terminus to facilitate purification of the protein using Ni-NTA. Also, 6x His-tag was used in this experiment as a standard to estimate the relative activity of PspA after release from the hydrogel. After release, the 6x His-tag PspA molecules from the hydrogel can be detected using western blot with anti-6x His-tag antibody while the anti-PspA antibody had been used to identify the active PspA after release (Q. C. Moore et al., 2006). Figure 4.5 validates the release of PspA at 0.12 mg/ml concentration from the hydrogel and confirms its activity due to its strong interaction with

Anti-PspA (IgG). These results confirm the released PspA is completely active, and the hydrogel system facilitates a high molecular weight protein delivery. Thus, the system is suitable for vaccine delivery.

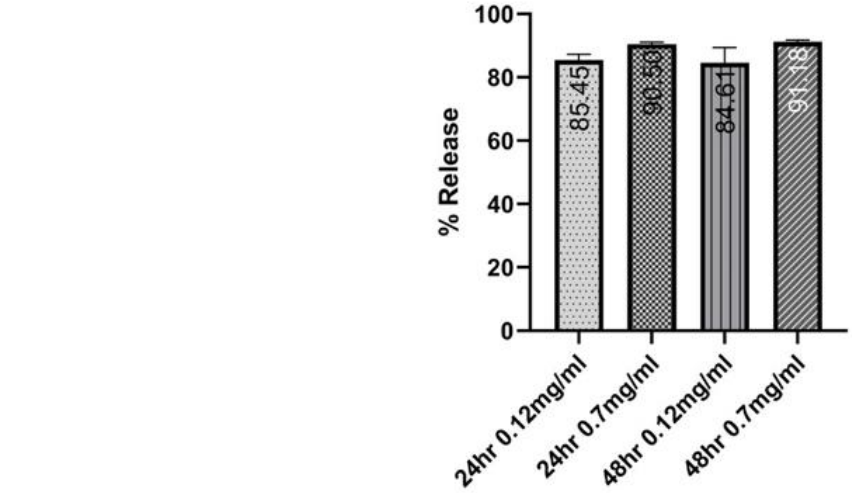

(a)

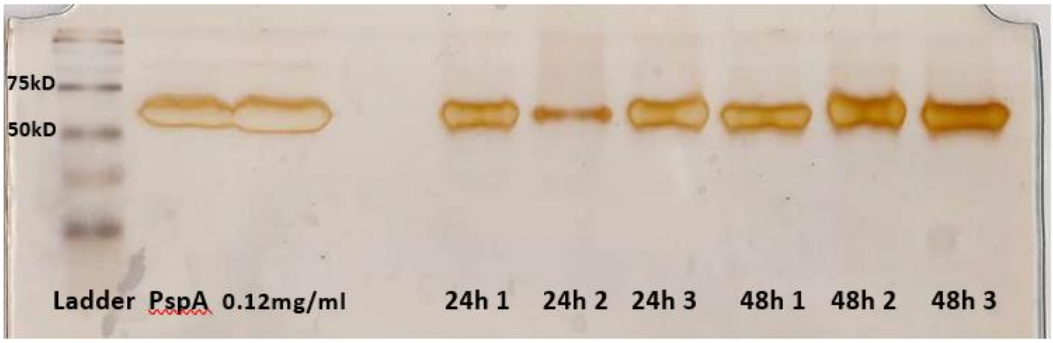

(b)

Figure 4.4 (a) *Protein release calculated from UV-Vis concentration;* ***(b)*** *The native gel of 0.12 mg/ml membrane release after 24 hours and 48 hours.*

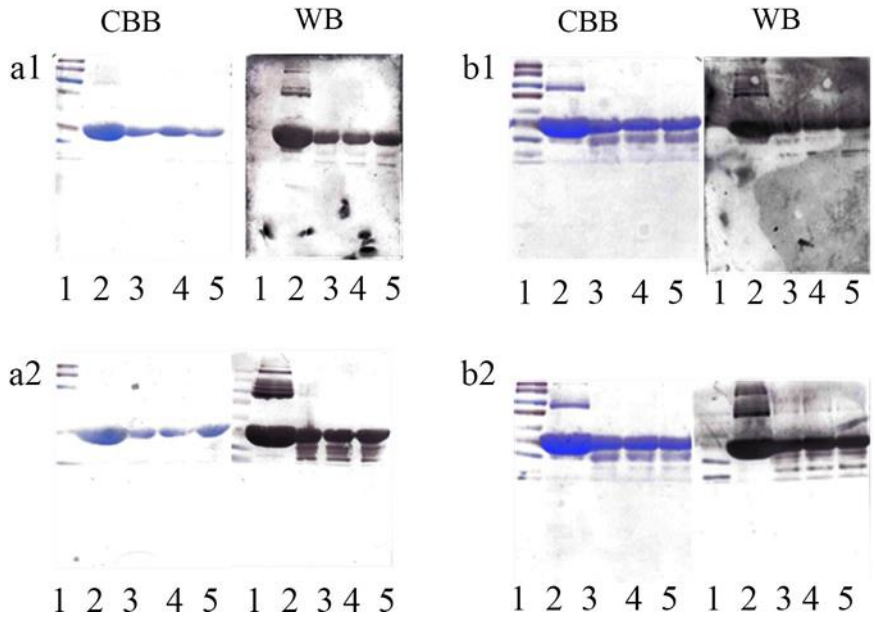

Figure 4.5 1. *Coomassie Brilliant Blue (CBB) staining and Western blot (WB) of PspA released from hydrogel using Anti-6x His-tag antibody.* ***2.*** *Coomassie Brilliant Blue staining and Western blot of PspA released from hydrogel using Anti-PspA antibody.* ***a1 & a2.*** *Release after 24 hours. Lane 1—molecular weight marker: 2—0.7 mg/ml PspA; 3 - 5—PspA release.* ***b1 & b2.*** *Release after 48 hours. Lane 1—molecular weight marker; 2—0.7 mg/ml PspA; 3—2 PspA released.*

ATR-FTIR spectroscopy

The interaction of cross-linkage was examined by Attenuated Total Reflection-Fourier Transform InfraRed (ATR-FTIR) spectroscopy. The resulting spectra show all major peaks (3300, 2940, 1731, 1141, and 1087) related to hydroxyl and acetate groups, which are indicative of a PVA hydrogel crosslinked with glutaraldehyde. Aldehyde peaks at 1735 (C=O stretch), 2850 (C-H stretch, and 1650 (OH def) cm^{-1} with intermolecular hydrogel bonding of water are also visible. The spectrum showed bands at 1140 (anti-sym) and 872 (sym) cm^{-1} indicative of the C-O-C-O-C stretch vibrations from acetal functional groups, which can represent an Acetal Ring Group or Ether Linkage Formation Structure resulting from binary functionalization. The PVA hydrogel with PspA incorporated displayed new vibration bands at 1648 and 1542 cm^{-1} in comparison to PVA hydrogel without protein (Chaouat et al., 2008; Prabhu et al., 2015); these bands represent the Amide I and Amide II similar to what others have seen when protein is present (Mansur, Oréfice, & Mansur, 2004; Reis et al., 2006). The

readings confirmed the incorporation of protein, seen in Figure 4.6. The appearance of these bands was decreased after release experiments, thus, indicating the release of PspA.

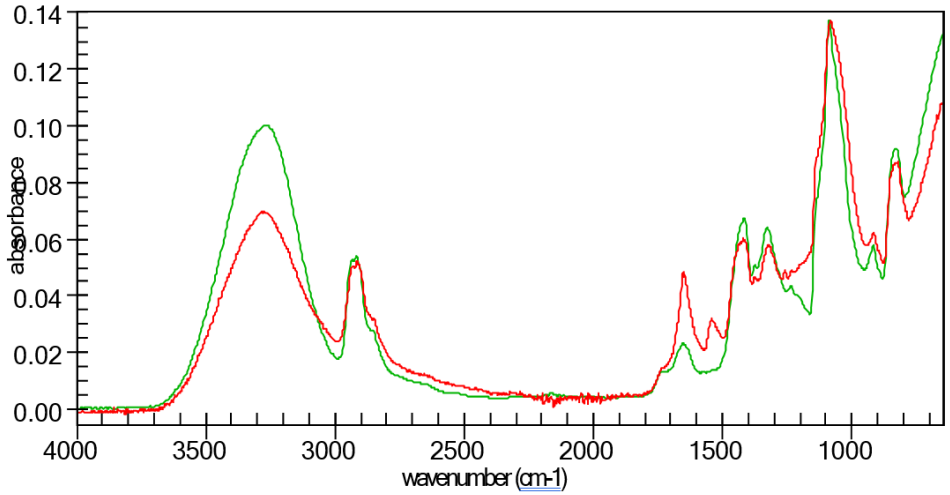

Figure 4.6 *ATR FTIR, spectra of 1% GA PVA hydrogel membrane (green), and 1% GA PVA hydrogel membrane with the protein, PspA, incorporated (red).*

Cytokines Expression and ELISA

As proof of the safety of the hydrogel system, cytokine antibody array analysis was utilized to investigate host immune factors that are involved in the ocular environment when the hydrogel is present and the release of the PspA protein. The corneal homogenates collected at post-exposure were analyzed using human inflammatory cytokine arrays. Chemiluminescent was used to detect signal intensities, and the signals were highlighted to show areas that had increased signals (Figure 4.7). The cytokine difference relative to the media and PspA hydrogel was determined and listed in Table 4.1. Of 60 cytokines assayed, there was a slight increase in the presence of GRO alpha and IL-8 in both conditions. The results demonstrated no contrasts in the cytokine expression profiles in the corneal homogenates collected from exposure to media alone and PspA hydrogel.

Table 4.1 *Cytokine profiles of Human Corneal Epithelial Cells Exposure to Hydrogel Drug Delivery System with PspA.*

Sample	IL-8[1]	Gro-alpha[1]
Control	0.167 ± 0.0718	0.048 ± 0.0033
PspA	0.153 ± 0.0956	0.045 ± 0.0033
Hydrogel System	0.151 ± 0.0590	0.046 ± 0.00042

[1]Numbers are expressed as Mean ± Standard Error of the Mean (SEM).

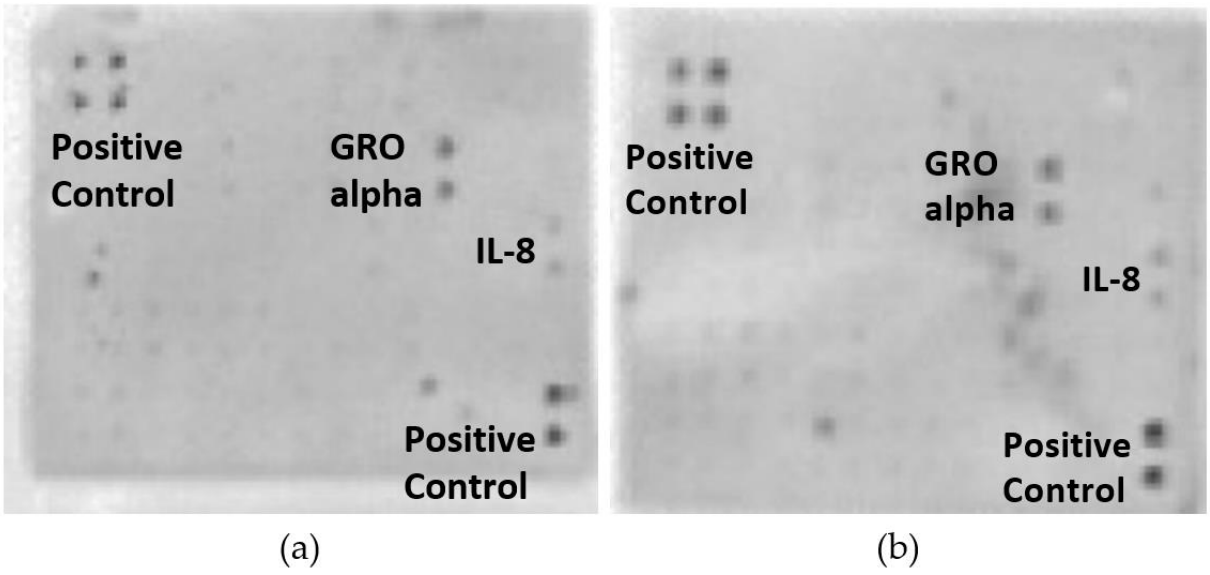

Figure 4.7 *12 Film images of cytokine arrays. A total of 60 cytokines were analyzed,* ***(a)*** *Representative of media 18 hours post-infection* ***(b)*** *Representative of PspA hydrogel 18 hours post-infection.*

To further evaluate the introduction of the hydrogel delivery system in the ocular environment, the innate immune response was assayed using cytokine antibody arrays. The results from the cytokine arrays were identical in cytokine expression. In these experiments, we identified GRO alpha and IL-8 were slightly upregulated in both media and PspA hydrogel. The immune response was further investigated utilizing specific ELISA assays of cytokines present during infection. It was noted that there was not an increase in the presence of the proteins, which is indicative of a normal immune response based on the data from the control samples.

Conclusion

With the isolation of a truncated fragment of PspA from *E. coli*, this study investigates the release of PspA from the open-mesh of hydrogel membranes. With the characterization of the PspA filled thin-film hydrogel membrane, it provides the necessary information to develop a modern biotechnology technique for the drug delivery system of high molecular weight proteins. This technique expands the current use of hydrogels and its application for vaccine delivery. The system represents a proof of concept and applies to proteins of similar size. The mechanism of hydrogel formation allows modifications that control protein entrapment and release. In conclusion, time and protein concentration affect the hydrogel pore size and drug release. Altogether, the data indicate that membranes with low protein concentration behave similarly to control membranes. Pore swelling and mesh size increase with time, with larger pores having higher protein release. Most of the protein within the hydrogel gets released within 24 hours, with membranes with 0.7 mg/ml concentration having the most release. The results from this study give insight into the minimum presence of cytokines, which are indicators of the innate immune response. Based on these findings, the presence of the hydrogel will not trigger an immune response that could potentially hinder the action of the drug therapy. Based on this study, we have provided evidence of an efficient hydrogel membrane system for protein delivery. With the characterization of PspA into a thin film hydrogel, it provides the necessary information of PspA transient entrapment within the membrane. This study provides the groundwork for applications of this hydrogel membrane delivery system in various infection models.

References

Ahmed, E. M. (2015). Hydrogel: Preparation, characterization, and applications: A review. *Journal of Advanced Research, 6*(2), 105-121. doi:https://doi.org/10.1016/j.jare.2013.07.006

Barbara, R. C. (2008). Recent Patents on Ocular Drug Delivery Systems. *Recent Patents on Drug Delivery & Formulation, 2*(1), 1-8. doi:http://dx.doi.org/10.2174/187221108783331410

Barzegar-Jalali, M., Alaei-Beirami, M., Javadzadeh, Y., Mohammadi, G., Hamidi, A., Andalib, S., & Adibkia, K. (2012). Comparison of physicochemical characteristics and drug release of diclofenac sodium–eudragit® RS100 nanoparticles and solid dispersions. *Powder Technology, 219*, 211-216. doi:https://doi.org/10.1016/j.powtec.2011.12.046

Briles, D. E., Tart, R. C., Swiatlo, E., Dillard, J. P., Smith, P., Benton, K. A., . . . McDaniel, L. S. (1998). Pneumococcal Diversity: Considerations for New Vaccine Strategies with Emphasis on Pneumococcal Surface Protein A (PspA). *Clinical Microbiology Reviews, 11*(4), 645-657. doi:10.1128/cmr.11.4.645

Bruno, B. J., Miller, G. D., & Lim, C. S. (2013). Basics and recent advances in peptide and protein drug delivery. *Therapeutic Delivery, 4*(11), 1443-1467. doi:10.4155/tde.13.104

Censi, R., Di Martino, P., Vermonden, T., & Hennink, W. E. (2012). Hydrogels for protein delivery in tissue engineering. *Journal of Controlled Release, 161*(2), 680-692. doi:https://doi.org/10.1016/j.jconrel.2012.03.002

Chaouat, M., Le Visage, C., Baille, W. E., Escoubet, B., Chaubet, F., Mateescu, M. A., & Letourneur, D. (2008). A Novel Cross-linked Poly(vinyl alcohol) (PVA) for Vascular Grafts. *Advanced Functional Materials, 18*(19), 2855-2861. doi:https://doi.org/10.1002/adfm.200701261

Craik, D. J., Fairlie, D. P., Liras, S., & Price, D. (2013). The Future of Peptide-based Drugs. *Chemical Biology & Drug Design, 81*(1), 136-147. doi:https://doi.org/10.1111/cbdd.12055

Figueiredo, K. C. S., Alves, T. L. M., & Borges, C. P. (2009). Poly(vinyl alcohol) films crosslinked by glutaraldehyde under mild conditions. *Journal of Applied Polymer Science, 111*(6), 3074-3080. doi:https://doi.org/10.1002/app.29263

Huang, X., Chestang, B. L., & Brazel, C. S. (2002). Minimization of initial burst in poly(vinyl alcohol) hydrogels by surface extraction and surface-preferential crosslinking. *International Journal of Pharmaceutics, 248*(1), 183-192. doi:https://doi.org/10.1016/S0378-5173(02)00433-7

Ibrahim, H., El-Leithy, IMan, Makky, Anna. (2010). Mucadhesive Nanoparticles as Carrier Systems for Prolonged Ocular Delivery of Gatifloxacin/Prednisolone Bitherapy. *Molecular Pharmetics, 7*(2), 576-585.

Jedrzejas, M. J. (2001). Pneumococcal Virulence Factors: Structure and Function. *Microbiology and Molecular Biology Reviews, 65*(2), 187-207. doi:10.1128/mmbr.65.2.187-207.2001

Jedrzejas, M. J., Lamani, E., & Becker, R. S. (2001). Characterization of Selected Strains of Pneumococcal Surface Protein A. *Journal of Biological Chemistry, 276*(35), 33121-33128. doi:10.1074/jbc.m103304200

Jensen, B. E. B., Dávila, I., & Zelikin, A. N. (2016). Poly(vinyl alcohol) Physical Hydrogels: Matrix-Mediated Drug Delivery Using Spontaneously Eroding Substrate. *The Journal of Physical Chemistry B, 120*(26), 5916-5926. doi:10.1021/acs.jpcb.6b01381

Juntanon, K., Niamlang, S., Rujiravanit, R., & Sirivat, A. (2008). Electrically controlled release of sulfosalicylic acid from crosslinked poly(vinyl alcohol) hydrogel. *International Journal of Pharmaceutics, 356*(1), 1-11. doi:https://doi.org/10.1016/j.ijpharm.2007.12.023

Kamoun, E. A., Chen, X., Mohy Eldin, M. S., & Kenawy, E.-R. S. (2015). Crosslinked poly(vinyl alcohol) hydrogels for wound dressing applications: A review of remarkably blended polymers. *Arabian Journal of Chemistry, 8*(1), 1-14. doi:https://doi.org/10.1016/j.arabjc.2014.07.005

Kiani, A., Shahbazi, M., & Asempour, H. (2012). Hydrogel membranes based on gum tragacanth with tunable structure and properties. I. Preparation method using Taguchi experimental design. *Journal of Applied Polymer Science, 124*(1), 99-108. doi:https://doi.org/10.1002/app.35038

Kulkarni, R. V., Sreedhar, V., Mutalik, S., Setty, C. M., & Sa, B. (2010). Interpenetrating network hydrogel membranes of sodium alginate and poly(vinyl alcohol) for controlled release of prazosin hydrochloride through skin. *International Journal of Biological Macromolecules, 47*(4), 520-527. doi:https://doi.org/10.1016/j.ijbiomac.2010.07.009

Mansur, H. S., Oréfice, R. L., & Mansur, A. A. P. (2004). Characterization of poly(vinyl alcohol)/poly(ethylene glycol) hydrogels and PVA-derived hybrids by small-angle X-ray scattering and FTIR spectroscopy. *Polymer, 45*(21), 7193-7202. doi:https://doi.org/10.1016/j.polymer.2004.08.036

Matsuyama, H., Teramoto, M., & Urano, H. (1997). Analysis of solute diffusion in poly(vinyl alcohol) hydrogel membrane. *Journal of Membrane Science, 126*(1), 151-160. doi:https://doi.org/10.1016/S0376-7388(96)00287-6

Mishra, R. K., Majeed, A. B. A., & Banthia, A. K. (2011). Fabrication and characterization of Chitosan/Poly (vinyl alcohol)-co-(vinyl acetate)-co-(itaconic acid) hydrogel membranes. *International Journal of Plastics Technology, 15*(1), 21-32. doi:10.1007/s12588-011-9012-2

Moore, M. R., Link-Gelles, R., Schaffner, W., Lynfield, R., Lexau, C., Bennett, N. M., . . . Whitney, C. G. (2015). Effect of use of 13-valent pneumococcal conjugate vaccine in children on invasive pneumococcal disease in children and adults in the USA: analysis of multisite, population-based surveillance. *The Lancet Infectious Diseases, 15*(3), 301-309. doi:10.1016/s1473-3099(14)71081-3

Moore, Q. C., Bosarge, J. R., Quin, L. R., & McDaniel, L. S. (2006). Enhanced protective immunity against pneumococcal infection with PspA DNA and protein. *Vaccine, 24*(29), 5755-5761. doi:https://doi.org/10.1016/j.vaccine.2006.04.046

Moore, Q. C., Johnson, L., Repka, M., & McDaniel, L. S. (2007). Immunization with PspA Incorporated into a Poly(Ethylene Oxide) Matrix Elicits Protective Immunity against Streptococcus pneumoniae. *Clinical and Vaccine Immunology, 14*(6), 789-791. doi:10.1128/cvi.00082-07

Nave, F. M., Luo, Y. Z., & Coleman, M. R. (2008). Impact of Mobile Phase Parameters on Transport Properties of Metal Affinity Hydrogel Membranes. *Separation Science and Technology, 43*(16), 4075-4098. doi:10.1080/01496390802414700

Norcross, E. W., Sanders, M. E., Moore, Q. C., 3rd, & Marquart, M. E. (2011). Pathogenesis of A Clinical Ocular Strain of Streptococcus pneumoniae and the Interaction of Pneumolysin with Corneal Cells. *Journal of bacteriology & parasitology, 2*(2), 108-108. doi:10.4172/2155-9597.1000108

Park, K. (2014). Controlled drug delivery systems: Past forward and future back. *Journal of Controlled Release, 190*, 3-8. doi:10.1016/j.jconrel.2014.03.054

Prabhu, P., Dubey, A., Parth, V., & Ghate, V. (2015). Investigation of hydrogel membranes containing combination of gentamicin and dexamethasone for ocular delivery. *Int J Pharm Investig, 5*(4), 214-225. doi:10.4103/2230-973X.167684

Reis, E. F. D., Campos, F. S., Lage, A. P., Leite, R. C., Heneine, L. G., Vasconcelos, W. L., . . . Mansur, H. S. (2006). Synthesis and characterization of poly (vinyl alcohol) hydrogels and hybrids for rMPB70 protein adsorption. *Materials Research, 9*(2), 185-191. doi:10.1590/s1516-14392006000200014

Siepmann, J., & Peppas, N. A. (2011). Higuchi equation: Derivation, applications, use and misuse. *International Journal of Pharmaceutics, 418*(1), 6-12. doi:https://doi.org/10.1016/j.ijpharm.2011.03.051

Sirousazar, M., Kokabi, M., & Hassan, Z. M. (2012). Swelling behavior and structural characteristics of polyvinyl alcohol/montmorillonite nanocomposite hydrogels. *Journal of Applied Polymer Science, 123*(1), 50-58. doi:https://doi.org/10.1002/app.34437

Sittiwong, J., Niamlang, S., Paradee, N., & Sirivat, A. (2012). Electric Field-Controlled Benzoic Acid and Sulphanilamide Delivery from Poly(Vinyl Alcohol) Hydrogel. *AAPS PharmSciTech, 13*(4), 1407-1415. doi:10.1208/s12249-012-9869-1

Thompson, A., Nguyen, D., & Nave, F. (2013). Characterization of PVA-IDA Hydrogel Crosslinked with 1.25%, 2.5% and 5% Glutaraldehyde. *GSTF International Journal on Education, Volume 1 Number 1, 1*(1). doi:10.5176/2339-5060_1.1.1

Varshosaz, J., & Hajian, M. (2004). Characterization of Drug Release and Diffusion Mechanism Through Hydroxyethylmethacrylate/Methacrylic Acid pH-Sensitive Hydrogel. *Drug Delivery, 11*(1), 53-58. doi:10.1080/10717540490265298

Yatim, M. M., Masri, S. N., Desa, M. N. M., Taib, N. M., Nordin, S. A., & Jamal, F. (2013). Determination of phenotypes and pneumococcal surface protein A family types of Streptococcus pneumoniae from Malaysian healthy children. *Journal of Microbiology, Immunology and Infection, 46*(3), 180-186. doi:https://doi.org/10.1016/j.jmii.2012.04.004

Zu, Y., Zhang, Y., Zhao, X., Shan, C., Zu, S., Wang, K., . . . Ge, Y. (2012). Preparation and characterization of chitosan–polyvinyl alcohol blend hydrogels for the controlled release of nano-insulin. *International Journal of Biological Macromolecules, 50*(1), 82-87. doi:https://doi.org/10.1016/j.ijbiomac.2011.10.006

Conclusion

Delivery systems continue to evolve to provide safer and more efficient alternatives to drug delivery. This dissertation presented four delivery systems specifically designed to overcome delivery barriers that affect drug bioavailability. In chapter 1, drug delivery to the ocular surface was enhanced by using chitosan-PEGDA nanoparticles for targeted delivery of gentamicin. This system showed better encapsulation efficiency, more stable and homogeneous particles, and greater antimicrobial properties than chitosan gentamicin nanoparticles without compromising lysozyme activity. In chapter 2, a chitosan-PEGDA film containing covalently linked nanoparticles was synthesized for ocular delivery. This study was a proof of concept for future contact lens synthesis. The results indicate that covalently attaching nanoparticles to the film did not disturb lysozyme activity, resulting in the successful release of the drug leading to bacterial growth inhibition. In chapter 3, the cytotoxicity of the polysaccharide fucoidan to cancer cells, MCF-7 and MDA-MB-231, were assessed and compared to chitosan encapsulated fucoidan. The data shows fucoidan to be more cytotoxic to MCF-7 than MDA-MB-231. However, cytotoxicity to MDA-MB-231 was increased by using chitosan nanoparticles. This study provides a new therapeutical approach to treating the hardier triple-negative cancers using a natural compound with low toxicity to normal cells. Lastly, in chapter 4, a PVA hydrogel for the delivery protein was synthesized, and its safety was assessed *in vitro*. Proteins possess incredible potential in disease treatment and prevention. However, their stability and size have hindered their capacity to be used on a broader scale. In this study, a poly(vinyl) alcohol membrane successfully entrapped and released a truncated version of PspA while maintaining the protein stability and activity after release. Furthermore, the data shows that hydrogel formation can be manipulated to control protein entrapment (concentration) and release (time), with lower protein concentrations having the most release. Therefore, PVA hydrogels are a suitable delivery

vehicle for proteins, and their application in microneedle drug delivery should be further investigated.